Advances in Colloid and Interface Science 284 (2020) 102246

Contents lists available at ScienceDirect

Advances in Colloid and Interface Science

journal homepage: www.elsevier.com/locate/cis

Historical Perspective

Silver nanoparticles: Synthesis, investigation techniques, and properties

Oleksandra Pryshchepa [a,b], Paweł Pomastowski [a], Bogusław Buszewski [a,b,*]

[a] Centre for Modern Interdisciplinary Technologies, Nicolaus Copernicus University in Torun, Wileńska 4, 87-100 Torun, Poland
[b] Department of Environmental Chemistry and Bioanalytics, Faculty of Chemistry, Nicolaus Copernicus University in Torun, Gagarina 7, 87-100 Torun, Poland

ARTICLE INFO

Article history:
15 August 2020
Available online 26 August 2020

Keywords:
Silver nanoparticles
Synthesis methods
Analytical techniques
Biological activity
Toxic mechanism

ABSTRACT

The unique silver properties, especially in the form of nanoparticles (NPs), allow to utilize them in numerous applications. For instance, Ag NPs can be utilized for the production of electronic and solar energy harvesting devices, in advanced analytical techniques (NALDI, SERS), catalysis and photocatalysis. Moreover, the Ag NPs can be useful in medicine for bioimaging, biosensing as well as in antibacterial and anticancer therapies. The Ag NPs utilization requires comprehensive knowledge about their features regarding the synthesis approaches as well as exploitation conditions. Unfortunately, a large number of scientific articles provide only restricted information according to the objects under investigation. Additionally, the results could be affected by artifacts introduced with exploited equipment, the utilized technique or sample preparation stages. However, it is rather difficult to get information about problems, which may occur during the studies. Thus, the review provides information about novel trends in the Ag NPs synthesis, among which the physical, chemical, and biological approaches can be found. Basic information about approaches for the control of critical parameters of NPs, i.e. size and shape, was also revealed. It was shown, that the reducing agent, stabilizer, the synthesis environment, including trace ions, have a direct impact on the Ag NPs properties. Further, the capabilities of modern analytical techniques for Ag NPs and nanocomposites investigations were shown, among other microscopic (optical, TEM, SEM, STEM, AFM), spectroscopic (UV-Vis, IR, Raman, NMR, electron spectroscopy, XRD), spectrometric (MALDI-TOF MS, SIMS, ICP-MS), and separation (CE, FFF, gel electrophoresis) techniques were described. The limitations and possible artifacts of the techniques were mentioned. A large number of presented techniques is a distinguishing feature, which makes the review different from others. Finally, the physicochemical and biological properties of Ag NPs were demonstrated. It was shown, that Ag NPs features are dependent on their basic parameters, such as size, shape, chemical composition, etc. At the end of the review, the modern theories of the Ag NPs toxic mechanism were shown in a way that has never been presented before. The review should be helpful for scientists in their own studies, as it can help to prepare experiments more carefully.

Abbreviations: AES, Auger Electron Spectroscopy; AF4, Asymetric flow field flow fractionation; AFM, Atomic Force Microscopy; BSA, Bovine Serum Albumin; BSE, Backscattered electrons; CE, Capillary Electrophoresis; CP-MAS NMR, Cross-Polarization Magic Angle Spinning Nuclear Magnetic Resonanse Spectroscopy; Cryo-TEM, Cryogenic Transmission Electron Microscopy; CTAB, Cetrimonium Bromide; CTEM, Conventional Transmission Electron Microscopy; DLS, Dynamic Light Scattering; DNA, Deoxyribonucleic acid; DSC, Differential scanning calorimetry; EDX or EDS, Energy Dispersive X-ray Spectroscopy; EELS, Electron Energy Loss Spectroscopy; EG, Ethylene glycol; ESEM, Environmental Scanning Electron Microscopy; FFF, Field Flow Fractionation; FTIR, Fourier Transform Infrared Spectroscopy; G4-DNA, G-rich Deoxyribonucleic acid quadruplex structure; HEPES, 4-(2-hydroxyethyl)-1-piperazineethanesulfonic acid; HPIV-3, Human parainfluenza virus type 3; HR-MAS-NMR, High-Resolution Magic Angle Nuclear Magnetic Resonanse Spectroscopy; HRTEM, High-Resolution Transmission Electron Microscopy; HSV-1, Herpes simplex virus type 1; IC50, Half-maximal inhibitory concentration; ICP-MS, Iductively Coupled Plasma Mass Spectrometry; IFE, Inner Filter Efect; LOH, Loss Of Heterozygosity; LP-TEM, Liquid-Phase Transmission Electron Microscopy; LSPR, Localized Surface Plasmone; MALDI-TOF-MS, Matix Assisted Laser Desorption/Ionization Time Of Flight Mass Spectrometry; MALS, Multi Angel Light Scattering; MHB, Mueller-Hinton Broth; MIR, Mid-Infrared Range; NALDI, Nanoassisted Laser Desorption/Ionization; NIR, Near-Infrared Range; NMR, Nuclear Magnetic Resonance; NP/NPs, Nanoparticle/Nanoparticles; NSOM, Near-field Scanning Optical Microscopy; PVP, Polyvinylpirrolidone; QDs, Quantum Dots; SAED, Selected Area Electron Diffraction; SE, Secondarry Electron; SEM, Scannig Electron Microscopy; SERS, Surface Enhanced Raman Spectroscopy; SIMS, Secondary Ion Mass Spectrometry; SP-ICP-MS, Single-Particle Inductively Coupled Plasma Mass Spectrometry; SPM, Scanning Probe Microscopy; STEM, Scanning Transmission Electron Microscopy; TEM, Transmission Electron Microscopy; TEOS, Tetraethyl orthosilicate; TGA, Thermogravimetric analysis; TOF-SIMS, Time Of Flight Secondary Ion Mass Spectrometry; UPS, Ultraviolet Photoelectron Spectroscopy; UV-Vis, Ultraviolet and Visible light range; XPS, X-ray Photoelectron Spectroscopy; XRD, X-ray Diffraction Spectroscopy.

* Corresponding author at: Department of Environmental Chemistry and Bioanalytics, Faculty of Chemistry, Nicolaus Copernicus University, Gagarina 7, 87-100 Toruń, Poland.
E-mail address: bbusz@chem.umk.pl (B. Buszewski).

https://doi.org/10.1016/j.cis.2020.102246
0001-8686/

Contents

1. Introduction

Over the past few decades, nanotechnology has reached an unprecedented scale. Thus, the increased interest of researchers in the field is not a surprise. Nanotechnology can be described as the field in science and technology involved in the engineering, production, and utilization of nanomaterials [1]. Nanoscale or nanometer objects, as defined by the prefix "nano" meaning 10^{-9}, in general, should fall within the limits of 1–1000 nm. However, according to the European Commission recommendations, to nanomaterials can be accounted any material of natural, incidental or engineered origin, which comprises at least 50% of the particles (in unbound or aggregated form) possessing one or more external dimensions in the range from 1 to 100 nm [2]. However, the objects that exceed the designated limits are often considered by researchers as NPs [3].

The NPs made from coinage metals attract attention due to their unique optical properties coming from the specific behavior under light irradiation, namely the appearance of Localized Surface Plasmon Resonance (LSPR). Among all "noble" metals, silver as a bulk material exhibits the highest electrical and thermal conductivities, the lowest melting and boiling points. Moreover, silver is the most reactive of the "noble" metals, and its cations exert toxic effects against various microorganisms [4]. Silver in form of NPs revealed even more unique properties, which enables them to be utilized in the multiple fields of technique and medicine: solar energy harvesting [5], electronic devices [6], advanced analytical techniques, e.g. SERS (Surface Enhanced Raman Spectroscopy) [7] and NALDI (Nanoassisted Laser Desorption/Ionization) [8,9], catalysis and photocatalysis [10,11], environmental applications [12], bioimaging [13] and bioanalysis [14,15], as antibacterial agent [16–18] or agent in anticancer therapies [19,20].

The utilization of Cu, Au, Pt, or Pd NPs for plasmonic applications is also considered. However, all the mentioned NPs cannot completely replace Ag NPs, since they have the highest quality factor in the plasmonic ability and exhibit the plasmonic band in a wide range of wavelengths (from near ultraviolet to near infrared spectrum), which is provided by numerous known nanostructures [21]. Moreover, in NALDI application the Ag NPs prepared by metal sputtering have shown the highest ion-desorption efficiency of analyte in comparison to Au, Pd, and Pt NPs [8]. Additionally, the Au and Pt NPs nearly a hundred times more expensive than Ag NPs, while Cu NPs utilization is much more complicated due to high susceptibility to oxidation and very few known nanostructures [21]. Lately, more attention is paid for the utilization of metal oxide NPs in the antibacterial applications, such as ZnO or ZrO_2 [22], which potentially can be a substitute for Ag NPs. However, long-time history of successful silver utilization in medicine as an antibacterial agent as well as the fact that till now it has been reported only one bacteria, *P. stutceri* (its natural habitat is silver mines), which completely resistant to Ag^+ [23], indicate that silver preparations, including in the form of NPs, is hardly can be replaced completely. Thus, Ag NPs still is the "hot topic" of numerous investigations.

One of the most important issues in nanotechnology is the possibility to engineer the NPs with desired properties for corresponding applications. The desired results can be achieved only in case of comprehensive knowledge about the NPs features regarding the synthesis approaches as well as exploitation conditions. A simple search in scientific publication databases reveals the hundreds of thousands of results on keywords like "Ag nanoparticles" or "silver nanoparticles". Unfortunately, a significant amount of the publications comprise highly restricted information regarding the Ag NPs properties, and how they are affected by the synthesis conditions. For instance, in the work by E.-Y. Ahn et al., among thirty utilized plant extracts only seven showed the capability to reduce Ag^+, the comparative characterization of the mentioned extracts or NPs surface functional groups were not performed [24]. Moreover, no correlation between NPs primary features (i.e. size, shape, surface charge, hydrodynamic radii) and biological activity could be derived. The authors attributed the toxicity of the synthesized Ag NPs to the extensively accepted theory of Reactive Oxygen Species (ROS) formation by released Ag^+. However, the Ag NPs show a much wider spectrum of possible toxic routs [25] and the surface chemistry strictly influences the NPs interaction with cells [26,27]. Hence, researchers should consider the possibility of a more comprehensive study of each individual investigated system, rather than to dissipate their resources.

Another subject that has poorly been covered in the literature is the influence of different analytical techniques on the obtained results during the study of Ag NPs. Still, some information can be derived from the scientists' reports, so it can be concluded that depending on the instrumental technique the studied features of Ag NPs can differ significantly [28]. Moreover, the results can be affected by artifacts introduced by the employed equipment, the utilized technique or sample preparation stages [29,30]. Even though the progress in the technologies allows us to eliminate a significant number of artifacts that can be introduced by the apparatus, it is rather impossible to consider or remove all the factors that influence the objects under investigation. Besides, the majority of the techniques have notable limitations and cannot provide exhaustive knowledge about the examined objects. Thus, researchers should carefully prepare their experiments and not avoid to perform additional analysis, as even simple chemical test may result in useful corroborative information.

The influence of Ag NPs on biological systems is also a sensitive issue, which induces numerous discussions in scientific society. Different effects, induced by Ag NPs in the prokaryotic and eukaryotic cells have been described in the literature [25]. Despite, the scientists' numerous attempts to distinguish separately the effects of each agent related to Ag NPs (stabilizer [31], Ag^+ [32], or the NP itself [33]), it is still impossible to perform completely, especially in terms of a time-resolved manner [34]. Moreover, the majority of the investigations are performed in vitro, which cannot reproduce the conditions of real biological systems. It was shown, that plasma proteins adsorption on Ag NPs surface [27,34] and Ag^+ chelation [17] change the NPs interaction with cells as well as their toxicity in general. Thus, the exact mechanism of AgNPs biological activity is still under consideration and is a challenge for future investigations.

Due to high interest in nanotechnology and in particularly in Ag NPs engineering and utilization in last decades a multiple studies have been performed, which in consequence was a reason for publication of several review articles. However, the issue of Ag NPs synthesis, properties, investigation techniques, the action mechanisms and application is so huge so it cannot be fit in the edges of one review. To give an example, M. Oćwieja et al. review is focused on the formation of layered structure of Ag NPs on different substrates [35]. In the article the basic approaches for the Ag NPs synthesis and characterization was shown. However, the main deliverable of the work is the excellent presentation of NPs deposition process on different substrates, including the adsorption kinetic of monolayers formation and its stability. In Rycenga et al. article the formation of Ag NPs structures for plasmonic applications has been revealed [21]. The authors, among others, have paid big attention to the plasmon phenomenon and possible ways to investigate it. P. Dubey with colleagues in their work has reviewed the Ag NPs cytotoxicity [25]. The review presents the information about numerous effects caused by Ag NPs to different cells. Moreover, the issues related to the Ag NPs properties and applications is developed continuously and hundreds of new research articles appears annually.

Thus, the purpose of the present study was to show the trends and achievements of the last years in Ag NPs synthesis and characterization. The latest development in the field of instrumental techniques offers new possibilities in materials science investigations. Hence, the manuscript was prepared with the main focus on the capabilities of modern instrumental techniques in line with NPs and nanocomposites investigations as well as their limitations. Finally, at the end of the review, the attempt to consider the toxic mechanism of Ag NPs on the molecular level was presented in a way that to the best of our knowledge has never been shown before.

2. Synthesis

Since the beginning of the nanotechnology, various routes for Ag NPs synthesis were introduced. The abundance of existing methods can be divided into two basic synthesis approaches, namely *top-down* and *bottom-up*. Top-down methods imply the creating of nanoscale structures starting from bulk material by reducing their size through "cutting" to required values. Instead, bottom-up approaches are the variety of synthetic techniques, which utilize the molecular, atomic, or ionic components to produce the more complex nanoscaled assemblies [36]. Further, synthesis techniques can be categorized according to the processes had been used, i.e. physical, chemical, biological methods (Fig. 1). The selection of an appropriate synthesis method is a major issue for engineered NPs production, as it affects their properties. For instance, galactose and mannose-capped Ag NPs possess lower toxicity against hepatocytes and neuronal-like cell lines in comparison to NPs stabilized with citrate [37], so they can be recognized as more biocompatible and therefore are more suitable for exploitation in medical applications. Instead, for NPs utilization in catalytic applications the size, shape, the unique dopants are more important than bioavailability [38]. Hence, the selection of synthesis rout usually is determined by desired NPs utilization features.

2.1. Physical approaches

Physical approaches include the exploitation of the physical agents, such as heat [39], electrical discharge [40], plasma [41], or electromagnetic irradiation [11]. The advantages of physical methods are their speed and minimal chemicals consumption. However, physical synthesis approaches have drawbacks to which the high energy of the process, the wide particle size distribution and low yield can be included [42]. Actually, the *top-down* approach is entirely based on physical synthesis methods. The arc discharge is frequently utilized for bulk silver atomization with subsequent Ag NPs formation, as in general, it considered as a fast and simple technique [43]. What is interesting, M. Miranzadeh with M. Z. Kassaee has shown that in the process the Ag NPs morphology and size can be controlled by utilization of different synthesis media [40]. However, authors have also claimed that synthesis medium influences not only NPs morphology but also their purity, the size distribution, stability against aggregation, and oxidation. Laser ablation is also well-known for NPs synthesis. The primary features (e.g. size, chemical composition) in the method can be influenced by the synthesis environment as well as laser parameters. The laser ablation in the water environment is a well-known technique for the production of ultrapure, monodisperse, and ultrafine Ag NPs [11]. The production of Ag NPs in the open air was also revealed [44]. However, the presence of the oxygen may lead to the undesirable formation of Ag_2O instead of metallic NPs, even with the utilization of Ar jet at the interaction zone. Moreover, the Ag NPs can be produced by thermal bulk silver evaporation/condensation. L. S. Kibis et al. have shown that within the method the final product properties can be changed by synthesis conditions [39]. For instance, the thermal silver evaporation with the simultaneous transfer in the convective gas flow of oxygen led to the formation of oxidized Ag_2O NPs. The same product was obtained with the silver sputtering by radio-frequency discharge in an oxygen atmosphere. By the changes of the oxygen to helium for the first method and to argon in the second case, it was possible to obtain metallic Ag NPs. The features of synthesized NPs by thermal evaporation were also affected by the position of the substrate relative to an evaporation device. Instead, the Ag NPs properties produced by sputtering can be partially controlled by the sputtering time. Another route was introduced by O. Kylian et al., they have produced polymer@Ag NPs deposited on the nylon 6,6 target by plasma during gas-phase synthesis [41]. Finally, for the production of Ag nanosized structures, the lithography can be utilized. The lithography is a technique, which offers precise control over the shape, size, and placement of the synthesized nano-assemblies, which is very desirable in plasmonic applications [36]. However, it should be mentioned that lithography is highly labor-extensive, making the utilization of obtained products very expensive. Some other physical, as well as chemical or biological approaches for Ag NPs synthesis can be seen in the Table 1.

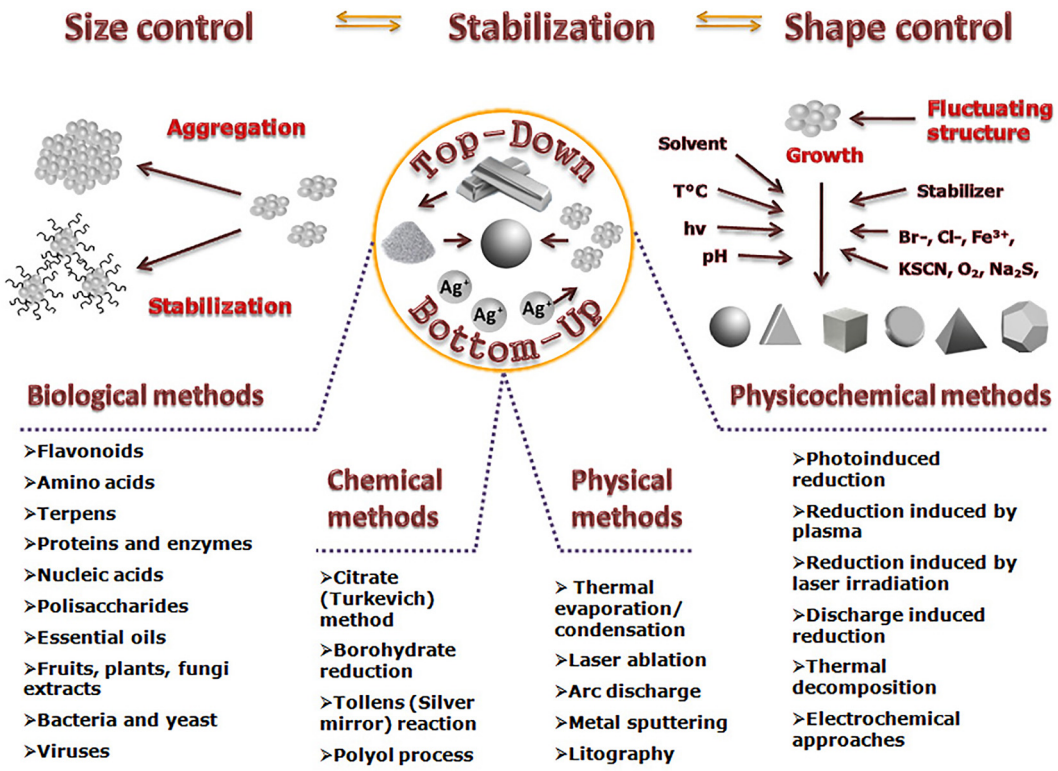

Fig. 1. The principles of Ag NPs synthesis.

2.2. Chemical synthesis

Chemical synthesis implies the NPs production through chemical transformations of the starting materials. The process requires the presence of three main components, namely metal precursor, reducing agent, and stabilizing/capping agents [42]. The fourth important component for NPs synthesis is a solvent, as the majority of the chemically and biologically conducted Ag NPs fabrication performed in the solution. However, in W. H. Eisa et al. the solid-state production of Ag NPs was performed by milling of *Zingiber officianale* powder with silver nitrate salt in desktop vibrating mill machine [45]. The distilled water and ethanol were utilized only at the end of the process for obtained NPs purification from unreacted species. The majority of chemically synthesized Ag NPs are made by four chemical reactions: citrate (Turkevich) method [46,47], borohydride reduction [48–51], Tollens (silver mirror) reaction [10], polyol process [52,53]. Turkevich method involves the utilization of $AgNO_3$ as the metal precursor and trisodium citrate both as a capping and stabilizing agent [46]. Even though the citrate method was one of the very first proposed for Ag NPs synthesis, it is still extensively utilized by researchers. The method is cost-effective and does not require advanced manipulation, so it is often utilized for NPs behavior investigations [47]. The borohydride reduction implies the utilization of $NaBH_4$ as a reducing agent. The borohydride exploitation for NPs synthesis seems to be the most popular among other chemical methods [48–51]. The popularity of $NaBH_4$ for Ag NPs production comes from the fact that it has higher reducing capability than citrate, and therefore it can be utilized for more precise size and shape control in Ag NPs synthesis [54,55]. To give an example, the utilization of $NaBH_4$ for the reduction of Ag_2O has provided the possibility to form hollowed Ag NPs [56]. Instead, the utilization of less active reducing agents led either to the formation of a hollowed structure with lower efficiency in case of hydrazine or even did not resulted in hollowed morphologies at all, as it was shown for ascorbic acid. Moreover, the precise utilization of $NaBH_4$ as a reducing agent allows to synthesize NPs with different shapes and sizes, such as spherical, rod-like, triangle, and even coupled "cookie-like" from the same set of the reagents [54]. However, the uniform colloid was possible to obtain only for spherical NPs, while rod-like and triangle together with spherical NPs occurred in solution as a mixture of different molar ratios. The silver mirror reaction involves the utilization of Tollen's reagent, $Ag(NH_3)_2OH$ as a precursor, and the aldehyde-group containing reducing agent (which may be sugars) for Ag NPs fabrications. The Tollen's reagent is not as popular in Ag NPs synthesis as $AgNO_3$, but in some cases provides additional possibilities for different valuable synthesis routes. To give an example, P. Yang with colleagues has shown the fascinating approach for tuning Ag@resorcinol-formaldehyde resin core-shell NPs to inverse resorcinol-formaldehyde-core@Ag shell NPs through the formation of Tollen's reagent by the mixture of NH_3/O_2 gases [10]. Moreover, J. Yoo et al. have produced the Ag NPs via hydrazine reduction of Tollen's reagent obtained from the dissolution of AgCl in ammonium hydroxide solution [57]. Insoluble nature of AgCl makes difficult to utilize it as a precursor in synthesis, but with the transformation to Tollen's reagent, it becomes possible to produce Ag NPs. In turn, the AgCl is one of the products that can be retrieved by recycling of silver-containing scrap. The utilization of polyols for Ag NPs synthesis is related to the possibility to engineer NPs with desired properties. By changes in the reaction conditions, such as temperature, reagent concentration, variations of polyol been used, or the presence of trace ions, the high degree of shape and size control can be achieved [52,53]. What is interesting, in the process polyol serves both as a reducing agent and the solvent. Some other synthesis approaches can be utilized, for instance Y. Tian et al. have prepared the flower-looked Ag NPs by reducing $AgNO_3$ in the presence of ascorbic acid and citrate ions as reducing and capping agents respectively [58]. Besides, the chemical transformation of precursor can be induced by different physical agents, such as heat or electromagnetic irradiation, so this group of methods can be defined as physicochemical approaches. To give an example, H. Le Trong et al. have synthesized Ag NPs by thermal decomposition of silver oxalate [59]. However, long

Table 1
Methods of AgNPs synthesis.

Method	Precursor	Synthesis conditions	Stabilization system	Product	Ref.
Physical	Ag 99.9%	Ar ion beam sputtering, Ag target (Ø 54 mm, 0,1 mm thickness), metal-support distance 80 mm, current 4 mA, t = 4 s, chamber flushed with argon, synthesis P = .04–.05 mbar	Deposited on glass support	Ag NPs 1.7–3.1 nm on glass coverslips	[8]
	Ag 99.9%	Thermal evaporation, Ag target (10 × 10 mm,0.2 mm in thickness) rolled into cylinder, placed in chromel wire helix (previously annealed in O_2 atmosphere at 1000 °C), heated to 700 °C in He (10 Pa) and O_2 (1 kPa) environment	Gold foil (99.9%) support	Ag NPs with 3–9 nm, mean 6 nm Ag_2O NPs 1–5 nm/twinned 8–10 nm (crystallite 2–3 nm)	[39]
	Ag 99.9%	Radio-frequency discharge sputtering, silver electrode Ø 2 mm in O_2 (25 Pa), support was preoxidazed in O_2 (100 Pa) at 300 °C, 30 min	Tantalum (99,9%) foil	Ag_2O/AgO NPs ≈ 4.5 nm	[39]
	Ag 99.9%	Target substrate distance 0.5–1.5 cm, Nd:YVO_4 laser, moving speed 100 mm/s, λ = 532 nm, 50 ns pulse, 20 kHz average output 6 W, irradiance of 100 MW/cm^2, open air, in jet of Ar	Deposited on glass support	Ag/Ag_2O NPs from 8 to 40 nm, with mean diameter 14.7 nm	[79]
	Ag 99.9%	Ag target (Ø 20 mm, 4 mm thickness), polished by sandpaper, washed with water and ethanol, immersed in deionized water, treated with pulsed laser ablation, Nd:YAG laser, λ = 1064 nm, 10 ns pulse, 10 Hz frequency, single pulse energy 435, 406 and 365 mJ/pulse	–	Average size Ag NPs depending on pulse energies 3.2 nm, 6.0 nm, 9.1 nm	[11]
	Ag 99.9%	Wires Ø1 mm used as electrodes, submerged in deionized water at 25 °C, arch discharged initial voltage of 135 V, 6,4 A peak current, on-pulse and off-pulse duration - 50 μs	–	Ag NPs with average sizes of 10 nm and 100 nm	[43]
	Ag 99.9%	Ag electrodes (Ø 2 mm, length 40 mm), exposed in different media (glucose/distilled water 10% and 25% w/w, glycerin/distilled water 10% and 25% w/w, phenol/distilled water 5% w/w, $Mg(NO_3)_2$•$6H_2O$/distilled water 0.01% w/w and 0,05% w/w, xylene, ethylene glycol, ethyl acetate, and phenol/toluene 5% w/w) with pulses of 5–10 A/cm^2, the cathode-anode gap was ≈ 1 mm, the NPs were separated by centrifugation and dried at 70 °C for 24 h	–	Ag NPs 35 to 100 nm, shape, depending on medium: rice shape, spheres, beads, grapes, platelets, balls, sponge particles, green bean shaped, cloudy leaflets, stacked plates, seeds	[40]
Chemical	$AgNO_3$	Twelve similar mixtures with sodium citrate, PVP and H_2O_2 were added to $AgNO_3$ solution under stirring. Different amounts of $NaBH_4$ solution were utilized for each mixture, stirred for 3 h, then filtered through 0.2 μmmembrane filter	Citrate	Triangle, sphere, rod-like and cookie-like Ag NPs Ø from 3 to 30 nm, different aspect ratios	[54]
	$AgNO_3$ $HAuCl_4$	$HAuCl_4$ solution was added to heated $AgNO_3$ solution, after mixture started to boil sodium citrate was added, keeped boiling for 30 min	Citrate	50 ± 9 nm $Au_{0.5}Ag_{0.5}$ NPs with Ag prevalence in the shell	[47]
	$AgNO_3$	$AgNO_3$ was added to 0.4 mM Cetyltrimethylammonium bromide (CTAB) solution under stirring, then $NaBH_4$ solution was added, obtained seeds kept in dark (1 h), then seeds were added to freshly prepared solution of $AgNO_3$, ascorbic acid and 10 mM CTAB	CTAB	Triangular Ag NPs with different edge length (the smallest 46 nm and 14 nm thickness)	[50]
	$AgNO_3$	$AgNO_3$ solution, NaCl and sodium citrate premixed together, quickly added to boiling water, reducing agent - ascorbic acid, heated and stirred for 1 h	Citrate	23 nm Ag NPs seeds	[3]
	$[Ag(NH_3)_2]^+$	Different amount of AgNPs seeds were added into water at room temperature, then ammonia complex solution and ascorbic acid was added, stirred for 1 h, the AgNPs separated by centrifugation and redispersed in sodium citrate solution	Citrate	40–300 nm Ag NPs, depending on amount of Ag NPs seeds	[3]
	$[Ag(NH_3)_2]^+$	Mesoporous silica was mixed with $[Ag(NH_3)_2]^+$, sonicated for 2 h, placed in dark at ambient temperature overnight, then dried at 60 °C in an air-circulated oven	Embedded in silica	Silica-silver nanocomposite	[12]
	$AgNO_3$	$AgNO_3$ with PVP mixed in ethylene glycol, heated at 120 °C for 1 h, cooled solution added to ethanol/water mixture, then TEOS and ammonia were added, stirred for 1 h at room temperature. Further, to induce AgNPs growth on surface the $NaBH_4$ was added to mixture, stirred for 1 h	Silica	65–90 nm Ag@SiO_2@Ag_{seed} NPs with surface seeds ≈ 5 nm 70–100 nm Ag@SiO_2@Ag NPs with surface Ag NPs ≈ 12 nm	[13]
	$AgNO_3$	The 1:15:15 M ratio of DNA:Ag^+:$NaBH_4$ was utilized. Previously the DNA assembly with specific sequences was prepared in phosphate buffer saline in 37 °C for 2 h, then Ag^+ ions were added and kept in dark at 4 °C for 1 h, subsequently $NaBH_4$ was added, the reaction maintained for 5 h in dark at 4 °C	DNA	DNA-harbored Ag clusters with ≈ 4 nm size	[15]
	$AgNO_3$	$AgNO_3$ and glutathione (molar ratio 4:3) was added to the flask under nitrogen flow with heated (120 °C) ethylene glycol, kept at 120 °C for 1 min to form colorless solution, then the temperature increased 165 °C with heating rate 20 °C/min. The reaction mixture cooled in ice-water bath in different time points (11, 13, 15, 16, 22, 28 min)	Glutathione	2–10 nm Ag_2S NPs, depending on reaction time	[14]
	$AgNO_3$	$AgNO_3$ solution and glutathione was added to ice cold water, pH raised to 12 by NaOH solution the formation of Ag_2O-NPs was observed. To the obtained Ag_2O nanocrystals separately the 1. $NaBH_4$ solution, 2. ascorbic acid, 3. hydrazine, 4. sodium sulfide or 5. sodium bromide was added at once	Glutathione	1. Hollow Ag NPs, 2. ordinary Ag NPs, 3. hollow in part Ag NPs, 4. hollow Ag_2S NPs, 5. hollow AgBr/Ag NPs	[56]

(continued on next page)

Table 1 (*continued*)

Method	Precursor	Synthesis conditions	Stabilization system	Product	Ref.
	CF_3-CO_2Ag	Ag trifluoroacetat was dissolved in isoamyl ether/oleic acid mixture at 160 °C under N_2 atmosphere, then precipitation was performed with sonication in ehtanol and subsequent centrifugation (3000 rpm)	Oleic acid	Hydrophobic Ag NPs ≈ 5.2 nm	[80]
	$AgNO_3$	$NaBH_4$ and citrate mixture heated to 60 °C for 30 min, then $AgNO_3$ was added drop-wise and temperature was raised to 90 °C, then the pH was adjusted to 10.5, the reagent excess was removed by centrifugation (12,000 rpm) and washing with deionized water	Citrate	Ag NPs with size 5–100 nm, depending on Ag^+ amount	[55]
	$AgNO_3$ AgCl	Ethylene glycol (EG) was heated to 140 °C, subsequently the HCl/EG, the $AgNO_3$/EG and PVP/EG solutions were simultaneously introduced, after 8 h the mixture removed from heat, the vial was kept loosely capped for 20 h and then tightened. The tests with addition of different amount of HCl, NaCl and HNO_3 were performed: 1. pure EG (with no HCl), 2. with addition of HNO_3 (no HCl), 3. with NaCl (no HCl), 4. standard procedure, 5. HNO_3 and NaCl (no HCl), 6. HNO_3 and HCl, 7. AgCl and HNO_3	PVP	1. Irregular/polydisperse Ag NPs, 2. truncated octahedra; 3. nanowires, nanocubes and irregular, 4. nanocubes, 5. cuboctahedra and truncated cubes, 6. nanocubes, 7. nanocubes	[52]
	$AgNO_3$	PVP/EG solution was heated to 160 °C, then NaBr/EG solution was added, subsequently dropwise $AgNO_3$ was introduced, kept for 35 min and then transferred to ice-water bath, the product crushed by acetone, separated (2000 rpm) and washed by water	PVP	Ag nanowires, ≈ 20 nm diameter	[53]
	$AgNO_3$	The synthesis in microfluidic device, where to the first inlet the mixture solution of $AgNO_3$, trisodium citrate and H_2O_2 and to the second inlet solution of $NaBH_4$ were introduced	Citrate	Triangular Ag NPs	[81]
		To the first inlet the triangular nanoparticles with TEOS and to the second inlet the ammonia in ethanol were introduced	SiO_2 shell	Triangular Ag@SiO_2 NPs	
Physico-chemical	$AgNO_3$	Laser ablation of 99.9% purity silicon target immersed in $AgNO_3$ solution, Nd:YAG laser, $\lambda = 355$ nm, pulses <40 ns frequency 5 Hz, power density per pulse <40 J/cm^2	Silica	Ag@SiO_2 NPs, with 11 ± 4 nm core and 1–2 nm shell	[82]
	$Ag_2C_2O_4$	Silver oxalate decomposition at 125 °C for 100 h	–	Ag NPs 5–20 nm	[59]
	$AgNO_3$	Dipped platinum anode and stainless-steel capillary tube utilized as cathode immersed in solution of $AgNO_3$ with fructose	Fructose	Polydisperse irregular Ag NPs	[63]
	$AgNO_3$	99.9% titanium anode and cathode Ø 2 mm were immersed in $AgNO_3$ solution, 15 A current and 3 V voltage	Citrate	Ag NPs ≈ 18 nm	[62]
Biological	$AgNO_3$	Flavone, chrysin, galangin, 3-hydroxyflavone, kaempferol, quercetin, myricetin, apigenin, luteolin, tricetin mixed with the $AgNO_3$ solution, pH adjusted to different values from 7.2 to 10.1, depending on flavonoid been used, the reaction carried at 23, 40, 70 °C	Flavonoids	Ag NPs 12–39 nm size, which depends on flavonoid been used and synthesis temperature	[7]
	$AgNO_3$	Different amount of beetroot extract were mixed with $AgNO_3$, reaction maintained overnight	Betanin	Ag NPs spherical, triangular and truncated triangular ≈ 15 nm	[75]
	$AgNO_3$	Lactoferrin, suspended in 0.09% NaCl, pH = 6, then $AgNO_3$ basic solution was added, the nanocomplex was separated by centrifugation 15,000 rpm, at 4 °C	Lactoferrin	Lactoferrin-conjugated Ag NPs with sizes 8–18 nm	[16]
	$AgNO_3$	Casein suspension in 0.05 M ammonium bicarbonate solution was mixed with $AgNO_3$ solution incubated at room temperature for 24 h, the nanocomplex was separated by centrifugation max speed for 8 min	Casein	Casein-conjugated Ag NPs in size range 4–100 nm	[83]
	$AgNO_3$	Essential oil of orange peel was mixed with $AgNO_3$ solution, stirred at 70 °C for 48 h	Compounds of essential oil	Ag NPs ≈ 3 nm	[66]
	$AgNO_3$	Solid state synthesis by milling of *Z. officinale* powder with 0,05–0,5 g of $AgNO_3$ salt, in hardened chromium steel jar with zirconia balls Ø 3 mm, 50 rpm, 30 min, balls:reacting powder was 15:1 w/w	Compounds of *Z. officinale* powder	Ag NPs with average size 11, 16, 20 and 24 nm, depending on $AgNO_3$ amount	[45]
	$AgNO_3$	Aqueous plant extract was mixed with aqueous $AgNO_3$ solution, kept in ambient temperature for 4 h	Compounds of *S. chinensis* L. extract	Coated Ag NPs with size in range 40–80 nm	[20]
	$AgNO_3$	To chitosan (50–190 kDa) dissolved in 0,5% acetic acid at 40 °C, cooled to room temperature, the $AgNO_3$ solution (to corresponding concentration 0.1, 0.2, 0.5, 1.0 and 1.5%) was added, then mixture was kept protecting from light to complete dissolution, films were formed on polystyrene plates and dried at 37 °C for 48 h	Embedded in chitosan	Ag NPs - chitosan films <5 nm, (Ag 0.1–0.5%) and Ag NPs 5–10 nm, (Ag content 1–1.5%)	[17]
	$AgNO_3$	*Bacillus licheniformis* biomass was mixed with $AgNO_3$ solution, then kept on shaker (200 rpm) at 37 °C for 24 h, then the biomass was removed by sonication and centrifugation (4000 ×*g*, 10 min), Ag NPs was purified by dialysis with 12,000 Da cut-off and by ultracentrifugation (200,000 ×*g* at 4 °C for 16 h) from HEPES buffer with sucrose gradient	Compounds of *Bacillus licheniformis* biomass	40–50 nm Ag NPs	[19]

Table 1 (*continued*)

Method	Precursor	Synthesis conditions	Stabilization system	Product	Ref.
	$AgNO_3$	*L. lactis* isolated from milk was incubated for 5 d at 26 °C in Mueller-Hinton broth, culture was centrifuged (9000 rpm), supernatant was combined with $AgNO_3$ solution, kept at 26 °C for 7 d, biocomposite separated by centrifugation (14,000 rpm) for 30 min	Compounds of L. *lactis* supernatant	Biocomposite with Ag NPs ≈ 19 nm	[84]
	$AgNO_3$	*O. limnetica* homogenate in phosphate buffer pH 7 mixed with $AgNO_3$ solution, kept at 35 °C under illumination for 48 h	Compounds of *O. limnetica* homogenate	Quasi-spherical Ag NPs with 3–18 nm size	[85]
	$AgNO_3$	Fungal cell filtrate of 1. *Alternaria* species, 2. *F. oxysporum*, 3. *Curvularia species*, 4. *C. indicum*, and 5. *Phoma* grown on potato dextrose broth at 28 °C for 72 h, mixed with $AgNO_3$ solution	Compounds of fungal cell filtrate	Ag NPs of 1. 7–20 nm, 2. 4–13 nm, 3. 5–23 nm, 4. 10–31, 5. 7–20 nm	[86]

heating caused metal sintering, which led to the formation of bigger NPs. Moreover, B. B. Bokhonov with coauthors has shown that thermal decomposition of silver salts of fatty acids led to the formation of self-assembled Ag NPs [60]. The authors have also observed the NPs sintering with an increase in temperature above 260 °C. It was suggested that fatty acids stabilize the Ag NPs assemblies, but the elevation of the temperature led to the desorption of carboxylic acids and subsequent aggregation. Y. Cai with colleagues has performed the deposition of uniform Ag NPs on stainless steel plates by $AgNO_3$ decomposition with laser irradiation [61]. They proposed the NPs formation mechanism, which comprises the $AgNO_3$ decomposition through Ag_2O formation with subsequent reduction to Ag under laser heating. However, the authors claim that the laser power should be controlled precisely. It was shown that low laser power was not sufficient to perform high efficient synthesis, while very high laser power led to overheating and to Ag NPs evaporation and sputtering. Additionally, even though, in general, arc discharge usually is utilized for the atomization of the bulk metal in NPs synthesis, it can also be utilized for $AgNO_3$ transformation to Ag NPs [62]. Moreover, the H. M. Yasin with coauthors has revealed the possibility to utilize micro-plasma for Ag^+ reduction in the solution to form fructose-coated Ag NPs [63]. The arc discharge as well as micro-plasma are the source of the fast electrons, which take part in the Ag^+ reduction. It is obvious that the amount of produced electrons plays a crucial role in the reduction process, thus providing an opportunity to control the synthesis. Moreover, the Ag NPs basic parameters can be controlled with the amount of utilized precursor and capping agent. It was shown, that a lower ratio of stabilizer to precursor led to the formation of bigger NPs with higher polydispersity, which can be explained by the increased contribution of aggregation in the NPs growth [63]. The electrolysis has also been used for Ag^+ reduction, where the mechanism of NPs formation is similar to that one with the utilization of micro-plasma [64]. Finally, the synthesis mediated by UV-Vis irradiation allows to change NPs shape [65]. It was suggested that UV-Vis irradiation increases the energy of small Ag nanoseeds, which then caused aggregation with the formation of Ag NPs of different shapes.

2.3. Biological methods

Recently, more attention is paid for the impact of the technologies on the environment. Thus, the so-called "green chemistry" becomes more popular. Regarding Ag NPs, the biological synthesis methods are considered to be eco-friendly, as for their production the harmful chemicals are not involved. Moreover, the biologically synthesized NPs in general exhibit lower toxicity to eukaryotic cells, so they provide a possibility for their exploitation in biomedical applications. The lower toxicity of biologically synthesized NPs is attributed to the fact, that the capping agent is formed with the compounds such as proteins [16], terpenes [66], flavonoids [7], which naturally can be found in an organism. Biological synthesis is based on the same principles as for chemical approaches, only the reducing and capping agents involved in the reactions should be of biological origin.

The "hot topic" in the biological synthesis of Ag NPs is the utilization of plants [45], fruits [20], plant seeds [67], or their extracts [68,69]. Moreover, the Ag NPs production with mushroom extract [70], marine algae [71] and even propolis [72] have been shown. To the active compounds, that can be involved in the Ag^+ reduction, and therefore NPs formation, the sugars [67], terpenes [66], amino acids [73], flavonoids [7], and other phenolic compounds [74] can be include. To give an example, R. K. Tomas et al. have produced Ag NPs with chlorogenic acid, which served both as a reducing and capping agent [74]. M. Svecova with coauthors has performed the Ag NPs synthesis with different flavonoids for SERS applications [7]. H. Veisi with colleagues has utilized the orange peel essential oil, composed mostly from limonene, to produce Ag NPs [66]. Moreover, the natural plant-derived pigments such as betanin [75] and curcumin [76] have also shown to be effective in the Ag NPs synthesis. What is interesting, the curcumin-based Ag NPs have revealed the synergistic antibacterial effect against *E. coli* and *B. subtilis*. Finally, in S. Shankar and J.-W. Rhim work the amino acid mediated Ag NPs formation was shown [73]. The authors have also utilized agar for the production of novel functionalized nanomaterials, which supposed to be useful in biodegradable packaging films formation.

The polysaccharide utilization for nanocomposites production in general is very popular in line with their medical applications. The Ag NPs-containing hydrogels and other polymer films are of the big interest for wound healing scaffolds and bandages production. Y. Jiang et al. have investigated the antibacterial and cytotoxic properties of Ag NPs-containing hydrogel based on konjac glucomannan and chitosan [77]. S. Ul-Islam et al. [78] as well as G. Lopez-Carballo et al. [17] have also utilized chitosan for production of new functional materials. Instead, A. K Kodoth et al. have revealed a possibility to utilize pectin for the synthesis of transdermal drug-delivery Ag-containing films [87]. J. H. Lee with coauthors has also exploit pectin and pullulan for antimicrobial films formation [88]. Proteins and nucleic acids are another biopolymers that show beneficial features in Ag NPs production. Recently, in our group, the synthesis of Ag NPs-containing nanocomposites based on whey proteins was performed [16,83]. Moreover, the Ag NPs formation through lysozyme [89], trypsin [90], and cytochrome C [91] was revealed. Finally, the self-assembled Ag NPs formation with G4-DNA has been shown by I. Libitz and A. Kotlyar [92].

Lately, it has become more popular to create Ag NPs via microorganism synthesis. It was shown that bacteria [19,84,93,94], fungi [86], cyanobacteria [85] and even viruses [95] can be utilized for NPs synthesis. The viruses capsid predominantly comprise proteins, so it can be considered as protein-mediated Ag NPs synthesis. Instead, the Ag NPs synthesized by cellular organisms can be performed in several different ways, namely intracellular and by utilization of culture supernatant, bacterial biomass, or cell-free extract [96]. The components of the synthesis mixture act both as a reducing agent and the stabilizer, forming

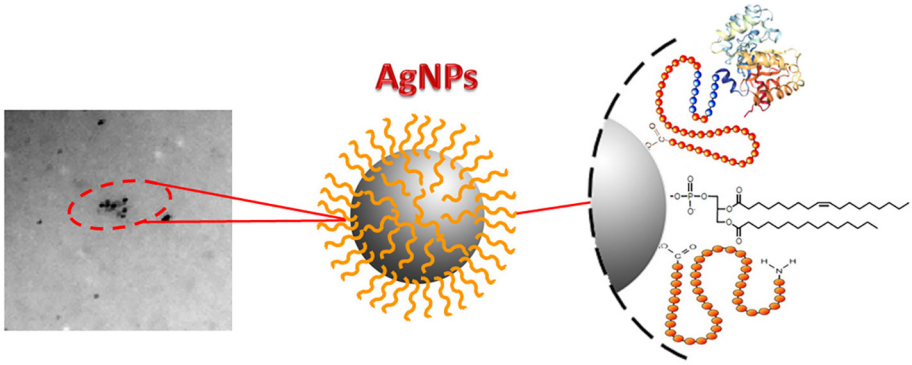

Fig. 2. The structure of AgNPs with organic deposits on the surface.

the organic deposits on the surface of the NPs (Fig. 2). Unfortunately, the exact mechanism and substances that are involved in the Ag NPs formation are still unclear. Moreover, S. M. Mehta et al. have revealed the possibility to exploit tryptone, the component of various culture media, for Ag NPs synthesis, which makes the interpretation much more complicated [97]. Additionally, a lot of culture media for microorganisms growth comprise casein hydrolysate, and investigations of our group have shown that casein is able to reduce Ag^+ without any additional conditions [83].

However, it should also be mentioned that with the utilization of the biological synthesis, the control of NPs basic parameters is less precise. Hence, the utilization of biologically synthesized Ag NPs is rather restricted in different devices or in advanced analytical techniques, where the desired optical features of the NPs are obtained by the changes in shape and size. Moreover, the biological systems may include some contaminants that disturb the synthesis. To one of such contaminants the Cl^- can be include, which forms the insoluble AgCl, thus tending to form non-metalic AgCl NPs [71]. Generally, the production of pure metallic NPs is a challenge in biological approaches, which attracts big attention of the scientists. The Cl^- is an integral part of culture media for microorganisms growth. Thus the utilization of microorganisms for Ag NPs synthesis often leads to the formation of undesirable AgCl or composed Ag/AgCl NPs. The main question, which appears during such a synthesis process is which kind of the product has been obtained. In some cases, the scientists make erroneous statements by incorrect interpretation of obtained data. N. Duran et al. have reviewed the articles focused on biogenic Ag and AgCl NPs synthesis and they noticed, that in some cases the researchers claim the production of metallic Ag NPs, while the XRD (X-ray Diffraction) for such products exhibited only the formation of AgCl [98].

2.4. Size and shape control

One of the major issues in the NPs production is a size control, as size determines NPs physical and biological properties. The NPs formation is the complex process, which in general can be divided into several main parts: nucleation, growth through Me^0 incorporation, and the aggregation. The nuclei formation is a thermodynamically dependent process [99]. The surface free energy always being positive, meaning that nuclei appearance is a thermodynamically disadvantageous process. Instead, crystal growth leads to a decrease in system energy. Thus, the growth process mainly depends on the possibility of mass exchange between NPs seeds and the solution as well as from the capability to aggregate. T. K. Nguyen et al. in their excellent review have revealed the theoretical details of the NPs nucleation and growth mechanisms in a solution [99]. It can be derived that Ag NPs size and size distribution are strictly dependent on the time-resolved Ag^0 concentration in the solution, which in turn depends on the amount of metal precursor, that have been used as well as the reaction rate of Ag^+ reduction. The excess of the metal precursor in general leads to bigger NPs formation [68]. Instead, the high reaction rate at the beginning of the process makes it possible to produce a bigger amount of NPs with a lower size. Thus, it can be derived that the reduction potential and utilized amount of reducing agent, which influences the reaction speed, is one of the major factors. The redox potential of Ag^+ can also be influenced by pH value. Obviously, the reaction can be affected by changes in temperature [3,56,68].

The aggregation plays an essential role in the NPs formation (Fig. 1). The widely accepted theory implies NPs growth through the aggregation of the crystal nuclei [68,99]. Moreover, the liquid-cell TEM have revealed the formation of sub-10-nm Ag nanorods through smaller quasi-spherical particles aggregation, which can be considered as the evidence of previously accepted theories [100]. However, uncontrollable aggregation can lead to the formation of more massive structures, that no longer possess the unique features of NPs. Thus, sufficient stabilization is an indispensable part of NPs synthesis and storage. Still, in A. Suresh et al. work the synthesized uncoated Ag NPs unexpectedly revealed zeta potential −42.5 mV in deionized water, which is considered to be enough for NPs stabilization through electrostatic mechanism [101]. The effect was attributed to the adsorbed nitrate ions on the NPs surface. The H. Kang et al. in their review have shown the variety of approaches involved in the stabilization of plasmonic NPs [102]. Besides the approaches that already have been shown above (i.e. citrate, PVP, flavonoids, proteins, DNA, polysaccharides, etc.) the utilization of inorganic shells induces high interest among the researchers. Silica coatings have shown beneficial properties during metallic NPs utilization [103]. To silica virtue, the high stability to the water environment, various chemicals, and elevated temperatures can be include. Moreover, silica is transparent for electromagnetic irradiation in the wavelength range from 300 to 800 nm, which makes it possible to utilize in the synthesis of different nanocomposites for optical applications. The different silica-containing structures can be easily produced through a highly-controllable Stöber process. More synthesis details and properties of silica-containing structures can be found in B. J. Jankewicz et al. work [104]. It should be noted, that besides the stabilization of the NPs the capping agent also determines the surface charge of the NPs, which in general is a reason for electrosteric stabilization mechanism. To give an example, A. Suresh et al. have synthesized Ag NPs with different capping agents [101]. The Ag NPs stabilized with poly (diallyldimethylammonium) have a positive surface charge of $+45 \pm 3.1$ mV, biologically synthesized NPs have a negative charge of -12 ± 2 mV, finally, the NPs capped with oleate revealed the negative charge of -45.8 ± 4.4 mV. However, the authors have investigated the cytotoxicity of as synthesized NPs, and it was shown that positively charged Ag NPs have revealed the highest cytotoxicity against both macrophage cells and lung epithelial cells. What is interesting, the biogenic Ag NPs, which supposed to be more biocompatible also have revealed higher cytotoxic properties than uncoated and oleate-coated

Ag NPs. The reason for such behavior partially can be explained by the same mechanism as for NPs stabilization, namely electrostatic interactions between charged objects. T. Silva et al., which also have synthesized the positively charged NPs with the utilization of the branched polyethyleneimine as a stabilizer, claim that possible higher toxic behavior is due to the interaction of such NPs with negatively charged cell wall [31]. In the case of biogenic Ag NPs, probably the relatively low surface charge was not able to prevent interaction with cell walls, thus causing a higher toxic effect.

Another approach for size control is the limitation of the NPs formation volume, which implies the utilization of templates. D. J. Lipomi et al. work can illustrate the approach in the simplest way [61]. Authors have produced the Au and Ag nanostructures by creating of protecting epoxy masks on the substrate and subsequent deposition of metallic thin films. The epoxy masks then were etched from the surface, leaving the highly structured plasmonic nanoarrays. Generally, the formation of NPs layers on the substrates is of high interest for multiple applications in technique and science. Therefore this issue is extensively investigated and shown in different articles. To give an example, in K.-M. Ng et al. work the NALDI plates were prepared by argon ion sputtering of Ag plates with subsequent NPs deposition on the glass substrate [8]. In T. Nakamura et al. the Ag NPs were deposited on the hydrogen-terminated silica by vaporization of Ag disk [105]. However, the presented processes is highly labor-extensive, moreover in L.S. Kibis work it was shown that the presence of the oxygen in synthesis zone may provide to formation of undesirable Ag_2O NPs [39]. Thus, the high interest attracts the possibility to form layered structures by deposition of Ag NPs prepared by chemical synthesis. M. Oćwieja with colleagues in their excellent review work have revealed different methods for the AgNPs layers deposition on the substrates together with the kinetics of the process as well as the stability of formed structures [35]. At the end of the work authors have revealed the possible applications of the obtained materials.

However, a more simple way is to use naturally formed templates for NPs size control. For instance, the polymers can be utilized for NPs synthesis, where inter-chain spaces serve as a reaction cavities for NPs formation [106]. Moreover, I. Moglia et al. have synthesized AgNPs in the human ferritin cavity [107]. T. W. Giessen and P. A. Silver have also utilized a bioengineered protein compartment (bacterial encapsulin system) derived from *T. maritima* for uniform and stable AgNPs synthesis [108]. The highly structured frustules of diatoms can also be utilized as a template for NPs synthesis [109]. Moreover, the viruses capside can be considered as nanoreactor for NPs production [110]. Still, the utilization of microfluidic devices in line with their possibility in NPs size and shape control were reported [18]. Moreover, the microemulsion method, where the micelles serve as a microreactors, has also shown to be efficient for size control in AgNPs synthesis [111].

The second important Ag NPs feature that should be controlled during synthesis is their shape, as it affected the NPs optical properties. The possibility to control Ag NPs shape is highly desired in plasmonic applications (surface-enhanced Raman spectroscopy, light energy harvesting, photocatalysis, etc). As it was mentioned above, the NP formation begins from the nuclei or NP seed formation, then it goes through a metastable fluctuating state where the primary structure can be formed. In the end, the particle obtained its final shape, which depends on multiple factors: temperature, the concentration as well as the type of reagents that have been used, the presence of trace ions [48,52]. To give an example, T. Huang with X.-H. N. Xu has performed the Ag NPs synthesis with various shapes by changes in the amounts of $NaBH_4$ added to the reaction mixture [54]. J. Wu et al. have shown that in DNA-mediated Ag NPs synthesis the nucleotide sequence can affect the final morphology [112]. I. Chakraborty with colleagues has also shown that synthesis with different proteins, i.e. lysozyme, apotransferrin, avidin, β-lactoglobulin, BSA (bovine serum albumin), hemoglobin, ovalbumin, and catalase, led to the formation of AgNPs with different shapes [113]. Moreover, the NPs shape can be changed by post-synthesis transformation under heating or light irradiation [65]. C. -M. Tsai et al. have also shown the AgNPs prisms conversion by KSCN, which was dependent on the reagent concentration [114]. The effect can be explained by NPs partial dissolution with subsequent structure rearrangement, namely the recrystallization process [115].

3. Investigation techniques

The properly planned experiment is a milestone in all investigations. Advances in science and technique have introduced numerous sophisticated devices, which can be utilized for nanomaterials study. The accurately chosen set of techniques can provide comprehensive information about the object under investigation. However, the received results can be affected by drawbacks and artifacts of utilized methods, and in consequence, can lead to false conclusions. Thus, the scientist should consider all possible problems during their investigations. Table 2 presents the scope of the techniques and approaches for AgNPs and their composites study, the more detailed description for them can be found below.

3.1. Optical imaging

Conventional optical microscope due to diffraction barrier is restricted in the ability to distinguish between two points separated by a lateral distance less than half the wavelength of visible light (≈200 nm), which in general makes difficult the direct investigation of nano-objects. However, T. Huang with X.-H. N. Xu in their work showed that the dark-field optical microscope (DFM) can be useful for single-NPs plasmonic microscope investigations [54]. The technique allowed to study Ag NPs LSPR properties in solution depending on their size and shape since NPs under DFM appeared as bright shining and colored spots. However, the dark-field optical microscopy and spectroscopy allow to study only the scattered light, therefore obtained single-NP LSPR represents the scattering of single NP, but not the absorption. Still, dark-field microscopy was useful for single Ag NPs oxidative dissolution monitoring [116]. The changes in the light intensity and color of the NPs over time clearly indicated the electrochemical dissolution process dependence from the applied potential. However, the technique usually requires an intense light source and long exposing time (up to several seconds) in order to collect spectra with satisfactory signal-to-noise ratio, so the fast dynamic observations can be impeded [151].

Fluorescent and confocal microscopy are frequently utilized for investigation of the Ag NPs toxicity and antibacterial properties. To give an example, in T. Liu with colleagues work fluorescence microscope have been utilized for investigation of the surface-attached bacteria and the influence of Ag NPs on bacteria capability to adhere [51]. Additionally, M. Assis et al. have studied the apoptosis and necrosis caused to MB49 and BALB/3 T3 cells by Ag NPs/α-Ag_2WO_4 composite [119]. C. G. Castro-Gonzalez with coauthors has observed the migration and accumulation of Ag NPs in *Stevia rebaudiana B.* leafs by multiphoton fluorescence microscopy, which allowed to identify preferable places of NPs accumulation [120]. The virtue of the fluorescent microscopy is that the cellular components may be labeled through specific molecules, allowing to observe the structures inside a live sample in real-time. However, the conventional fluorescent microscope is limited by low spatial resolution, which is near 200–300 nm in the lateral direction and 500–700 nm in the axial direction [152]. Lately, new possibilities were implemented with such techniques as stimulated emission depletion microscopy and super-resolution fluorescent microscopy performed with single molecule imaging, so the resolution can be enhanced to ≈ 30–40 nm in an axial direction [152]. Still, it should be noted that for NPs tracking in different parts of an organism the fluorescent labeling by different ligands is often utilized. However, in C. Kastner et al. work it was shown that the low stability of such complexes may lead to false results, as enhanced fluorescence may be due to free ligand but not the complex [153]. They showed that tyrosine may provide

Table 2
Instrumental techniques for study of Ag-containing NPs and NCs.

Technique	Study purpose	Information	Artifacts/problems	Ref.
Dark-field microscopy	Ag NPs features	Single-NP scattering LSPR for NPs with different shapes were defined	Low sensitivity, which requires intense light source and long exposing time (up to several seconds)	[54]
	Ag NPs dissolution kinetics	Changes in the NPs color and scattering LSPR intensity, which were dependent from applied potential were revealed		[116]
	The influence of surrounding media on LSPR	The red-shifts in Ag NPs LSPR were observed with increasing in refractive index of surrounding media		[117]
	Ag NPs interaction with green algae	The light scattering enhancement from the algae cells treated with Ag NPs was observed in comparison to control sample		[118]
Fluorescent microscopy	Attached bacteria on the surface	The results have shown the lower quantity of attached bacteria on the surfaces doped with Ag NPs	Low spatial resolution, low affinity of labeling molecules to NPs can lead to misinterpreta-tion	[51]
	The Ag NPs/α- Ag_2WO_4 toxic activity to cells	MB49 and BALB/3 T3 cells stained with acridine orange/ethidium bromide revealed the changes in the color intensity and uniformity, indicating the apoptosis and necrosis		[119]
	NPs migration in leafs	Multiphoton fluorescent microscopy revealed the places of NPs distribution in stem and leafs of *Stevia rebaudiana B.*		[120]
SEM	Ag NPs morphology	SEM images revealed predominantly spherical Ag NPs shape	Non-conductive samples surface charging, sample damage and transformation (i.e. reduction), artifacts from sample preparation (aggregation, size reduction, shape change, sample cracking)	[57,66]
	Surface morphology changes	Images revealed the formation of Ag NPs shell on silica rods and spheres, Ag NPs deposition on polyester and linen fibers		[78,121,122]
	Ag NPs biological activity	SEM revealed damage caused to bacterial cells *B. subtilis, E. coli, S. aureus.* The epidermal fissuring *in C. elegans* was shown		[76,123,124]
	Ultrathin surface morphology	The images of the surface morphology of *R. subcapitata* exposed to Ag NPs were made by more sensitive SE electrons		[118]
	Ag NPs uptake by FIB/SEM	The presence of 3138 ± 722 Ag NPs within one macrophage was revealed, mostly agglomerated, the distribution inside cell organelles cannot be discriminated		[125]
TEM	Ag NPs features	Ag NPs size and size distribution were defined Ag NPs shape and structure were defined The lattice spacing in crystals was measured	Non-conductive samples surface charging, sample damage and transformation (i.e. reduction), aggregation during sample preparation, the technique requires ultra-high vacuum, thin sample < 100 nm	[48,126] [54,127] [16,90]
	Ag NPs growth	LP-TEM revealed the formation of Ag-nanorod through small spherical NPs aggregation		[100]
Cryo-TEM	Ag NPs assemblies	The formation of chain-like Ag NPs aggregates mediated by 2,2′-bipyridine decorated peptoids was defined		[128]
	Ag^+ remediation	The adsorption of Ag^+ and distribution all over the bacterial cell surface with subsequent Ag NPs formation was revealed (made by EDX mapping)		[129]
AFM	Ag NPs size	The measured size for 100 NPs ≈ 20 ± 8 nm, while measured by TEM were 22 ± 6 nm	Electrostatic charging, which can change the movements of cantilever	[130]
	Surface morphology	Spherical Ag NPs formed by glucose were in size 10.3 nm and uniformly distributed on the support surface, while formed with dialdehyde nanofibrillated cellulose were with diameter of 19–37 nm and deposited along the fiber position		[131]
NSOM	Ag NPs	The LSPR for Ag NPs was performed, which revealed the red shift in comparison to UV-Vis due to coupling effect The NPs spherical shape and topography was defined	The interference of emitted by tip light with scattered, coupling effect with conducting tip	[132]
DLS	Ag NPs size	Measured size was 79 ± 0.5 nm in water, 71 ± 0.2 nm in cell culture medium	Aggregation, measurements are highly dependent from the surrounding media (the concentration of NPs, ions, proteins and other molecules, pH, viscosity, etc.)	[125]
	Ag NPs aggregation, ζ-potential	ζ-potential of citrate-capped was −27.7 ± 5 with hydrodynamic radii 27.8 nm (TEM - 10.1 ± 1.8 nm), prepared with green tea extract −36.2 ± 5 with hydrodynamic radii 87.7 nm (TEM - 8.3 ± 3.6 nm). The Ag NPs prepared with green tea extract showed higher aggregation stability in solutions with different content of NaCl, glucose, glutamine, cell culture component and different pH		[49]
UV-Vis	Ag NPs LSPR	Au@Ag nanocuboids longitudial band ≈552 nm, and transverse ≈461 nm	The sample should be clear with no dust and bubbles	[133]
		Spherical $Au_{0.5}Ag_{0.5}$ NPs band ≈ 470 nm		[47]
		Hollow Ag NPs LSPR band ≈ 480 nm		[56]
		Triangular Ag NPs, out-of-plane quadrupole band 339 nm, out-of-plane dipolar band 414 nm, in-plane dipolar resonance 523–585 nm		[50]
	Ag NPs stability	The freshly synthesized NPs LSPR ≈ 400 nm, the NPs exposed to sunlight for 25 days get another bands (470, 600 nm)		[130]

Table 2 (*continued*)

Technique	Study purpose	Information	Artifacts/problems	Ref.
Fluorescence	Pb^{2+} quantification	1.45 ± 0.3 nm Ag NPs capped with polymethacrylic acid revealed linear fluorescent enchantment depending on Pb^{2+} concentration in range from 0.0 to 1.0 μM	Inner Filter Effect (IFE I and II), absorbance by impurities and quencher in fluorescent band, the presence of fluorescent impurities	[134]
	Dopamine quantification	Fluorescent AgNPs ≈ 10 nm capped with 4-mercapto phenylboronic acid and 40-aminobenzo-18-crown-6 revealed linear quenching depending on dopamine content (0.001–0.1 mM) due to NPs aggregation		[135]
FTIR	Ag NPs formation and functionaliza-tion	1214.5 cm^{-1}, 3072.4 cm^{-1} bands appearance, increase in 1455.7 cm^{-1}, shift 1635.7 cm^{-1} → 1627 cm^{-1} after ampicillin binding	The specific bands hardly can by discriminated due to overlapping and significant shifts depending on molecular structure	[136]
		Presence of 1694 cm^{-1} stretching band of C═O group and 734 cm^{-1} of weak S–S vibration revealed alpha-lipoic acid binding		[137]
		The AgNPs formation and binding to lactoferrin affected the infrared spectra in range 1650–1400 cm^{-1}		[16]
Raman	Ag NPs functionaliza-tion study	The vibration between Ag(0) surface and pyridine nitrogen was revealed by appearance of 241 cm^{-1} on spectra	Fluorescence of sample and impurities as well as adsorption by matrix can burdened the study, heating may damage the sample and can cause blackbody thermal emission	[128]
	SERS study	All SERS spectra of Ag NPs with lyzozyme, BSA, cytochrome-C and hemoglobin has band ≈ 240 cm^{-1} attributed to Ag–N and Ag–S, band ≈ 1630 cm^{-1}, which replaces the amide I band at 1655 cm^{-1}, the shifts near 1375 cm^{-1} in cytochrome and hemoglobine can be assigned to hem bands		[89]
NMR	Mechanism of Ag NPs formation	The hydride intermediates ($[Ag_7(H)\{Se_2P(O^iPr)_2\}_6]$ and $[Ag_7(H)\{S_2P(OEt)_2\}_6]$) formation was revealed by appearance of doublets 1125. ppm (d, J_{AgH} = 39.7 Hz) and 1116.7 ppm (d, J_{AgH} = 41.1 Hz) at 298 K as well as octet at 3.50 ppm ($^1J_{H-Ag}$ = 39.4 Hz) at 293 K and broad peak 5.65 ppm, ($^1J_{H-Ag}$ = 39.6 Hz) at 223 K	Considerably low sensitivity, requires the core digestion of big NPs, $^{107/109}$Ag has low gyromagnetic ratio and big T1 value, which requires special devices and long term analysis	[138]
	Ag NPs effect on cell glutathione content	The glutathione signals in the range 2.51–2.55 ppm have disappeared after Ag NPs treatment, revealing its complete depletion		[139]
	Role of stabilizer and reducing agent in Ag NPs formation	Significant changes in chemical shifts of sodium dodecyl sulfate protons 4.086 ppm → 4.037 ppm, 1.360 ppm → 1.320 ppm, 0.952 ppm → 0.900 ppm after Ag NPs formation in the mixture with trisodium citrate, the decreased intensities of signals from trisodium citrate protons		[140]
XPS	Quantitative binding affinity of taurine	≈2% of Ag as in unbound (elemental) state, Ag–O, Ag–N and Ag–S bounds were found to be ~71%, 11% and 16%, respectively, which revealed the sulphonate group binding to Ag	Sample charging, the sample transformation (i.e. reduction), sample can be examined only on 2 nm depth, requires ultra-high vacuum	[141]
UPS	Photoelectron emission yield	Doped with ≈ 4.5 nm Ag NPs hydrogen-terminated Si (111) show the photoelectron yield with p-polarization: $2.8•10^6$, while that without Ag NPs has $1.4•10^4$		[105]
AES	The morphology of Ag growing on Fe_3O_4	The data showed that Ag gas atoms adsorbed on Fe_3O_4 according to hemispherical cap model, which revealed the formation of separated Ag NPs but not the Ag layer	Sample charging, small examination depth, requires ultra-high vacuum, the sample transformation and damage	[142]
	Ag NPs formation	The technique revealed that small (5 nm) particles comprised from Ag have formed on bismuth silicate		[143]
EELS	LSPR modes for Ag NPs embedded in SiO_2	LSPR evolves depending on electron dose from $2.1•10^6 e^-Å^{-2}$ to $18.7•10^6 e^-Å^{-2}$, under lowest dose no LSPR shift was observed, with increasing of electron dose blue-shifts were observed from 2.8 to 3.2 eV (for NP ≈ 7 nm)	Sample charging, requires ultra-high vacuum, the sample transformation and damage	[144]
	Elements distribution over the NPs	In the middle of the NPs the electron energy losses corresponding to Ag atoms was observed, on the edges the presence of C, N and Ca was shown		[89]
XRD	in situ annealing behavior of Ag_2S NPs	For NPs heated in air the 2θ signals at ≈29°, 31.5°, 38°, 41°, corresponding to monoclinic acanthine α-Ag_2S disappeared, and the 2θ signals 39° and 43° of pure silver appeared. For NPs heated in argon, the XRD pattern changed to more complex, which may be attributed to monoclinic non-stochiometric acanthine α-$Ag_{1.95–1.98}S$	Preferred orientation of non-spherical NPs, low signal intensity for NPs below 10 nm, 2% sensitivity limit for composites	[145]
SAED	Ag NPs crystalline phase examination	Measured d-spacing (nm) were 0.233, 0.203, 0.141, 0.121 which are in good correspondence with Ag(0) hkl (nm) 0.236, 0.204, 0.145, 0.123, and AgO hkl (nm) 0.237 and 0.143	Sample charging and damage, requires ultra-high vacuum	[79]
ICP-MS	Changes in Ag, Fe, N and Mg content in *Stevia rebaudiana B.* treated with Ag NPs	With changes of Ag NPs concentration in culture media from 0 to 200 mg/L the changes in N (38,067.3 ± 45.3 to 55,339.7 ± 31.1 μg/g), Mg (882.4 ± 9.5 to 1292.6 ± 11.2 μg/g), Fe (289.3 ± 4.5 to 143.3 ± 0.7 μg/g) and Ag (0.13 ± 0.0 to 188.2 ± 1.6 μg/g) content (calculated on dried weigh) were observed	Atomic (Cd) and polyatomic interferences, samples usually requires mineralization	[120]

(*continued on next page*)

Table 2 (*continued*)

Technique	Study purpose	Information	Artifacts/problems	Ref.
SP-ICP-MS	Ag NPs callular uptake by Neuro-2a cells	Cells treated with 2 μg/mL of Ag NPs with sizes 50 and 75 nm revealed the uptake of 1662 and 605 number/cell respectively, while treated with 10 μg/mL of Ag NPs revealed the uptake 1989 and 1740 number/cell	Aggregation, lower size limit (20 nm), impossible to distinguish different Ag form	[146]
TOF-SIMS	Ag NPs interactions and transformations in municipal wastewater	In positive mode silver-amine ions were observed $AgC_2H_6NO^+$, $AgC_3H_4NO^+$, $AgC_4NO_2H_3^+$ at 167, 177, 203.9 mass and Ag bonded with sulfur $AgSC_2H_3N^+$, $AgSC_3H_6N^+$ at 179.90 and 194.93, mass. In negative mode $AgCOOHCNH_2^-$, $C_3H_2NO_2Ag^-$, $C_5N_3O_2Ag^-$ at 179.91, 192, 241 and $AgC_2H_3SN^-$, $C_3H_2SNAg^-$, $C_3H_7SNO_2Ag^-$ at 179.89, 190.89, and 227.92 mass were observed	Spatial resolution is limited by diameter of primary ion beam, which is often bigger than NPs size	[147]
MALDI-TOF MS	NALDI analysis of benzpyridi-nium	With changes in laser fluence from 15 to 80 mJ/cm^2 the normalized total ion intensities for Ag NPs were from 5 to 35 •10^4 count/mm^2, while for Au NPs from 0 to 21•10^4 count/mm^2	NPs aggregation, analyte fragmentation	[8]
AF4	Ag NPs determination in environmental samples	1. the recoveries of PVP-capped NPs with sizes 30, 60 and 90 nm were shown to be 90.2, 78.6, 69.4 and 55.6% for tap water, river water, effluent and influent of wastewater treatment plant respectively; 2. the better resolution was shown to be in order effluent > river water > influent > tap water (based on UV-Vis detector); 3. the better consistency between measured and original sizes was observed in tap water and effluent (based on DLS detector); 4. ICP-MS detector showed the good separation only in tap water	Membrane fouling by irreversibly bonded NPs, NPs aggregation, non-selective upon size detectors (UV-Vis/MALS)	[148]
CE	Ag NPs separation	1. migration time in single standard analysis for 40 nm capped with branched polyethylenimine, PVP, citrate and polyethylene glycol were 958 ± 21 s, 1048 ± 15 s, 1275 ± 115 s and 958 ± 32 s respectively; 2. four component mixture was not possible to separate; 3. citrate capped was possible separate from PVP and polyethyleneglicol capped in two-component mixture	Aggregation, NPs sticking to capillary walls, low selectivity	[149]
DSC	TiO_2-Ag NPs doped gelatin films stability	Glass transition values by DSC were 59.52, 51.77, 52.19, 51.8 and 52.61 °C for films with 0, 1, 2, 3 and 4% of TiO2-Ag respectively	Heating rate is crucial	[150]

unreliable results, since it desorbs from the Ag NPs surface very fast, while fluorescent-marked BSA showed satisfactory Ag NPs-ligand stability.

3.2. Electron microscopy

The very first techniques that should be utilized for NPs characterization are SEM (Scanning Electron Microscope) and TEM (Transmission Electron Microscope) since they give invaluable information about structure and surface morphology of the materials. SEM is an imaging technique which in general deals with backscattered electrons (BSE) [154] and allows to investigate surface morphology of NPs [57,66], further the interactions of NPs with different systems can be studied. The Ag NPs deposition on silica spheres and rods [121], on polyester fibers [122] or on linen [78] and the investigation of the damage caused by Ag NPs to microorganisms [76,123] and nematodes [124] was observed by SEM micrographs. However, some other signals such as secondary electrons (SE) can also be obtained within this technique.

SE show higher sensitivity to surface morphology therefore can provide images with better quality [118]. In SEM incident beam electrons with energy in range 1 keV–30 keV are utilized, which can provide a complementary information, as depending on the electron energy sample can be scanned on the different depth (up to 100 nm for SE and 500 nm for BSE) [118,154,155]. Further extension of the technique can be made by combination with a focused ion beam (FIB), typically Ga^+, to make sample cross-sections and imaging by SEM [125]. The non-conducting sample charging is one of the most significant SEM problems that influence the image quality and therefore its interpretation. The negative charged surface can produce undesirable SE and influence on landing energy of the incident electrons, which lead to field enhancement between the surface and the electron detector. Instead, positive surface charging transforms the sample to an electron trap [156]. An environmental scanning electron microscope (ESEM) is one of the techniques that can deal with the charging effect due to the presence of water vapor in the microscope chamber. What more, wet mode prevents samples from dehydration, which can introduce additional artifacts such as size reduction, shape change, and cracking, so it is extremely useful for biological systems examination [155,157]. For instance, ESEM was utilized to investigate the changes that occurred in earthworms after Ag NPs exposure [158]. Finally, to SEM drawbacks the low signal-to-noise ratio and spatial resolution, in comparison to TEM, can also be included [154].

TEM is one of the most common techniques for NPs structural features study. It provides information about size, shape, arrangement, and NPs structure. TEM exist in several different forms to which CTEM (Conventional TEM), HRTEM (High-resolution TEM), and STEM (Scanning TEM) can be include. The image in CTEM is formed with an appropriate detecting system by transmitted through sample electrons. Adhikari et al. use TEM images to determine size and size distribution of synthesized Ag NPs [126]. However, they noted that in some cases NPs sizes could not be reliably determined due to disproportionate aggregation during sample preparation for analysis. Polte J. with colleagues were also unable to distinguish the Ag NPs sizes due to large aggregation caused by simple drying [48]. Generally, the NPs aggregation is one of the main problems in Electron microscopy (EM) investigations. Donald A. et al. have observed the transformation of AgNPs to a core@shell and hollow Ag@Ag_2SNPs, TEM images clearly indicate the changes in structure [127]. Still, TEM-images have 2D-character, so 3D-images made by SEM can provide more details regarding the morphology of the NPs [58,123]. HRTEM technique is based on observation of interference of the electron beam by the sample. This allows to obtain high phase-contrast images, that show details finer than 0,2 nm. In particularly HRTEM provides direct images of the atomic

structure of the samples [159]. By HRTEM it was possible to distinguish the protein coating of different protein-conjugated Ag nanocomposites [89,90] and the lattice spacing between neighboring fringes as it was made for trypsin-Ag conjugates [90]. Still, TEM has its drawbacks to which labor-intensive sample preparation can be include, as the sample should be very thin, so it can allow passing electrons through the sample (not more than 100 nm if possible). In some cases for HRTEM samples should be as thin as 10 nm (generally 50 nm). Additionally, TEM handles with high-voltage electrons (80–300 keV) that may damage the sample [159].

In STEM instruments the principles of the SEM and TEM are combined, where the sample is scanned across by sub-nanometer diameter probe, and the image is formed through transmitted electrons. Microscopy and spectroscopy techniques are shown to be complementary techniques, and the utilization of both can help to avoid inadequate characterization of material [154]. STEM instrument in comparison to CTEM can be employed to spectroscopic analysis, as within the technique some additional valuable signals can be measured, such as SE, BSE, characteristic X-rays, and electron energy loss, so it provides information with much better resolution about sample structure and is also suitable for chemical composition determination [159]. Energy dispersive X-ray spectroscopy (EDX or EDS) is a technique, usually coupled with electron microscopy, where the characteristic X-ray radiation from excited atoms is measured. Within the technique, it is possible to estimate both the compositional information of the whole sample as well as the location of individual elements across the surface. In Pomastowski et al. work by EDX detector the prevalence of Ag ions in synthesized NPs was estimated (Fig. 3), but also the presence of C, O, S and P confirmed the protein participation in NPs stabilization [16].

Blommaerts et al. conducted an EDX mapping of the Au/Ag NPs. The analysis shows the core-shell structure of the particle, with the prevalence of Ag on the surface [47]. EELS (Electron Energy Loss Spectroscopy) combined with STEM was also useful for the chemical composition determination of lysozyme-Ag nanocomplex [89]. Within STEM the Selected Area Electron Diffraction (SAED) can also be conducted. SAED is widely utilized to distinguish crystal structure of AgNPs and it was shown that obtained data is complementary to that one from XRD analysis [74]. Another extension of the technique is Cryo-TEM approach. This technique together with liquid cell sample preparation TEM, which also called liquid-phase TEM (LP-TEM), allow to investigate nanoscale materials formation and nano-objects behavior in solutions. Both techniques are very labor-extensive but partially can fill gaps left by other methods [160]. By LP-TEM in situ particle growth in detail can be observed, as it was made for Ag nanorods [100]. However, the dynamic nature of LP-TEM processes and the presence of liquid decreases the resolution, what more important the incident electron beam can influence on synthesis process [160]. During Cryo-TEM analysis thin (up to 100 nm) frozen films of sample solutions are examined. As all processes in the samples are arrested it became possible to perform X-ray spectroscopic and EELS analysis, what more the 3D structure can be outlined. Ahmad et al. studied silver remediation from aqueous solutions by microorganisms. By Cryo-TEM coupled with EDX mapping the extra- and intracellular Ag NPs formation through silver ion adsorption and conversion was observed [129]. Moreover, Cryo-TEM technique confirmed the presence of chain-like Ag NPs assemblies, mediated by 2,2′-bypiridine decorated peptoids, in solution, as such structures could also be introduced through NPs aggregation induced by dried sample TEM preparation [128]. Still, the object under investigation is highly sensitive to electron beam exposure, which can damage both the sample and vitrified solvent, so the interpretation of the images became more complicated [160].

3.3. Scanning probe microscopy

Scanning probe microscopy (SPM) exploits a very sharp probe tip for local characterization of materials surface and can provide a structural map of the surface in the atomic-resolution scale. Among other SPMs, an atomic force microscope (AFM) is one of the most employed techniques for surface topography determination and is also common for nanostructures investigation. In AFM the moving probe across the surface changes its vertical position depending on roughness and electric properties of the sample, which in most cases is detected by the position-sensitive photodetector. The AFM has been utilized for investigation of Ag NPs deposition on dialdehyde nanofibrillated cellulose. It was possible to determine the Ag NPs sizes distribution, which was in the range between 19.0 and 37.0 nm with an average size 28.14 nm [131]. I. Romer et al. also investigate the Ag NPs by various techniques, the average size of citrate capped AgNPs was measured as 20 ± 8 nm by AFM, while TEM showed the NPs size as 22 ± 6 nm [130]. It should be noted that AFM measurements can be burdened with unwanted artifacts and signals including the motion of the macroscopic body of cantilever due to electrostatic effects between the cantilever body and the sample, which can lead to misinterpretation of obtained results [161].

Near-field scanning optical microscopy (NSOM) is another scanning technique, that can be assumed as an improved version of the conventional optical microscope. In NSOM the properties of evanescent waves are utilized, which implies that scanning probe during the analysis is located not further away than aperture diameter. Thus, it is possible to overcome the resolution limit and obtain information about the optical properties of the sample. Within the technique both the image and the relevant spectra can be obtained [162]. M. Beleites et al. have performed the NSOM topographical investigation of the Ag NPs. They also performed transmission mode measurements, which showed that Ag NP was surrounded with a halo with the increased transmission on the distance up to 200 nm. Such a phenomenon can be explained by interference of the light emitted by scanning tip and scattered light from NP. Finally, it was shown that the LSPR for Ag NPs measured by transmission NSOM exhibit the redshift in comparison to UV-Vis analysis, which may be explained through the coupling effect with the conductive probe [132].

3.4. Dynamic light scattering

Dynamic light scattering (DLS) is a technique with a short time required for measurements and relatively low cost of the apparatus, therefore it frequently exploits for NPs sizing. For instance, DLS is often utilized as the detector during the NPs separation by A4F [148]. However, in general the particles size values derived by DLS are overestimated. In R. Ma work the measured by TEM size for nanostructured Ag NPs was 76.6 ± 20.7 nm, calculated from XRD diameter was 30.4 nm, while hydrodynamic radius measured in 1 mM $NaHCO_3$ was 89.1 ± 1.5. It should be mentioned, that in TEM only the size of the NPs metallic core can be estimated. Instead, in DLS the hydrodynamic radius, which is defined as hypothetical hard sphere that diffuses with the same speed as the particle assayed in DLS [30], of the particles is measured. By XRD the size of crystallite can be calculated, which in case of twinned or poly-crystallite NPs can be several times smaller than whole particle core. In practice, NPs in colloidal dispersion are the combination of the metal core with solvated corona, which has a dynamic character and fluctuates depending on the surrounding environment. Such a phenomenon was shown in Guehrs et al. work where DLS analysis of commercially produced 75 nm size Ag NPs have been performed, the measured values were 79 ± 0.5 nm and 71 ± 0.2 nm for particles dispersed in water and in cell culture media respectively, while TEM measurements revealed NPs sizes as 74 ± 8 nm [125]. Song et al. have also characterized Ag NPs synthesized by silver nitrate reduction with curcumin, and the measured hydrodynamic radius ranged from 30 nm to 90 nm [76]. TEM analysis has revealed that as mentioned Ag NPs were of spherical shape with a relatively uniform diameter of 35 ± 5 nm. Generally, the high concentration of different molecules in the culture media, especially proteins, through surface adsorption can drastically change the hydrodynamic radius of dispersed

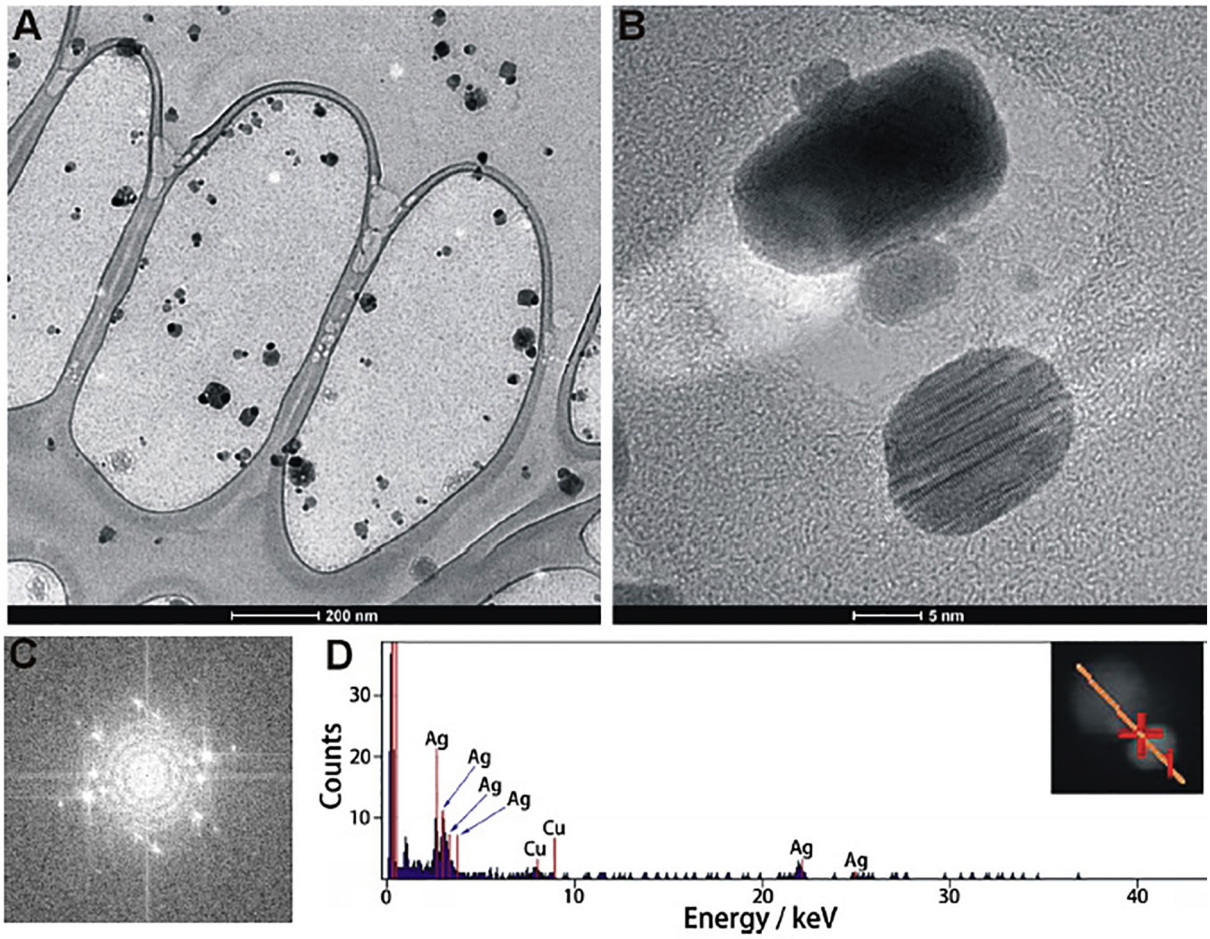

Fig. 3. TEM image of Ag-Lactoferrin nanocomplexes. Bar: (A) 200 nm, (B) 5 nm, (C) Fast Fourier Transformation, and (D) EDX spectra. Reproduced with permission from ref. [16]. Copyright 2016 American Chemical Society.

NPs. Moreover, adsorption is a complex process, which needs time to stabilize, so obtained results can change over time. However, the measurements are also not recommended to perform in deionized water, as it always leads to size overestimation up to 10 nm, which is due to the long-distance interactions between particles in the absence of ions [30]. Additionally, the hydrodynamic radius in DLS is derived from Stokes-Einstein relationship, in which the calculations for spherical shape particles are considered, so for anisotropic particles, it does not correspond to any of their geometrical dimension and can be accounted to the DLS drawbacks. Moreover, in DLS the cumulative analysis for average size estimation is utilized, which is not suitable for polydisperse systems [35]. However, it should also be mentioned that for NPs the anisotropic inelastic Mie scattering is observed that has an angle-dependent character [30]. Moreover, for smaller NPs the absorption cross-section is dominant over scattering cross-section [5,163] thus smaller NPs reveal the lower intensity of scattered light. In some older versions of the DLS instruments the backscattered light was gathered at the angle of 90°, presently detectors are placed at 173°, which allows to avoid the excess of scattered light and unmask scattered light of low intensity, thus contributing in the higher resolution of measurements [30].

The dependence of measured size from solvent characteristics (refractive index, viscosity) was also revealed, which should be considered during the investigations [30]. Belteky et al. have investigated the influence of different electrolytes and pH on Ag NPs hydrodynamic radius and aggregation behavior, which is considered to be the most frequent problem in DLS analysis [49]. Besides environmental conditions, the aggregation may also appear due to NPs high concentration. Moreover, to the high concentration effects the multiscattering occurrence can be attributed, which results in artificially smaller measured NPs size [30]. Changes in pH and electrolytes concentration in solution also influence charge of NPs surface, which commonly expressed in ζ-potential (or electrokinetic potential) changes. ζ-potential cannot be measured directly, therefore it can be expressed through electrophoretic mobility deduced from Henry's equation [35]:

$$\zeta = \eta\mu_e/\varepsilon f(\kappa d_p) \quad (1)$$

where η – solutions viscosity; μ_e – electrophoretic mobility; ε – dielectric constant of the dispersant, $f(\kappa d_p)$ – Henry's function of dimensionless parameter.

In case when the electric double layer thickness is much smaller than the radius of the particle in particularly for particles much bigger than 100 nm, the Henry's equation with some approximation can be modified to Smoluchowski equation [30,164]:

$$\zeta = \eta\mu_e/\varepsilon_r\varepsilon_0 \quad (2)$$

where η – solutions viscosity; μ_e – electrophoretic mobility; ε_0 – electric permeability in vacuum, ε_r– dielectric constant of the solution.

Instead, for NPs dispersed in low salt concentration, when the electric double layer thickness is much bigger than particle radius and Henry's function of dimensionless parameter is taken as 1 the Hückle equation can be utilized:

$$\zeta = 3\eta\mu_e/2\varepsilon_r\varepsilon_0 \quad (3)$$

where η – solutions viscosity; μ_e – electrophoretic mobility; ε_0 – electric permeability in vacuum, ε_r– dielectric constant of the solution.

However, the Hückle equation is shown to be not applicable for aqueous solutions [30]. Thus, most often the Smoluchowski model is utilized. However, some scientists claim that Smoluchowski equation should not be utilized for NPs ζ-potential estimation as the measured values by this model in general are smaller than real one, which can be obtained only from Henry's model [35].

The electrokinetic potential is often measured within DLS analysis, as it was made in the above-mentioned work of P. Belteky with coauthors. They have investigated the Ag NPs synthesized with green tea extract in comparison to Ag NPs stabilized with citrate. In consequence, NPs stabilized with green tea extract had about 8,5 mV lower ζ-potential than citrate capped (−27,8 mV), which caused better stability in solutions with different content of NaCl, glucose, glutamine, cell culture component and different pH [49]. Generally, the surface charge of the NPs determines their electrokinetic stability in the suspension. In turn, the magnitude and the sign of the surface charge are determined by the adsorbed molecules on the surface of NPs, in particular the capping agent. For instance, the Ag NPs stabilized with poly (diallyldimethylammonium) have positive surface charge, while uncoated Ag NPs which probably contain adsorbed nitrate ions on the surface were negatively charged [101]. According to Derjaguin—Landau—Verway—Overbeek (DLVO) theory, the stability of the NPs suspensions against aggregation is a result of interplay of two opposite forces, i.e. the attractive van der Waals forces and repulsive Coulombic forces of charged particles [102]. It is suggested that absolute ζ-potential values greater than ±25 mV are required for NPs and biocoloids systems stability against rapid aggregation, where the particles would stay in dispersion for a longer period [16]. In work performed in our group, the measured ζ-potential of AgNPs was 0 ± 0.5 mV in pH range 2–4, which in consequence led to the AgNPs aggregation and therefore the measured by DLS sizes varied from 1500 nm to 200 nm [93]. Instead, ζ-potential values in pH range 4.5–10 decrease up to – 25 eV, and the NPs size was estimated as 100 ± 1.5 nm [93]. However, the transfer of NPs from a synthesis solution to the environment of the investigated systems usually leads to the exchange of the surface adsorbed molecules with dissolved one, which in consequence can change the charge and magnitude of the NPs surface and therefore influence their stability and interaction behavior [27,34,147].

3.5. UV-Vis and fluorescence spectroscopy

UV-Vis spectroscopy is a fast, simple and sensitive technique, thus it is widely utilized for Ag NPs initial characterization. UV-Vis spectroscopy can provide both quantitative and qualitative information about investigated material [35]. For example, UV-Vis detectors are typical in separation techniques, such as CE (capillary electrophoresis) or FFF, for Ag NPs quantification and therefore the information about NPs absorption in the UV-Vis range is so valuable [148,165]. However, it should be mentioned that for organic compounds the UV-Vis spectrum is a consequence of the presence of the chromophores, while UV-Vis enormous light absorption extinction of metal NPs is connected to LSPR appearance. LSPR is a complex process and described as excitation and coherent oscillation of electrons under the electromagnetic field of incident light [166]. The main feature of the LSPR in NPs is that the oscillation of the excited electrons is limited by the volume of the NPs [166]. Thus, it plays a dominant role in the excited electrons oscillation frequencies and therefore on the wavelength of the resonant light band. Still, the complexity of LSPR phenomenon implies the influence not only the NPs volume but also their composition [133] and structure [56], shape [50], surrounding media (especially that one that is in the closest vicinity to NPs, in particularly the capping agent/adsorbed molecules on the NPs surface) [166], and interactions with other NPs (including aggregation) [121,167], which alone with NPs size distributions have an influence on the width of the absorbance band, the shifts of the resonant wavelength as well as the appearance of the additional absorption band [46,166]. For spherical silver NPs the LSPR absorption light band normally is near 400 nm, while for triangular Ag nanoplates the maximum absorption in a range 500 nm - 1000 nm was observed [50,168] and aggregation of the NPs, as well as rod-like shape, leads to the appearance of two peaks: one near 400 nm and additional in the range from 500 nm to 1000 nm [46,169]. The influence of the NPs size distribution on the broadening of LSPR band was shown in M. A. Garcia work [166]. It was calculated that AgNPs with a size of 10 nm and deviation of ±8.5 nm has three time higher full-width-at half maximum of LSPR band than for NPs with the same size but dispersion of ±4.5 nm. T. Huang and X.-H. N. Xu have also shown significant LSPR band broadening in AgNPs of different shapes and size distributions [54]. The majority of the reports note the appearance of the intense absorption band in UV-Vis range as evidence of NPs production and by the changes in the absorbance intensity explain the completeness of the process [93]. To give an example, J Polte et al. have observed the in-situ intensity changes in UV-Vis spectra during $AgClO_4$ reduction by $NaBH_4$. However, during the process they noted that the formation of hydrogen bubbles on the cuvette walls disturbs the kinetic study [48]. Some scientists try to exploit LSPR for synthesizing process development and optimization [68,168]. UV-Vis spectra are also suitable for NPs stability investigation [130]. However, experimental data along with mathematical calculations indicate that seemingly negligible changes (including those related to synthesis) in nanostructures may cause significant changes to the optical features of the Ag NPs [144]. Thus, it should be paid more attention to NPs LSPR investigation, as it may have an influence on results during exploitation in different optical applications such as biosensing and biolabeling, photocathalysis, different photoelectric devices, etc. The knowledge about potential applications associated with plasmonics may be extracted only from a complete understanding of LSPR appearance phenomena, which will contribute in the design of highly specific nanostructures with desired optical properties.

The fluorescence spectra of Ag NPs-containing systems usually are measured in line to determine the possibility for different substances quantification in biological or environmental applications. It was reported that extremely small Ag NPs, which sometimes also called Ag nanoclusters or Ag quantum dots (Ag QDs), exhibit fluorescence emission. Changes in the closest vicinity to Ag QDs surface can either enhance the effect, as it was investigated for Pb^{2+} ion interaction in water [134], or decrease in case of dopamine binding [135]. Additionally, the aggregation of the Ag QDs also lead to the fluorescence disappearance, which was utilized for anti-digoxigenin antibody immunoassay analysis [15]. A.V. Pansare with coauthors exploited Ag QDs synthesized with *N. cadamba* extract to determine the BSA fluorescence quenching [170]. However, it should be strongly considered the mechanism of fluorescence intensity changes during the process, especially for such complex mixtures as in the last example, since some flavonoids, which usually are abundant in the extracts, can exhibit fluorescence properties [171]. In general fluorescence measurements can be affected by Inner Filter Effects (IFE), which include IFE I - the absorbance of exiting energy by impurities and IFE II - the reabsorbance of the emitted light by quencher or other impurities. Finally, the presence of unknown fluorescence substances in the mixture can also interfere the analysis [29].

3.6. Infrared and Raman spectroscopy

At the early stage of infrared investigations, it was noticed that certain functional groups are associated with specific characteristic absorption, and after years of painstaking work of many scientists, it became a technique for the determination of characteristic groups in the sample [172]. The majority of publications that are focused on Ag NPs usually

exploit Fourier Transform Infrared Spectroscopy (FTIR) in MIR (Mid-Infrared extends from 4000 cm^{-1} to 400 cm^{-1}) range as a reliable technique for Ag NPs characterization. FTIR is frequently used for surface functional group investigations [84], surface functionalization control [136,137] or for investigation of the possible groups which take part in Ag NPs formation and/or stabilization by different extracts [45], proteins [16,90], polysaccharides [87], etc. On the flip side, the significant shifts in the characteristic absorption band due to perturbation emerging from neighboring groups or the spatial geometry of the molecule together with the fact that in general more than one functional group absorb in the same region [172], make possible to determinate the individual functional groups only in case when FTIR is coupled with other techniques, which can be NMR (Nuclear magnetic resonance) [173]. To give an example, while it is relatively easy for simple compounds as alpha-lipoic acid to discriminate which groups are involved in Ag NPs binding [137] it becomes more complicated when we try to investigate how metal interacts with proteins or polysaccharide-based nanocomposite [16,87], and almost impossible for extracts or propolis, which are multicomponent mixtures [66,69,72]. NIR-range (Near-Infrared extends from 12,500 cm^{-1} to 4000 cm^{-1}) spectra can serve as an extension of the technique since it can provide valuable information about different hydrogen-containing groups (the majority of the absorption bands in the NIR region are due to CH, NH, and OH) [172]. Furthermore, some Ag NPs exhibit LSPR in NIR absorption region, which also should not be skipped in the Ag NPs investigations [168,169].

In Raman spectroscopy, inelastic scattering of the electromagnetic waves in the infrared range is measured and information about vibrational and rotational modes of the molecules can be gathered. The virtue of the technique is that the groups, which may be weak or inactive under FTIR analysis can exhibit strong bands in Raman spectra, so it provides complementary information. Raman spectra were utilized to investigate the binding of the Ag NPs to 2,2′-piridine decorated peptoids, the presence of the band at 241 cm^{-1} clearly indicate the existence of Ag(0)-(pyridine)N interaction [128]. Pomastowski et al. have also observed the changes that occurred in the Raman spectra of lactoferrin after Ag-ions uptake [16]. Moreover, in the last decades metal nanoparticles are widely studied for SERS. S. Reymond-Laruinaz et al. have observed the enhancement of the signals in Ag- conjugates with lysozyme, BSA, cytochrome-C, and hemoglobin in comparison to intact proteins [89]. However, during spectra interpretation, it should be considered the heating effect of the sample, which may lead to sample decomposition or baseline increasing due to blackbody thermal emission. Additionally, the fluorescence of the sample or the impurities may lead to the appearance of additional bands. Finally, the matrix effect should be considered as it can absorb the scattered waves and decrease the signals [174].

3.7. Nuclear magnetic resonance spectroscopy

NMR is a powerful tool for identification and quantification of molecular species, as it can provide information about the molecular structure of the compounds and the resonance strength is directly proportional to the number of the particular nuclei. The NMR spectra can be recorded for atoms that have a non-zero spin number (have an intrinsic magnetic moment) but the most frequently NMR spectra for ^{1}H, ^{13}C, ^{15}N, and ^{31}P nuclei are recorded. ^{1}H NMR is widely utilized for surface functional group determination and quantification [175]. Regarding Ag NPs it was shown that ^{1}H NMR could be useful for determination how organic compounds are involved in the synthesis process. V. Shah with coauthors suggested the decrease of some signals in ^{1}H NMR spectra was due to tri-sodium citrate oxidation [140]. What more, ^{1}H NMR can be utilized for quantitative determination of ligands participation in NPs stabilization [176]. However, quantitative information about adsorbed ligands often requires the NPs core digestion, as they cause significant signal broadening, especially in case of the NPs with larger size [177]. In Pawłowski et al. work the changes in silver caprylate spectra during Ag NPs synthesis by thermal decomposition can be observed [178]. The authors also noted the broadening of all signals in spectra of silver caprylate in comparison to caprylic acid spectra, which they attributed to presence of small amounts of Ag(0) atoms, exhibiting paramagnetic properties and therefore influence on nuclear spin relaxation. Such effect was utilized by L.E. Marbella and colleagues to investigate magnetic susceptibility of AuCo NPs by Evans' method [179]. C^{13} NMR spectra were also useful in the investigation of Ag-doped Pt NPs formation. The L. C Jones with coauthors noted that PVP-Pt NPs C^{13}-NMR spectrum is very similar to only-PVP spectrum, but after adding of $AgNO_3$ the new shifts at 20 ppm, 46 ppm, and 63 ppm appeared and spectrum became more similar to that one from Ag-PVP. The differences may indicate the differences in Pt and Ag interactions with PVP and also it provided an insight into possible intermediates that play role in directing the Pt_xAg_yNP shape [180]. What is interesting, the analysis was performed with the utilization of cross polarization, which is extremely useful for solid-phase NMR, in particular Cross Polarization Magic Angle Spinning NMR (CP-MAS NMR). ^{31}P NMR spectra were also useful for investigation of Ag NPs formation through $[Ag_7(H)\{E_2P(OR)_2\}_6]$ (E = Se, S) conversation. The spectra indicated the creation of $[Ag_8(H)L_6]^+$ as an intermediate prior to the formation of Ag_7H clusters. Moreover, the presence of a hydride within the heptanuclear silver was determined by ^{1}H and ^{109}Ag NMR-analysis [138]. However, the $^{107/109}Ag$ nuclei suffer from low gyromagnetic ratio, which decreases the sensitivity and generally requires specialized measurement devices. Moreover, the T_1 value of Ag nuclei is on the order of hours, so the technique is a highly time-consuming [177]. The conventional NMR in general posses considerably low sensitivity, especially in comparison to other spectroscopic techniques, e.g. fluorescence measurements can be performed for single molecule [181]. Still, the signal-to-noise ratio can be enhanced by magnetic field enhancement. Additionally, Fourier-transform pulsed NMR allows to more than 100-fold increase in sensitivity by utilization of short radiofrequency pulses, which can cover a wide range of excitation frequencies at the same time. Some other approaches for NMR sensitivity enhancement can be found in J. H. Lee et al. work [181]. However, at the end of the last century, the HR-MAS NMR (High-Resolution Magic-Angle Spinning NMR) technique has been introduced and showed high sensitivity and selectivity in the investigation of complex mixtures [182]. Such an approach can be used for the identification and quantification of metabolites from biofluids affected with Ag NPs. For instance, M. J. Piao et al. have measured by HR-MAS NMR the changes in glutathione quantities in human liver cells treated with Ag NPs [139].

3.8. Electron spectroscopy

Photoelectron or photoemission spectroscopy is a technique, where the discrete energy levels (electron orbitals) are studied by measurements of ejected electrons energies from material illuminated with light of a certain length. Depending on the wavelength of utilized light the technique is divided into X-ray Photoelectron Spectroscopy (XPS) and Ultraviolet Photoelectron Spectroscopy (UPS). In XPS the most common Mg Kα and Al Kα X-ray sources with energies 1253.6 eV and 1486.6 eV are utilized, which allows to investigate the core states of the atoms [183]. Taurin interaction with Ag NPs has been studied by XPS as a common technique for chemical composition determination. The technique allowed to estimate not only the percentage composition of Ag, O, N, and S elements on the surface, but also the percentage of Ag–O, Ag–N, and Ag–S bonds [141]. The XPS has also been utilized for chemical composition estimation of Pt NPs doped with Ag. ICP-MS quantification of such composite showed the lower values of Ag in comparison to XPS, which suggested to be due to the limited photoelectron free pass (nearly 2 nm), so the differences may be attributed to Ag surface enrichment [180]. The composition of Ag-content formulations was possible to estimate by Ag 3d level shifts measurements, which also were shown to be sensitive to NPs size. T. Radu with colleagues has measured

the Ag 3d shift dependence from Ag NPs size embedded into bioglasses volume [184]. The authors showed that for bioglasses containing Ag NPs with the average size of 9 ± 0.2 nm the peak position of Ag 3d level on XPS spectra shifted to lower binding energies by 0.3 eV comparing to bioglasses containing Ag NPs with the average size of 7.4 ± 0.2 nm, which was assigned to the influence of Ag NPs dimensions. Still, the final peak position shift which may be observed on the spectrum is due to the competition of two phenomena: initial state effects (partial electron transmission to the clusters) that implies a tendency to shift the peak to lower binding energies and final state effect, which influences the relaxation energy of the system with a tendency to shift the peak to higher binding energies. These two phenomena imply not only the impact of the NPs size and shape but also the nature of the supporting substrate [185]. The extension of the technique – near-ambient pressure XPS, which allows to study NPs in suspension. However, the Ag 3d peak under near-ambient XPS showed the shift in 0,7 eV in comparison to Ag NPs studied in the dried sample on Si-wafer [186]. What more, S. Dahle with colleagues has investigated the interaction of Ag ions with glucose, and by XPS they observed the unexpected reduction of OH groups, which may be attributed to charging effect on insulators during the study [187].

UPS utilizes electromagnetic waves with energies in the range from 3.10 eV to 124 eV, which is suitable for valence and conductive bands investigation [183]. Such information is very valuable since Ag NPs-containing nanocomposites in the last decades are often investigated for photoelectric conversion in different optoelectronic devices [188]. UPS was used for the estimation of photoelectron emission yield for Ag NPs on a hydrogen-terminated Si surface [105]. Still, for all electron spectroscopy techniques, in general, the ultra-high vacuum is essential, which can be included to their drawbacks. The necessity of the ultra-high vacuum is related to the fact, that the electrons have limited free path and additional collisions are unacceptable. Moreover, the molecules presented in the gas phase as well as adsorbed on the surface can lead to the appearance of additional signals. Finally, the high-energy beams can heat the material causing additional changes in their structure [183].

Auger electron spectroscopy (AES) is based on an analysis of electron energies emitted from excited atoms through a series of internal relaxation events, which also called the Auger effect. Auger electrons are very specific regarding elements from which they were ejected, so the technique is common for surface scanning and imaging. J.C. Sharp et al. have studied the growth of Ag NPs on Fe_3O_4 (111), the results indicated that Ag formed 3D islands on the surface with a fixed particle density of 4×10^{12} particle/cm^2 and the average size was ≈ 4 nm [142]. A. E. Abbass et al. have used Auger spectroscopy to investigate Ag NPs embedded in bismuth silicate [143]. They noted that the study was burdened with sample charging effect, which was overcome by providing good sample contact to rough copper holder. Moreover, even though Auger spectroscopy have confirmed the formation of Ag NPs smaller than 5 nm, the information about its distribution through all the sample was not possible to extract, since AES makes possible to scan surface only on the depth of few nm.

Electron energy loss spectroscopy is a technique where the difference in energy of electrons in the incident beam with inelastically scattered electrons are compared. Depending on the level of energy loss the information about bandgap, plasmon modes, valence, and core energy levels can be obtained. EELS in general is integrated in an electron microscope and can be used for imaging as well as for estimation of spatially resolved information [189]. EELS was utilized for chemical composition estimation in Ag NP-lysozyme bioconjugates. The results clearly indicate the presence of Ag, C, N, O, and Ca at different measurment points. The presence of Ca at NPs edges provided additional confirmation of Ag NPs binding to lysozyme, since it was derived from chicken egg white with 90% purity and calcium is a major component of eggs [89]. A. Campos with coauthors has investigated plasmon modes of Ag NPs embedded in silica by STEM-EELS [144]. They noticed that the electrons incident beam influenced both the NPs and surrounded silica structure, which in consequence influenced LSPR shifts. Initially, the NPs did not exhibit a clear plasmon resonance, as the synthesis conditions have led to Ag_2O formation. The NPs interface clearance from oxygen due to reduction caused the plasmon peak appearance on EELS spectrum and the matrix damage appeared as shifts to higher energies. Moreover, they conclude that small Ag NPs size does influence on LSPR shifts, but these are often masked by environmental influences.

3.9. XRD and SAED investigations

XRD is based on measurements of the angles and intensities of diffracted X-ray beams. Depending on the wavelength of incident X-ray, the wave amplitude can be enhanced due to constructive interference and detected during the analysis. Such enhancement is observed, when Bragg's law is fulfilled, which allows to estimate the relation between the wavelength of the incident electromagnetic radiation to the diffraction angle and the lattice spacing in crystalline sample [190]. The XRD analysis is a common technique by which the crystalline structure of both single Ag NPs [55] as well as incorporated in nanocomposite [87] can be detected. However, the intensity of signals obtained from Ag NPs embedded in organic films usually are at a very low level, so it barely could be noticed [17,87] and signals from Ag NPs deposited on the ZnO were not noticeable at all [191]. Generally, for mixed materials, the detection limit is shown to be approximately 2% [190]. Moreover, within the XRD technique by the Debye−Scherrer equation the NPs size can be estimated as it was made for Ag NPs doped in dialdehyde nanofibrillated cellulose, the calculated crystallite size was in the range from 14,03 to 16,63 nm, while SEM measurements indicated NPs size in the range 20.75 nm - 38.25 nm, which was suggested to the presence of aggregates consisting several crystallites [131]. The NPs size estimation by XRD is based on the fact, that the decrease in particle size leads to peak broadening in XRD patterns. However, for particles with sizes from 1 μm to 50 nm the peak broadening is almost negligible and mainly caused by instrumental effects. In turn, the significant peak broadening for NPs with sizes less than 10 nm lead to extremely low signal intensity and peaks overlap, which in consequence hardly can be distinguished. Such the situation burdened both the NPs size determination as well as crystal characterization [192]. What is interesting, the NPs shape can influence the intensities of the individual signals. The cubic or rod-like particles under the drying process or during precipitation tend to orient with flat faces parallel to the substrate, which called “the preferred orientation” of the sample. The phenomenon can provide additional valuable information but generally is undesirable, especially in quantitative XRD analysis [192].

Selective area electron diffraction (SAED) is another technique for materials crystalline structure investigation. The principle is similar to XRD, only instead of X-rays, the diffraction pattern of the electron beam is obtained. The virtue of the technique is that it can be performed during electron microscopy investigation and that the analysis can be made from a selected area of the sample, which allows obtaining information about the crystalline structure of different parts in composite materials, in particular for individual NPs. To give an example, the SAED analysis was made for Ag NPs derived from thermal decomposition of fatty acids silver salts. Such synthesis allowed to obtain self-assembled Ag NPs with a diameter near 4,5 nm (in the temperature range from 230 to 270 °C) and SAED analysis confirmed the long-range order structure [60]. G. Shen and D. Chen have synthesized the ZnO nanowires decorated with Ag NPs and performed the SAED analysis, in which selective character showed the possibility to investigate area corresponded to ZnO nanowire only. The results indicated that the obtained ZnO nanowires appeared as single crystals with the preferred growth directions alone the [0001] orientation [191]. However, in the XRD analysis by the characteristic angles, the inorganic crystal compounds can be identified, while SAED gives only information

about basic parameters of the materials crystal structure, which often is not enough to distinguish two different compounds. To give an example, B. Boutinguiza et al. have shown that measured by SAED interplanar distances of 0.233 and 0.141 can correspond both to Ag (theoretical 0.236 and 0.145) as well as to Ag_2O (theoretical 0.237 and 0.143) crystal structures, so the discrimination of these Ag forms is complicated.

3.10. Mass spectrometry

The widespread employment of Ag NPs in numerous applications requires very precise techniques for its investigation, as the influence of nanomaterials on different systems is huge, while caused by agents in insignificant amounts. Inductively Coupled Plasma Mass Spectrometry (ICP-MS) has shown to be a powerful tool for accurate trace analysis of Ag content in the samples and possesses excellent detection limit, high resolution power that can reach 10,000. Moreover, the ICP-MS can be utilized for multi-elemental investigations as well as for measuring elemental isotope ratios [193]. Regarding nanosized Ag or its composites the ICP-MS is frequently utilized for silver uptake quantification in different systems. In our group, we have investigated the Ag adsorption by whey proteins lactoferrin [16] and casein [83] during the nanocomposite synthesis. Moreover, C. Tiantian with coauthors has utilized ICP-MS for Ag content estimation in silver-silica nanocomposites [12]. ICP-MS is also suitable for different biological samples investigation. To give an example, C. G. Castro-Gonzales et al. have utilized ICP-MS to study the Ag uptake by *Stevia rebaudiana B.* under exposure of Ag NPs with different concentrations in the culture media [120]. Additionally, J. Tang with colleagues has measured the time-resolved silver distribution in the different parts of rat organism after treatment with Ag NPs and Ag microparticles injections [194]. The Ag NPs biological activity is frequently attributed to the possibility of Ag^+ production. Thus, the ICP-MS is commonly utilized for quantification of Ag^+ release from different silver-containing nanomaterials, as it was made by T. Liu al. [51]. They have investigated the Ag^+ release from Ag NPs enclosed in superhydrophobic polyelectrolyte films, as a possible agent of nanocomposite antibacterial properties. However, as every ICP-MS investigation, the Ag determination is suffered from numerous interferences. The interferences in the quantification of ^{107}Ag are the $^{91}ZrO^+$, $^{90}Zr^{16}OH^+$, and $^{89}Y^{18}O^+$, while to ^{109}Ag interferences the $^{93}Nb^{16}O^+$, $^{92}Zr^{16}OH^+$, and $^{92}Mo^{16}OH^+$ can be included [193].

Lately the single-particle ICP-MS (SP-ICP-MS) is frequently utilized for Ag NPs behavior investigations in different environmental and biological systems. SP-ICP-MS implies the utilization of very diluted NPs suspensions, so it allows to introduce single particle into ICP-MS during the analysis. Moreover, the measurements in SP-ICP-MS mode are performed with very short dwell time, so it allows to estimate both the concentration of the dissolved metal and incorporated in NPs in the sample at the same time [148]. Thus, the technique is frequently utilized for NPs size estimation and quantification. I.-L. Hsiao et al. has investigated the cellular uptake of TiO_2 and Ag NPs for Neuro-2a cells [146]. They utilized conventional ICP-MS, SP-ICP-MS, and laser ablation ICP-MS. The performed analysis showed that the Ag uptake was higher in case with cell treatment by bigger NPs but the higher particle number uptake for smaller NPs. However, the sample preparation for conventional ICP-MS could contribute to a higher quantity of estimated silver uptake, as some of quantified particles may be not due to cell absorption but adsorbed on the culture media plate. On the other hand, the NPs aggregation as well as limited size for detection (20 nm for Ag NPs [148]) can contribute to SP-ICP-MS analysis results. Moreover, A. Keri with colleagues has performed an SP-ICP-MS analysis of Au/Ag bimetallic NPs with different structures and was able to estimate NPs size and their elemental composition [195]. It was shown that in SP-ICP-MS mode the sequential determination of Au and Ag in the particles with calibration by different sized monometallic NPs and subsequent mathematical estimation was the most precise and accurate for both size and molar ratio investigation. The drawbacks of the utilized method are its time- and labor-consuming character. Moreover, as it can be deduced, the chemical composition, as well as the size, were measured not for each particular NP, but for all NPs population. Thus, the obtained data presents the average parameters of all quantified NPs and can be applied with high credibility only for spherical, monodisperse, and uniform in terms of chemical content particles. However, in S. Naasz the size and chemical composition of Au@Ag core-shell NPs were also determined [196]. The authors reported that due to restrictions within the SP-ICP-MS coupled with quadrupole analyzer it is not possible to perform multi-isotope analysis, thus the determination of Au and Ag content in the NPs was performed in two separate runs. Instead, the SP-ICP-MS coupled with the TOF analyzer was able to distinguish all isotopes simultaneously. Moreover, in the work the determination of the chemical composition of more complex multi-component $BiVO_4$ and $(Bi_{0.5}Na_{0.5})TiO_3$ particles was performed. It was shown, that in case of Au@Ag NPs the SP-ICP-MS coupled with TOF instrument could simultaneously detect Au and Ag in 97% of particles events, while the simultaneous determination of Bi and V for $BiVO_4$ as well as Bi and Ti for $(Bi_{0.5}Na_{0.5})TiO_3$ was possible to perform in >90% of all particle events.

Secondary ions mass spectrometry (SIMS) is a technique that implies the surface sputtering of the sample by focused primary ion beam and the analysis of ejected secondary ions. Such technique is suitable for surface 3D chemical mapping with detection sensitivity for even ppb scale. S. Wagener with colleagues has investigated the textiles functionalized by Ag NPs, and it was shown that TOF-SIMS (Time of flight-SIMS) was able to determine not only the chemical composition of Ag species on the fiber surface but also provided the information about its spatial distribution [197]. Additionally, TOF-SIMS allowed to estimate changes that occurred on Ag NPs surface after exposure to wastewater. The analysis indicated that Ag NPs after 72 h in wastewater in TOF-SIMS analysis produce different sulfur-content ions in both negative and positive mode, which may be attributed to the presence of Ag_2S and other silver sulfide species in the sample. Instead, the results from XPS analysis was more precise, and it was possible to distinguish the Ag–S–C organosulfur bonds, which appeared on the Ag NPs surface [147]. Still, SIMS is greatly limited by the diameter of the primary ion beam. The size of NPs, in general, is in order or even smaller than the diameter of primary ion beam, therefore it is rather difficult to investigate the thin structure of nano-objects [198].

Matrix-assisted laser desorption/ionization, that most often coupled with time of flight analyzer mass spectrometry (MALDI-TOF MS), is considered to be a soft ionization mass spectrometry technique as in general within it pseudo-molecular ions are produced. It was shown in S. Dhanya et al. work that small Ag nanocluster with up to 11 atoms could be ionized and analyzed by MALDI-TOF MS directly [199]. E. Oliveira with coauthors have also investigated the Ag nanoclusters, they were able to distinguish nanoclusters with 21 Ag atoms [200]. However, lately, more attention paid to the fact that Ag NPs unique optical properties make possible to use it as a matrix, which contributed to the new approach in MS – NALDI. To give an example, K.-M. Ng et al. has investigated different noble NPs as a possible promoter for benzylpyridinium ionization [8]. The investigation showed that Ag NPs have the biggest ion-desorption efficiency in comparison to Au, Pd, and Pt NPs. However, Ag NPs lead to slight analyte fragmentation and to metal cluster ion appearance (Ag^+ and Ag_2^+). M. Yang with coauthors has shown that signals can be enhanced even more in case of deposition of Ag NPs on zeolite [9]. They suggested that zeolite as a supporter can make the distribution of Ag NPs more homogeneous and prevent the NPs aggregation, which is one of the widest problems in NALDI approaches. Moreover, the active sites on zeolite may influence the electronic state of Ag NPs by reducing the excitation energy threshold. What interesting, in MALDI-TOF-MS analysis the enhanced signals may come from compounds directly bounded to NPs, as it was shown in our work, where we observed the greater signal for α-casein (Fig. 4), which we assumed to be due to it prevalence role in Ag NPs bounding [83]. Finally, it was shown that MALDI-TOF MS is suitable

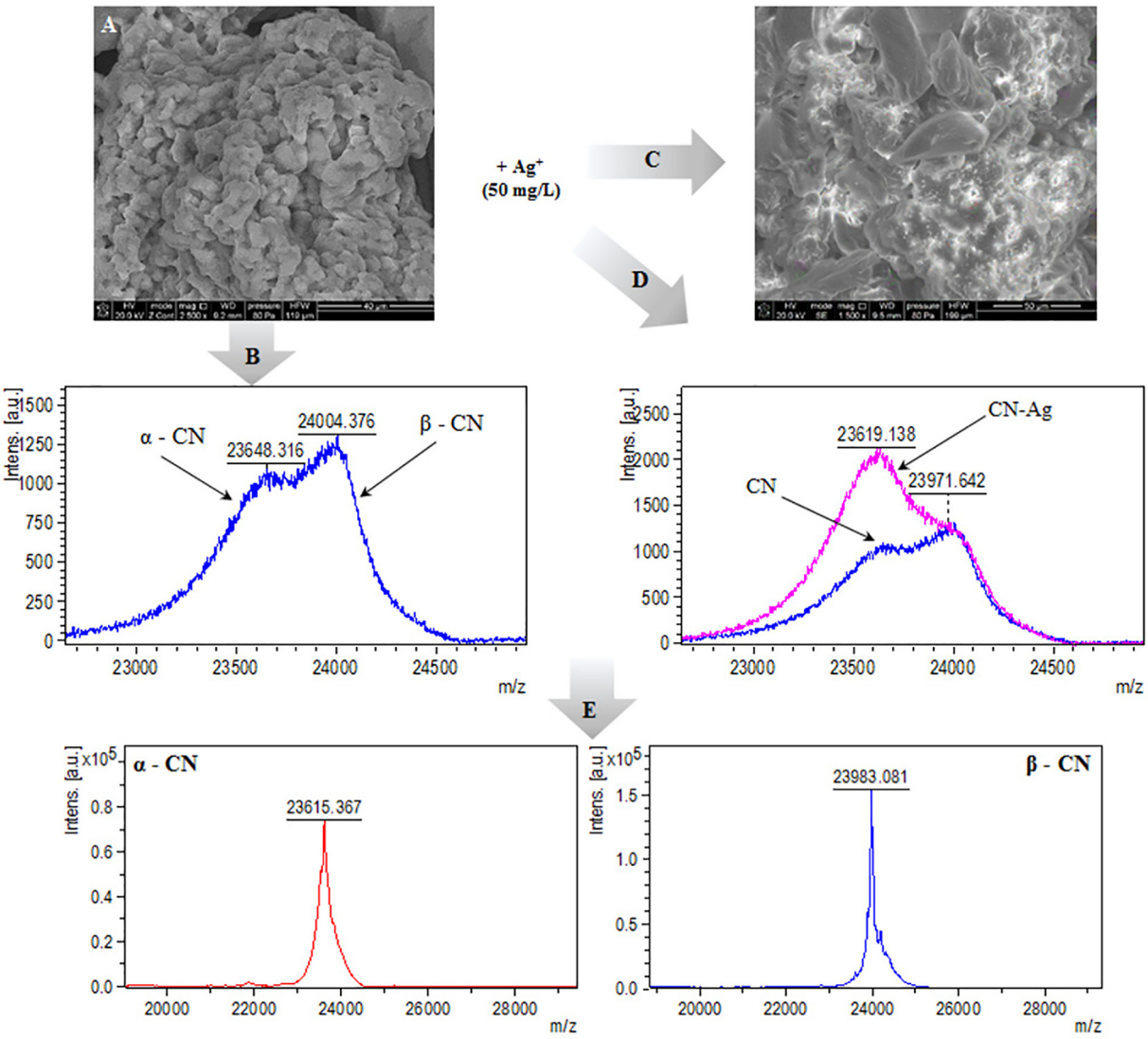

Fig. 4. SEM image of native casein (A); mass spectrum of intact casein (B); SEM image of casein-silver complexes (C); mass spectrum of casein-silver complexes (D) and mass spectrum of intact α- and β-casein standard solutions (E), respectively [83]. Copyright 2019 by the authors. Licensee MDPI, Basel, Switzerland.

for tracking how Ag NPs alone with modification by antibiotics influence the protein profiles of bacteria [201].

3.11. Separation techniques

The physicochemical and biological properties of the NPs are strictly dependent on their size. In the above sections of the article, numerous techniques for size determination were presented, but each of them suffers from limitations, especially in the case of polydisperse samples. Field flow fractionation is frequently mentioned as an effective and low-cost method for NPs sizing. The separation in the technique occurs due to different mobility of particles under the field applied perpendicularly to the parabolic main flow. The applied field may be of several different natures: made by cross-flow and asymmetric cross-flow, centrifugal, gravitational, or thermal field. Asymmetric flow field-flow fractionation (AF4) is one of the most popular variations of the technique and the most typical detectors are UV-Vis, DLS, and MALS (Multi angel light scattering) [148,165]. However, off-line and on-line ICP-MS can also be utilized. In AF4 only one wall of the flow channel makes up of semi-permeable membrane, so it makes possible to perform NPs focusing before fractionation. In consequence, the focusing step prevents peak broadening and improves resolution [165]. S.T. Kim with colleagues in their work has shown the possibility for AF4 utilization in stability study of Ag NPs-protein conjugates, as they performed the investigation of the aggregation behavior in different conditions of Cytochrome C - conjugated Ag NPs [91]. K. Loeschner et al. reported the successful utilization of the technique for Ag NPs determination in chicken meat [202]. However, they noted that the extracted from meat Ag NPs have shown the earlier elution in comparison to the pristine Ag NPs suspended in water. As the TEM and SP-ICP MS have shown no changes in the NPs size, the difference was attributed to the presence of enzymes. Moreover, in W.-C. Lee et al. work it has been shown that carrier liquid, as well as capping agent, have an influence on the obtained results [148]. The analysis of 30 nm, 60 nm, and 100 nm Ag NPs capped with citrate and PVP has shown that for NPs capped with PVP suspended in deionized water the highest recovery can be obtained. Instead, the fractionation by AF4 could not be efficient for PVP-capped Ag NPs carried in surfactant FL-70 due to interactions between the functional groups of FL-70 and Ag NPs. T. K. Mudalige et al. has also reported the process dependence on the carrier mixture as well as a stabilizing agent of the NPs [203]. They noted that irreversible NPs binding to AF4 membrane at the focusing side leads to membrane fouling, which in consequence

decreases the NPs recovery. The problem was possible to overcome by membrane functionalization and NPs stabilization.

NPs in aqueous solutions occur with surface charge originated from functional groups of stabilizing agents or from adsorption on the NPs surface of ions present in the solution. The NPs surface charge makes it possible to use electrophoresis for its separation. Electrophoretic separation is based on differences in electrophoretic mobility of the particles, which in general depends on its charge and size [165]. In CE the separation process is performed in fused silica capillary, which inner surface can be modified on purpose to alter the electroosmotic flow and decrease the analyte adsorption onto capillary walls [204]. H. Qu et al. have performed the optimization for the separation process of both the Ag NPs an Ag^+ by CE [205]. They noted that alkaline conditions are more suitable for such purposes, as it prevents the Ag NPs dissolution and aggregation. Additionally, the necessity of chelating agent usage for Ag^+ capture as well as non-ionic surfactants was emphasized. Moreover, D. Mozhayeva with C. Engelhard has shown that CE can separate Ag NPs with the same size but different coatings [149]. Still, in the case of a five-component mixture, the migration time of 20 nm citrate capped Ag NPs was in the same time window as the migration of 40 nm and 60 nm PVP-capped particles. The investigation has shown that the Ag NPs migration times depend on the mixture, in which they are injected. Thus, the correct discrimination of different species is possible only in case of combination with other techniques, for example, SP-ICP-MS. Finally, B. Michalke and I. Vinkovic-Vrcek in their work have shown, that methods presented in literature not always can be applied for real samples, which was the liver extract [206]. They have tested six different approaches to find satisfactory conditions for Ag NPs and Ag^+ separation. The optimized method proposed by authors implies a strong alkaline condition, usage of tetramethyl-ammonium hydroxide and reverse polarity. The beneficial influence of tetramethyl-ammonium hydroxide was attributed to Ag NPs-sticking prevention.

Gel electrophoresis is another separation technique, which commonly is associated with biopolymers separation and study, i.e. proteins or nucleic acids. The principle is the same as for CE, but the process is performed in the gel. Lately, with progress in nanotechnology gel electrophoresis become popular for NPs and nanocomposites characterization. M. Hanauer with colleagues has shown that metal NPs with different shapes and sizes can be separated by gel electrophoresis [207]. They noted that different capping agent can influence the separation efficiency. Moreover, they performed a mathematical calculation to explain quantitatively the NPs behavior in the process, which also allows to estimate the packing density of polyethylene glycol absorbed on the NPs surface. Gel electrophoresis is also useful for observation of NPs interaction with different biomolecules. I. Moglia et al. have investigated Ag NPs formation in recombinant human L- and H-ferritine [107]. Gel electrophoresis allowed to confirm the formation of Ag NPs in L-ferritine by chemo- and photo-reduction, while chemo-reduction in the H-ferritine did not appear. What is more, the formation of protein dimers and higher monomers induced by Ag^+ was observed. I. Lubitz with A. Kotlyar has performed the preparative gel electrophoresis for G4-DNA-AgNPs (G-rich DNA-quadruplex structure) conjugates, which they subjected for TEM [92]. During the process, the G4-DNA-Ag NPs separation on three different bands was observed. In consequence nanocomposites from each band showed the different NPs content (from one to three pieces). Finally, gel electrophoresis was useful for the observation of changes that take place in cells treated with Ag NPs and their composites. For instance, S. Meenakshisundaram with colleagues has observed the expression levels of various anti-apoptotic, cell cycle regulators and apoptotic genes caused by Ag NPs synthesized with *A. muricata* leaf extract[208].

3.12. Thermal analysis

Thermal behavior is a crucial characteristic of Ag NPs, as their utilization in electronics and catalysis implies the elevated thermal conditions. Moreover, the NPs are often incorporated in different materials in line to give antibacterial properties, so it may alter the thermal stability of such composites. Thus, thermal analysis is frequently utilized for Ag NPs and Ag-nanocomposites characterization, which can be performed in several different ways. S. I Sadovnikov et al. have carried out high-temperature in situ XRD analysis of nanosized Ag_2S, which is a promising substitute for germanium and silicon-containing semiconductors [145]. The results indicated that in the oxidizing medium the NPs were in form of α-Ag_2S up to 448 K and in the form of β- Ag_2S in the temperature range from 453 to 623 K. After the temperature has reached 673 K the formation of metal Ag has begun and in the temperature range from 723 to 773 K signals only from metal Ag were observed. The thermal annealing of as mentioned NPs has also been performed under conditions without oxygen and moisture at 393, 423, 453, 493, and 930 K. The analysis showed the appearance of monoclinic non-stochiometric acanthine α-$Ag_{1.95-1.98}S$ and the NPs size growth at a temperature above 453 K.

Another technique for thermal investigation is thermogravimetric analysis (TGA), where the mass loss of the sample over the temperature dependence is investigated. S. M K. Thiagamani with coauthors has utilized TGA for cellulose-based hybrid nanocomposites investigation [209]. It was shown, that nanocomposite comprised from cellulose matrix, banana peel powder as a filler and incorporated Ag NPs was more resistant to thermal decomposition in comparison to pure cellulose. This might be due to the higher thermal stability of the banana peel powder filler. S. Boughriba with colleagues has investigated the changes in thermal stability in *Rhinobatos cemiculus* gelatin films modified by TiO_2-doped Ag NPs [150]. The first three stages for all films were attributed to water (60–100 °C) and glycerol (250 °C) evaporation as well as small weight gelatin fraction decomposition. Gelatin films modified with 2, 3, and 4%of TiO_2-Ag NPs showed enhanced stability, so the degradation peak at 500 °C was not present in comparison to material with less amount of filler. Moreover, the differential scanning calorimetry (DSC) was performed for as-prepared samples. DSC is a thermoanalytical method, which allows to study phase changes. The technique is based on measurements of the temperature changes depending on the portion of applied heat. At transition point the heat is spent on the changes in the structure, the additional heat portion does not lead to temperature growth till all samples turn into other phase states [210]. *Rhinobatos cemiculus* gelatin glass transition temperature (Tg) was estimated as 150 °C, while gelatin film Tg value was about 59,5 °C. The TiO_2-AgNPs incorporation decreases the Tg value up to 52,6 °C for 4%-composite. The changes were attributed to a disordered state caused by NPs among the gelatin molecule's net-like structure.

4. Physicochemical properties

The first most important property of the Ag-content NPs is their chemical composition. Metallic Ag NPs are the central object of the majority of publications. However, other forms of nanosized Ag should also not be avoided, as they exhibit beneficial features, so they can be utilized in different applications. Ag_2S NPs have shown to be a promising biocompatible contrast agent for dual-energy mammography and computer tomography [14]. Ag_2O NPs are reported to be a good filler for pastes for the production of printed electrical devices [6]. Additionally, the Ag_2O NPs the same as Ag NPs showed the antibacterial properties against various Gram-positive and Gram-negative bacteria [211]. Moreover, the metallic Ag NPs can undergo changes through sulfidation, chlorination, oxidation, and aggregation, which drastically change their properties: decreasing in bioavailability and bioactivity, poor solubility, etc. S. Karimi et al. have shown that utilization of the marine algae extract of *Chaetomorpha sp* for Ag NPs synthesis led to Ag@AgCl NPs formation [71]. Additionally, M. Azodi with coauthors has shown the metallic AgNPs transformation in the complex mixtures, which the wastewater is, through surface oxidation to Ag_2O and subsequent S-content NPs formation [147]. D. Chen et al. have also reported the

Ag_2S surface formation in presence of $S_2O_3^{2-}$ ions [212]. They emphasized the crucial role of phenolic groups of the tannic acid, which served as Ag NPs stabilizing agent, in the $S_2O_3^{2-}$ reduction. All these indicate that the presence of different ions in the synthesis mixture or in the investigated systems should be considered, as the formation of different Ag-containing impurities may influence on the obtained results.

To the Ag-containing NPs variations can be include several different groups: pure Ag NPs, alloys, core-shell, and doped metallic NPs (AgAu [47,195], AgPd and AgPt [180], etc.), nanocomposites (Ag/TiO_2 [213], Ag@AgCl [71], SiO_2@Ag [122], etc). To the Ag NPs chemical features the capping agent and/or surface modifier can also be include, as it determines NPs physical, chemical, and biological behavior. The capping agent is directly responsible for the sign and magnitude of the NPs surface charge, which in turn influences hydrodynamic radii and aggregation stability [49]. Moreover, the metallic NPs LSPR plasmon maximum is strictly dependent on the stabilizer, as it changes the dielectric constant of the surrounding media near the NPs surface. Finally, C. D. Walkey et al. have investigated the influence of the surface modifiers on the NPs interaction with serum proteins [26]. It was shown that the capping agent has influenced the protein corona composition, which formed on the NPs surface. Thus, the stabilizer may influence the NPs mechanism interaction with cells and therefore can influence cell regulation routes [27].

Size is another important feature, which together with chemical composition determines the majority of NPs properties. The size-dependent characteristics of NPs are attributed to the so-called "quantum size effect". The properties of bulk material are determined by the average of all the quantum forces affecting all the atoms from which the material is made. By decreasing the size of the objects it can be reached the point, where the averaging no longer works. The distinctive behavior of the atoms or molecules in small clusters in comparison to that one from bulk material is called quantum size effect. Besides, the surface energy excess also contributes to specific properties of the nanoscale objects, as the specific surface is increased drastically with decreases in the particles size [214]. However, the size of the NPs can be determined by several methods and each of the methods will provide controversial data. It was shown, that size measured by DLS, in general, is overestimated. R. Ma with coauthors in their study has shown that the DLS measured NPs size can be even 20 times bigger, than that one obtained by TEM [28]. The hydrodynamic diameter for Ag NPs coated with gum arabic was measured as 99.1 ± 1.1 nm by DLS and 5.5 ± 1.7 nm by TEM. The effect is attributed to hydrated corona on the NPs surface, which behave rather as a hard shell than the liquid causing the light scattering [30]. Moreover, the NPs aggregation also could result in higher measured values of NPs size. Even though DLS estimated size is not the exact radii of the NP, it may contribute to the results obtained for desirable NPs characteristics. DLS is a spectroscopic technique operating in the visible part of the electromagnetic radiation. Thus, it may indicate the alters in the UV-Vis spectra, conventionally utilized for LSPR measurements. B.-J. Liu et al. have shown in their work, that depending on the NPs size and shape the scattered and absorbed light contribution in the overall extinction spectrum may differ significantly [163]. They also noted, that in fact the direct discrimination of the scattered and absorbed part of the light is cannot be performed with existing measurement tools, therefore only mathematical calculations may slightly shed light on the issue. In the abovementioned work of R. Ma et al. the XRD diameter evaluation was also performed [28]. The crystallite diameter for uncoated Ag NPs and coated with PVP, in general, have shown the calculated sizes twice lower than TEM investigations. The obtained data may be due to the presence of twinned particles, which cannot be distinguished by TEM.

Shape influence on the metallic NPs properties may be assigned to several factors. Firstly, the shape factor alters the specific surface area, and therefore the thermodynamic characteristics of the NPs. In the simplest approximation for two NPs of the same volume, the spherical NP will have 2.5 times lower surface in comparison to the rod-like NP with a 16:1 aspect ratio [215]. The second effect may be explained by the limitations for electron movement inside the metallic NP surrounded by an insulator. The electron behavior in the metallic particles was explained by M. A. Garcia, where the rod-like shape influence on LSPR was illustrated [166]. The electromagnetic field of the incident light causes the electron movement to the NPs surface. Such electron accumulation on one side of the NP causes the negative charge, whereas other electron-deficient part stays positively charged. The created dipole forces electrons to return to the equilibrium position, causing the electron oscillation with a certain frequency, named the plasmonic frequency or resonant frequency. Larger electron displacement creates larger dipole and in consequence larger restoring force altering the resonant frequency. The electron movement along the rod axis in rod-like NPs creates greater charge accumulation on the surface, which in consequence shifts the resonant frequency to a higher wavelength. However, the shape-depended NPs properties caused by more complex phenomena. Besides the light adsorption, the NPs shape also alters the light scattering [5]. Moreover, the anisotropic NPs structure changes the energy distribution on the surface. In general, the atoms on apexes and edges possess more energy than atoms on faces, which for example causes the faster Ag NPs dissolution on the apexes [216]. Additionally, the adsorption, desorption processes as well as adsorbed molecules distribution changes on the NPs with different shapes [217]. The higher surface-to-volume ratio implies the higher adsorption, which in consequence changes the surface charge and therefore the behavior in the solution, making possible for example to separate NPs with different shapes by gel electrophoresis [207]. Moreover, R. Vankayala et al. have revealed that singlet oxygen formation by Au and Ag NPs greatly depended on the NPs shape [218]. The authors noted, that oxygen exists in molecular form only on the Ag(111) plane, and decompose on the atomic form on both Ag(100) and Ag(110). Finally, the NPs shape influences their interaction with cells [219]. S. Dasgupta et al. by calculations of the curvature energies of lipid bilayer membranes combined with a contact adhesion energy for the particle−membrane interaction have revealed the complexity of the endocytosis process for non-spherical/non-ellipsoid NPs [220]. The calculations showed that cellular uptake depends not only on global parameters like aspect ratio but also on local geometrical parameters, like extrema of the local mean curvature.

The combination of three abovementioned NPs characteristics determines other physicochemical and biological NPs properties. To the features that differ the Ag behavior in the form of NPs from that one in the bulk material, the optical, thermal, and catalytic properties can be included. The optical properties of Ag NPs are the most emphasized and discussed in the literature. As it was mentioned in the other sections of the review the LSPR is the major effect of the unique behavior of the metallic NP and commonly is related to the light absorption of specific wavelengths. The absorbed light depends on the size and shape of the NPs, and in consequence, determines the NPs color (Fig. 5). T. Huang with X.-H. N. Xu has synthesized Ag NPs with different colors [54]. The color of synthesized colloids was dependent from the shape of the NPs and was light yellow for spherical NPs with a diameter of 2.6 ± 0.8 nm (λ_{max} = 393 nm) and orange-red for the mixture of predominantly spherical NPs (91.2%) with a diameter of 9.5 ± 3.2 nm and rod-shaped NPs (7.9%) with size 13.5 ± 4.2 nm × 10.5 ± 3.9 nm (λ_{max} = 461 nm). The colloids with the purple, purple violet, violet and blue colors (λ_{max} = 536 nm, 552 nm, 572 nm, and 606 nm respectively) were the mixtures of a nearly equal amount of spherical NPs with sizes 16.7–20.3 nm and rod-shaped NPs with aspect ratios 23–27 nm × 15–19 nm (37–54% of each), and with small amount of triangle NPs (8.8–15.2%). However, the LSPR is also significantly modified by surrounding media, in particular, the refractive index has a big influence on the changes in resonant wavelength and therefore in the NPs color. J. J. Mock et al. have observed the NPs color changes subjected to dark-field microscope investigation [117]. In their work, the spherical 40–90 nm-sized Ag NPs immobilized on SiO_2 wafer appears in the blue color in the local dielectric interface of air, while in oil with refractive index 1,44 the color is shifted to green/yellow.

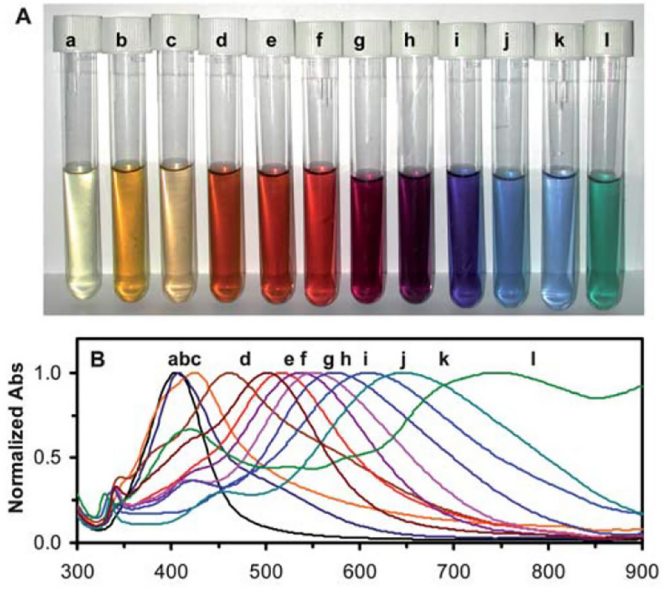

Fig. 5. Study of absorption and scattering plasmonic optical properties of colloidal Ag NPs using UV-Vis absorption spectroscopy: (A) photos of colloids with AgNPs of different shapes, (B) normalized absorbance of UV-Vis absorption spectra of AgNPs colloids shown on (A). Reproduced with permission from ref. [54]. Copyright 2010 Royal Society of Chemistry.

A. P. Kulkarni et al. have also investigated the influence of the refractive index on the LSPR band, they performed the Ag NPs transition from a water environment to polar organic solvents [221]. The transfer of Ag nanoprisms to methanol, 2-propanol, dimethylformamide, and dimethylsulfoxide have shown that the in-plane LSPR band slightly broadened and redshifted, the relevant shifts were higher in case of higher refractive indexes. Instead, the change of water media to acetone causes significant in-plane band broadening.

To LSPR induced effects the formation of so-called "hot electrons" (electrons with high kinetic energy) can be included [222]. The hot electrons formation can be utilized in solar energy harvesting. Moreover, hot electrons can directly interact with molecules adsorbed on the metal surface. Thus, Ag NPs exhibit enhanced catalytic properties in photochemical reactions. To give an example, P. Jiang et al. have observed the dehalogenation of 4-iodothiophenol, 4-bromothiophenol, and 4-chlorothiophenol by in-situ SERS detection [223]. It was shown, that dehalogenation reaction rate performed on 80 nm Ag NPs was much higher than that one for 40 nm or 80 nm Au NPs. Finally, as it was mentioned earlier, the optical properties of NPs also include fluorescence, which was reported for extremely small NPs with diameters below 10 nm. For example, L. Burratti et al. [134] have investigated the fluorescence features of NPs with 1.45 ± 0.26 nm size. C. Li et al. [15] also reported the fluorescence behavior of 3.9 ± 0.7 nm-sized NPs. However, Oliveira with colleagues [200] suggested that the fluorescence exhibit only extremely small Ag-clusters containing several silver atoms (up to 4). The fluorescence of larger nanoparticles is a consequence of as mentioned nanoclusters adsorption on the surface of the particles. Oliveira et al. in their work concluded that the investigation of such small objects is impossible due to low stability under the electron beam of HRTEM. Bigger Ag NPs also can exhibit photoluminescence properties, but the excitation mechanism greatly differs. To force the big NPs to emit light the two-photon excitation can be utilized. F. Han with coauthors has investigated the influence of the Ag NPs size on the two-photon excitation photoluminescence intensity [224]. Moreover, they have utilized the plasmon coupling, which was reported to be responsible for the enhancement of the phenomenon. The 14-fold enhancement of two-photon excitation photoluminescence was observed for coupled with poly(diallyldimethylammonium chloride) 50 nm Ag NPs, which is the maximum enhancement among all studied Ag NPs. The obtained results may be due to increased extinction at the excitation wavelength, which was caused by the formation of a strong longitudinal band, resonant with the excitation band.

The discrete character of the NPs makes them a semiconductor even though silver as a bulk material has the highest electrical conductivity among all metals. The NPs behavior as a semiconductor emerges from the fact that the size of the NPs is in the same order as the exciton Borh radius, which is a distance between electron and hole of exciton. The electron-hole pair, called the exciton, is originated from the excited state of the semiconductor when the electron leaves the hole on the valence band by transferring to the conductive band [1]. The UV-Vis spectroscopy usually is exploited for optical band gap determination. The band gap study, in general, shows the properties of the whole Ag NPs-containing system rather than Ag NPs alone, as the metallic NPs are often utilized in order to improve the optoelectronic properties of the materials. W. L. Wang et al. has investigated the TiO_2 nanotubes decorated with AgNPs [225]. It was shown that the band gap of TiO_2 nanotubes were 3.18 eV and by changes in Ag content from 12.5% to 17.8% it was possible to adjust the cut-off for band gap from 420 nm (2.95 eV) to 430 nm (2.88 eV). Instead, S. I. Mogal with coauthors has noticed that the band gap for pure TiO_2 particles was 3.08 eV [213], which is between the measured values for anatase (3.2 eV) and rutile (3.0 eV) [226]. The modification with 0.75% Ag shows two ban gaps 2.99 eV and 2.35 eV. The further increase of Ag content caused the shifts in band gap absorption edges and the disappearance of the visible absorption band. These indicated the absence of a doping effect for composites with higher Ag-content. The XPS analysis of as-prepared nanocoposites shows that on the surface of low silver-content NPs predominant silver species were in the form of oxides and increase of the silver content led to Ag^0 nanoclusters formation. However, it was shown by N. T. Tsendzulghul et al. that AgO, depending on deposition condition, had the band gap in the range between 2.3 eV (539 nm) and 3.1 eV (388 nm) [227]. Moreover, as it was shown earlier the XPS analysis of insulators can cause the surface group reduction due to charging effect, which could contribute to results shown by S. I. Mogal et al. Still, K. H. Mahmoud et al. have also noticed the non-linear influence of Ag NPs on band gap of the gelatin [228]. The authors have calculated the optical band gap changes from 4.60 eV for pure gelatin to 3.85 eV for gelatin doped with 0.6% of Ag NPs and 4.2 eV for gelatin doped with 1.0% Ag.

The thermodynamic properties of the material can be divided into two constituents: bulk quantity and surface quantity [229]. The significant size reduction leads to considerable magnification of surface component influence on the material properties. The result of the relatively highly-energetic state of the Ag NPs is a lower melting temperature in comparison to the bulk material. C.-W. Chiu et al. have investigated the melting point of Ag NPs synthesized in the interlayer space of synthetic fluorinated mica clay [230]. The DSC analysis indicated that 8.1 nm Ag NPs has melting point ≈ 118 °C, while 11.7 nm particles ≈135 °C. R.-X. Dong et al. have also studied the thermal stability of 26 nm Ag NPs synthesized on bentonite clay, the reported melting point was 110 °C [223]. However, the investigation was performed in a different way, namely the Ag NPs after synthesis were subjected for 2 h drying at 110 °C, and then observed under FE-SEM. The coalescence of as-prepared NPs has been revealed. Such behavior can be explained by Hanszen's theory of the pre-melting process, which implies the appearance of a quasi-liquid film on the NPs surface before melting, which can occur even at temperatures lower than the melting point and cause the NPs coalescence [231]. Under the pre-melting process, the NPs core can stay solid, while DSC analysis shows the ending point of the phase transformation process for whole NPs volume.

5. Biological activity

Biological activity can be defined as direct action (positive or negative) on a living organism, i.e. bacterial, plant, or animal cells [232].

The Ag NPs biological activity frequently is associated with their antibacterial properties. Indeed, Ag NPs and their composites were reported as effective agents for a variety of Gram-positive and Gram-negative bacteria's growth inhibiting. The trypsin-conjugated Ag composite was able to inhibit the growth of *E. coli* and *S. aureus* [90]. Besides, B. Das et al. have demonstrated the effectiveness of Ag NPs synthesized with *Ocimum gratissimum* leaf extract in case of a multidrug-resistant form of the abovementioned microorganisms [123]. A. Rogowska et al. have reported the antimicrobial activity of Ag NPs synthesized with *Actinomietes* strain CGG11n against Gram-negative *K. pneumoniae*, *E. coli* and *P. aeruginosa* as well as Gram-positive *S. aureus* and *S. epidermidis* [136]. Finally, K. Rafińska with colleagues has shown the susceptibility of *B. subtilis* to as-mentioned CGG11n-synthesized Ag NPs [201]. Still, Ag^+ ions were more effective, as they completely inhibited the *B. subtilis* growth in the concentration of 12.5 μg/mL, while the Ag NPs in the concentration of 100 μg/mL inhibited the growth only by about 13% in comparison to the control.

In addition to antibacterial properties, Ag NPs and their nanocomposites were reported as antifungal, antiamoebic, antiviral, antiangiogenic agents. S. S. Dakshayani et al. have shown both the antibacterial activity against *E. coli* and *S. aureus* as well as antifungal against *A. niger* of Ag NPs synthesized with *Selaginella* plant extract [69]. The Ag NPs conjugated with Guanebenz have been shown to be toxic for *Acanthamoeba castellanii* and *Naegleria fowleri* [233]. S. Gaikwad et al. have synthesized the Ag NPs by different fungi (*Alternaria species*, *Fusarium oxysporum*, *Curvularia species*, *Chaetomium indicum*, *Phoma specie*) and the as-synthesized NPs were subjected to antiviral capability investigations [86]. The Ag NPs produced with *Alternaria species* and *Phoma species* revealed to be toxic at a concentration of 10 mg/mL, but the viral inhibition with lower Ag NPs concentrations was on a relatively low level (between 0% to 40%). Instead, the inhibitory activity against herpes simplex virus type 1 (HSV-1) and human parainfluenza virus type 3 (HPIV-3) of Ag NPs synthesized with *F. oxysporum* and *C. indicum* showed the highest scores. The reduction in virus infectivity can be reached up to 80% for Ag NPs produced by *F. oxysporum* against HSV- 1, and 90% for Ag NPs produced by *C. indicum* against HPIV-3. Ag NPs produced by *Curvularia species* shows the resembling activity as *F. oxysporum* and *C. indicum* for HSV-1 virus, however no effect with HPIV-3. Moreover, L. Lu with colleagues have revealed that compounds with Ag in various oxidation states, such as $AgNO_3$, [Ag^{II}(*meso*-tetraphenylporphyrin)], and [Ag^{III}(*meso*-triphenylcorrole)], had no significant anti-viral activity against hepatitis B virus (HBV) [234].

Ag NPs also exhibit toxic effects against a variety of cancer and normal cell cultures. Additionally, the Ag NPs anticancer activity can be attributed to their antiangiogenic properties. S. Gurunathan with colleagues has investigated the antiangiogenic properties of Ag NPs synthesized with *Bacillus licheniformis* [19]. The antiangiogenic properties for as-prepared NPs were attributed to decreased viability of endothelial cells (up to 50% in the concentration of 500 nM), their reduced migration and altered formation of tubular structures. The Ag NPs synthesized with *Bacillus* spp. were shown to affect the viability of breast cancer cells MCF-7 [94]. The cell toxicity was dose-depended and at the concentration of 30 μg/mL the cell viability was calculated as 80%, while at the concentration of 50 μg/mL cell viability was substantially decreased as 15%. Even though the growth inhibition was not very significant, the Ag NPs treated cells also exhibit decreased adhesion capacity, changes in cell shape and size. K. Jadhav et al. have also performed the in vitro investigation of anticancer activity for phytosynthesized 40–80 nm-sized Ag NPs against a number of cancer cell cultures, among others liver HepG2, lungs L-132, pancreas MIA-Pa-Ca-2, breast MDA-MB-231, oral KB cells, prostate PC-3, and cervical HeLa cancer cell lines [20]. The IC_{50} value (half-maximal inhibitory concentration) was estimated as 6.31, 4.002, 5.228, 8.452, 14.37, 7.46, and 6.55 μg/mL for each abovementioned cancer cell cultures respectively. Moreover, the cytocompatibility assay with normal human fibroblast L929 cell lines indicated that the as-synthesized NPs have no significant toxicity in therapeutical concentration (the viability was ≥95% in the presence of 78.62, 39.31, 19.65, 9.82, 4.91, and 2.45 μg/mL of NPs). Finally, the Ag NPs in the concentration of 78.67 ± 3.60 μg/mL displayed <3% hemolysis, which lies within the biocompatible range in accordance to ISO/TR 7406 [20]. However, Ag NPs can exhibit toxic properties against normal cell cultures. A. K. Suresh with coauthors has investigated the cytotoxic effect of Ag NPs against mouse macrophage and lung epithelial cell lines [101]. Four different types of Ag NPs were utilized, namely poly (diallyldimethylammonium)-Ag, biogenic-Ag, uncoated-Ag, and oleate-Ag with sizes in the range 4–9 nm. The IC_{50} concentrations for RAW-264.7 cells were found to be 0.1, 0.125, 1.1, and 4.9 μg/mL for each of the abovementioned Ag NPs respectively and 0.45, 0.7, 1.6, and 6.3 μg/mL for C10 lung cells. The authors emphasized that the surface coatings alone had no toxic effect, but the direct correlation between the Ag NPs surface charge and toxic effect can be observed. Moreover, the authors revealed that as-mentioned oleate-coated Ag NPs nanoparticles were found to be nontoxic or noninhibitory to prokaryotic Gram-negative *E. coli, S. oneidensis*, and Gram-positive *B. subtilis*.

Ag NPs can cause various physiological effects on the cell level and therefore on an organism in general. The Ag NPs can activate mitochondria-mediated stress. For instance, J. S. Teodoro et al. have revealed that Ag NPs impaired the oxidative phosphorylation capacity and depressed transmembrane potential in isolated rat liver mitochondria [235]. Moreover, the authors have shown that mitochondria pre-incubated with Ag NPs exhibit increased susceptibility to calcium-induced permeability transition. P.V. AshaRani with colleagues has also investigated the cellular Ca^{2+} homeostasis and changes in mitochondria permeability of Ag NPs-treated human lung fibroblast [236]. However, the perturbation in Ca^{2+} cellular homeostasis influences not only the mitochondria normal functioning, but also injures the cytoskeleton. The cytoskeleton injury blocks the chromosome segregation and cytokinesis. Similarly, in the M. Piao et al. work the Ag NPs treatment influenced the mitochondrial transmembrane potential and caused the cytochrome C release [139]. The authors have shown, that transmembrane potential loss is a result of the down-regulation of Bcl-2 and up-regulation of Bax. A. Sachdev et al. have also shown that carbon dots-Ag@ZnO nanocomposite down-regulated the Bcl-2 gene, which could lead to the expression of pro-apoptotic genes [237]. R Zhang et al. have revealed that Ag NPs can induce the endoplasmic reticulum mediated stress by affecting the PERK/eIF2α signaling pathway, IRE1 phosphorylation, and ATF6 cleavage [238]. The Ag NPs were also shown to alter the ion interplay in the biological fluids, among other the formation and accumulation of Ag_2Se and Ag_2S insoluble salts [239]. Moreover, the high Ag^+ affinity to S and Se can affect the selenoprotein synthesis [240] or S-containing peptides, proteins and enzymes activity, such as glutathione or dehydratases [241,242]. Besides, glutathione is considered to be a major cell antioxidant that removes ROS from an organism and maintains cellular oxidation-reduction homeostasis. However, the Ag NPs mediated oxidative stress is connected not only with glutathione elimination. The cells subjected to NPs exposure had the decreased activity of antioxidant enzymes [243] and the changes in expression of genes connected to oxidative stress regulation [244]. N. Mei with colleagues has shown that 5 nm Ag NPs induced the expression of 59 from 84 genes related to oxidative stress in mouse lymphoma cells [245]. Moreover, they have revealed the mutagenic activity of Ag NPs. The authors presented the results of LOH (loss of heterozygosity) analysis in dose ranged of 3–6 μg/mL, the mutant formation in cells treated with 5 μg/mL Ag NPs was sevenfold higher than in control. Ag NPs can also influence cell proliferation and differentiation. The Ag NPs can enter cells in several different ways: autophagy (through membrane channels), clathrin-mediated or caveolar endocytosis, phagocytosis, pinocytosis. In P. Dubey et al. work the routes of NPs in-cell intercalation and distribution are presented in a more detailed way [25]. Additionally, a more exhaustive description of effects, that Ag NPs can cause to living cells is presented.

5.1. Mechanism of Ag NPs biological toxicity

The toxic mechanism of metallic NPs is the main issue of a large number of scientific publications. Even though the numerous effects can be observed in bacterial and eukaryotic cells treated with Ag NPs the exact molecular mechanism of their action still has no clear elucidation. Fig. 6. graphically presents the scope of the chapter. There is plenty of publications, which attributed the biological activity of the Ag NPs to their possibility to release Ag^+ by oxidation. Such a mechanism, where Ag NPs are considered only as an Ag^+ carrier, some researchers called "Trojan horse" mechanism. The Ag^+ was reported to have an affinity to phosphate, carboxyl, amino, and thiol groups. The O. Gordon et al. have investigated the impact on bactericidal properties of Ag^+ ions in the presence of DNA, phosphate, cysteine, and glutamine amino acids [241]. The authors concluded, that only the Ag^+ interaction with thiol groups is the reason for their bactericidal properties, as only the presence of thiol-containing amino acid abolished the antibacterial activity. Further, to confirm the theory, the Ag^+ influence on succinate dehydrogenase deactivation was shown, which was possible to avoid by adding cysteine-containing tripeptide glutathione. Moreover, in C. N. Banti et al. the lipoxygenase inhibition by Ag^+ complexes with anti-inflammatory agents (2-hydroxybenzoic acid, salicylic acid, and aspirin) has been shown [246]. However, the as-mentioned Ag^+ containing complexes were also able to interact with DNA. The hypochromism observed in the UV spectra for Ag-containing complexes with calf thymus DNA was attributed to the intercalated or electrostatic binding mode. Additionally, the Ag^+ complexes with anti-inflammatory agents caused the DNA fragmentation in leiomyosarcoma cancer cells.

The Ag^+ is also considered to be responsible for ROS formation. H. J. Park et al. has shown that Ag^+ induced the expression of superoxide-sensor protein production, which can indicate the superoxide radical formation [247]. The authors noticed that earlier studies had shown the controversial results, but the process is depended on Ag^+ concentration and dramatically decreases at a concentration higher than 0.5 mg/L, which could be the reason for negative results. Furthermore, the hydroxyl radical formation in *S. epidermidis* treated with Ag^+ was observed, which could be due to the silver interactions with enzyme iron-sulfur clusters [241]. The addition of the Fenton reaction-specific quencher, thiourea, which does not consist thiol groups, led to decreased hydroxyl radical occurrence. Even though, the ICP-MS measurements in *S. epidermidis* lysates indicated that silver itself is not able to liberate coordinated Fe ions, their role in ROS formation cannot be dismissed completely. F. F. Xu et al. have also investigated the influence of Ag^+ on $[4Fe\text{-}4S]^+$ clusters of dehydratases, in particular fumarase [242]. They noticed, that malate (fumarase substrate/product) can partially prevent the damage, as the malate by the active site occupation make it more difficult for Ag^+ reach it.

The Ag^+ has also reported to electrostatically interact with membrane phospholipids and proteins, which can cause the depolarization and destabilization of cellular membrane and leakage of H^+ [248]. The Ag^+ release from the Ag NPs is a generally accepted fact, as it was confirmed by multiple investigations [32,77,249,250]. The Ag^+ release through the oxidative dissolution of the Ag NPs is the main issue in the assessment of their toxicity and fate in biological systems and the environment. M. Azodi et al. has investigated the dissolution behavior of Ag NPs in municipal wastewater [147]. The process was dependent on the amount of dissolved oxygen and the initial concentration of the Ag NPs. For deionized water suturated with oxygen the highest dissolution rate was revealed, while the presence of the inorganic reduced sulfur in the form of HS^- in the wastewater may contribute to a lower dissolution by forming insoluble sulfides. Moreover, the utilization of higher concentration of Ag NPs (1000 ppb over 10 ppb) led to a smaller extent particles size reduction, but to a higher Ag^+ content in the solution. S. Kittler et al. have performed the dialysis study of citrate and PVP-stabilized Ag NPs, which confirmed the low-rate NPs dissolution even in the absence of specific oxidizing agents [249]. The authors suggested

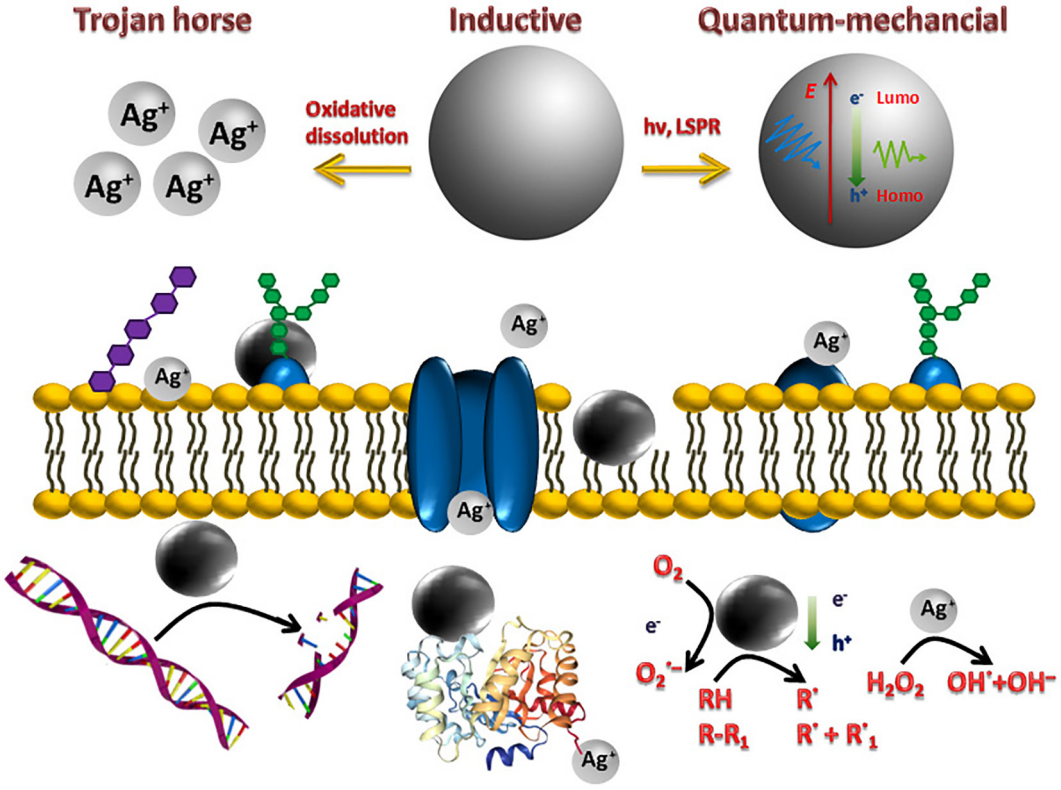

Fig. 6. The mechanisms of silver nanoparticles toxic action.

the process occurrence due to dissolved oxygen in the solution, but noticed that observed dissolution kinetic can be explained neither by the possible oxygen diffusion nor by residual solved oxygen, which may indicate the more complex process. In R. Ma et al. work the size-dependent dissolution of Ag NPs has shown [28]. It was revealed that the solubility of Ag NPs was increased in the case of smaller particles. However, the dependence was not linear in accordance with the surface area of the NPs, meaning that the ratio of released Ag^+ to the surface area was not constant for NPs of different sizes. Thus, it can be concluded that surface area alone could not explain the differences in dissolution rate, but the surface tension may provide reasonable information about Ag NPs solubility in the aqueous solubility. Additionally, the investigations also showed that the coating type and synthesis method has no significant impact on the Ag NPs dissolution kinetic. Finally, in C. Graf et al. the shape-dependent character of Ag NPs dissolution has been revealed [216]. The authors observed fast dissolution of the nanoprisms' tips, followed by a slowdown of the process when NPs become spherical, which was attributed to a higher energy on apexes and edges. In general, the oxidative dissolution is a dynamic process, which depends on environmental conditions. In B. Tang work it was shown that under light irradiation the Ag NPs can be partially dissolved, which in consequence led to changes in NPs shape from nanoprism to nanodisc [251]. The authors have revealed that after removing the light irradiation, the dissolved Ag^+ adsorbed again on the NPs surface, so the final size of the Ag nanodisc was larger than that one which can be inscribed in the initial nanoporism. Moreover, it was possible to turn nanodisc to nanoprisms again, with addition of extra citrate. However, the newly obtained nanoprisms were of larger size than the initial one.

Still, the Ag^+ release only cannot explain the higher biological activity of Ag NPs. A. Ivask et al. have shown that the Ag NPs toxicity increased with decreasing in size, and the correlation was observed for all investigated organisms: *E. coli*, *P. fluorescence*, *S. cerevisiae*, *P. subcapita*, *D. magna* and murine fibroblast line BALB/3 T3 [250]. What is interesting, the highest size-depended difference in toxicity was observed for *D. magna*, while the smallest for mammalian fibroblast. The size-depended toxicity was attributed to the Ag^+ release capability, which correlated for all tested NPs size, except the smallest one (10 nm). The authors suggested that 10 nm Ag NPs have additional not-dissolution driven toxicity. The C. Beer et al. work has also shown that suspension of Ag NPs with 16–20 nm size revealed higher toxicity against A549 human lung carcinoma cell, than its corresponding supernatant with Ag^+ fraction between 1 and 2.6% [32]. Still, the Ag NPs suspension with higher Ag^+ fraction (5.5–6.0%) did not differ in toxicity from their supernatant.

The Ag NPs itself can disorder the different cell organelles function due to adhesion to their surface. The NPs then can induce changes in structure or activate cellular destructive mechanisms, which leads to organelles' inappropriate functioning, therefore it can be called "Inductive" toxicity mechanism. Ag NPs adhesion can occur in several different ways, i.e. through electrostatic attraction or weak interaction forces, where the capping agent has a dominant role. X. Sun with colleagues has shown that Ag NPs can induce the VE-cadherin (endothelium specific cell-adherent protein) internalization in human umbilical vein endothelial cells, while the Ag^+ had no effect [33]. The direct evidence for Ag NPs adhesion on the cell surface was proved by BSE-SEM imaging and EDX spectra. Moreover, the experiment with direct and indirect (trough ultrathin 1–2 nm membranes) Ag NPs treatment was carried out. The results indicated, that in both cases the total cell VE-cadherin amount in lysates was not affected, but the direct exposure to Ag NPs influenced on a higher amount of internalized VE-cadherin. Additionally, M. E. Villanueva et al. have investigated the Ag NPs interaction with model biomembranes [80]. The oleic acid was used as a stabilizer with the aim to provide hydrophobic properties to Ag NPs. The changes in surface pressure-area isotherms of the membrane lipids indicated the Ag NPs incorporation into the films as a non-ideal mixture. The changes in surface compression modulus value C_s^{-1} for Ag NPs/lipids mixtures as a function of the surface pressure provided the information about monolayer in-plane packaging elasticity. The decreased C_s^{-1} values for lipid monolayer in the presence of Ag NPs at low and high pressure were observed, which indicated the higher compressibility and therefore the more fluidic and expanded character. Thus, the Ag NPs induce greater disorder at the molecular level of lipid layers. Moreover, the Brewster Angle Microscopy was able to distinguish the coexistence of different phases in stratum corneum mimic membrane, which indicated the phase segregation induced by Ag NPs and can be as evidence of their destructive role on cell membranes.

The charge influence on the Ag NPs toxicity has been shown in T. Silva et al. work [31]. The toxicity of positively charged branched polyethyleneimine-coated, moderate negatively charged PVP-coated and negatively charged citrate-coated Ag NPs were inspected. The positively charged Ag NPs exhibited higher toxicity both to prokaryotic (*E. coli*) and eukaryotic (*D. magna*) cells, which is attributed, similar to Ag^+, to the possibility for more easy interaction with negatively charged cell membranes. However, A. Lesniak et al. have compared the polystyrene-NPs adhesion to human adenocarcinoma alveolar basal epithelial A549 cells, and they noted that protein corona formed on NPs surface influenced on their adhesive properties [34]. The cells exposure to NPs in complete cell culture medium supplemented with 10% fetal bovine serum indicated lover adhesion rate than that one cultured in serum-free medium. Additionally, S. Juling et al. have revealed that the metabolic response to the Ag NPs treatment in Caco-2 human intestinal epithelial cells is dependent on the protein corona formed on the NPs surface [27]. G. Lopez-Carballo et al. have also noticed the higher antibacterial capacity against *E. coli* and *S. aureus* of chitosan films, containing silver nanoparticles, in diluted MHB comparing to normal culture media [17]. The effect was attributed to the chelating capability of proteins, that decreased the availability of ions to exert antimicrobial activity. Hence, even though the primary stabilizer has an influence on the NPs toxicity, it can be changed significantly depending on the surrounding environment. The A. Lesniak et al. has also emphasized that in general the adhesion process as well as NPs uptake is difficult to disentangle as they occur simultaneously, so the time-resolving toxic mechanism investigation is the task for future investigations [34].

The third Ag NPs toxicity mechanism can be attributed to the consequence of plasmon modes and quantum states of the metallic NPs - the unique light propagation, enhanced reactivity of hot electrons, or the relaxation mechanisms of excited NPs. Thus, it can be denominated as a "Quantum-mechanical" mechanism. As a consequence of such a mechanism, the photodynamic therapy with metallic NPs can be performed. In classical photodynamic therapy, the molecule of the photosensitizer can receive the long-term excited triplet state by a non-radiative transition from the singlet state, which the molecule reached after photon absorption. The photosensitizer triplet state can be decay by energy transfer to surrounding molecules producing radicals, radical ions, or excited singlet oxygen ($^1O_2$) [252]. The LSPR-induced hot electron dynamics and thermalization is also described in the literature. The hot electrons in noble NPs can decay through two different actions, namely electron-electron and electron-phonon interactions [253]. The successful transfer of Ag NPs energy, provided by LSPR, through electron-electron interactions requires the direct substrate molecules deposition on NPs surface. R. Vankayala et al. have revealed that Ag NPs were able to promote the formation of $^1O_2$, but only in the lightened conditions, confirming the LSPR-depended nature of the process. Moreover, the sensitization process has shown to be strongly dependent from NPs morphology [218]. To give an example, O. Erdogan et al. have investigated the photo-induced enhanced toxicity of the Ag NPs synthesized via *Cynara scolymus* leaf extract [243]. The as-synthesized NPs alone had no influence on adenocarcinoma MCF7 cell viability in concentration 10 μg/mL, but in combination with photodynamic therapy, it inhibited the cell growth, viability, and migration by 50%. The ROS formation under the irradiation was confirmed by the decrease in the

superoxide dismutase, catalase and glutathione peroxidase activity. In contrast, the electron-phonon interactions lead to thermal diffusion (heat transfer) outside the NPs, which is the basis for photothermal therapy. K. Manivannan et al. have shown that core-shell $Ag@SiO_2@Ag_{seed}$ NPs can reach 43 °C under visible light irradiation, so it is enough to get the tumor cell cytotoxicity and tumor vascular tissue destruction, which occurs at 41.1 °C and 43 °C respectively [13]. However, for the $Ag@SiO_2@Ag$ NPs, the visible light was able to induce heat only up to 40.5 °C. Moreover, the $Ag@SiO_2@Ag_{seed}$ NPs exhibited fluorescence properties, so it can be utilized as a bioimaging probe. The utilization of metallic NPs in the photodynamic and photothermal therapies has multiple virtues in comparison to conventional photosensitizers. The NPs are more stable under irradiation, metallic NPs have significantly higher extinction coefficient due to LSPR, which additionally can be tuned by changes in NPs form and size, so their adsorption band will be in a biological transparency window (650 to 1300 nm) [218,252]. An additional virtue of NPs is that they can be utilized as a carrier for different substances, which can enhance the photodynamic and photothermal action [254]. In the case of Ag NPs the increased Ag^+ production under irradiation is also considered. G. Fuertes with colleagues has shown that Ag NPs coated with silica received the antimicrobial properties against *E. coli* only in case of irradiation with light of LSPR band [255]. The irradiation with light of 387 nm wavelength caused the changes in NPs structure and characteristic "staining" of bacterial cells, so the NPs toxic properties were assigned to photo-induced Ag^+ release.

6. Conclusions and perspectives

Ag NPs have shown to be the objects with unique properties that allow to exploit them in multiple applications such as electronic devices and solar energy harvesting, advanced analytical techniques, medical diagnostics and treatment, catalysis and environmental applications. Ag NPs show different physical properties comparing to bulk silver, among other decreased melting point and enormous extinction in UV-Vis range due to LSPR. Additionally, they exhibit catalytic and photocatalytic properties, which were presented in the article. Moreover, the Ag NPs biological activity attracts high researchers' interest, among other antibacterial, antifungal, antiviral, antiameobic, antiangiogenic properties as well as cytotoxicity against cancer and normal cell lines, so this issue was also revealed in the article.

Herein we reviewed different aspects of the Ag NPs synthesis and their influence on the NPs features. It was shown that the basic NPs properties (size, shape, etc.) can be controlled by synthesis system selection, e.g. using different precursors, stabilizers, pH, and temperature changing as well as using different advanced synthesis devices. Moreover, the synthesis can be influenced by multiple physical agents such as electromagnetic irradiation or sonication. Further, the multiple techniques were shown, that can be utilized for the Ag NPs and their composites investigation. The basic principles and capability of the techniques were revealed. The drawbacks and artifacts of the technique, that may appear during measurements were shown. According to the provided information, it should be strongly considered the flaws in the experiments to avoid results misinterpretation and therefore the appearance of erroneous statements.

In the final part of the review, the Ag NPs physicochemical and biological properties were shown. It was revealed that Ag NPs size has a significant impact on their features, which is related to the so-called "quantum size effect". However, the NPs shape also influences their properties, as it leads to changes in surface-to-volume ratio, and therefore the NPs surface energy. Moreover, the presence of faces, edges, and apexes leads to NPs surface differentiation according to energy level or electrons distribution. Additionally, the influence of chemical composition, including the capping agent, was revealed. Finally, the several ways of Ag NPs toxicity mechanism were presented, which in general may have a collaborative effect. The Ag NPs toxicity mechanism is highly discussed in the literature, however, its exact elucidation is still unknown, and is the issue of future investigations.

Even though the study of Ag NPs has begun several decades ago there is still a lot of unclear aspects in their properties. The continuous development of more sophisticated techniques brings new knowledge about objects under investigation. The new facts about Ag NPs properties allow to utilize them in a more precise way and provide a possibility for a more wide range of their applications. In turn, new applications encourage to develop new routes for Ag NPs synthesis, which will satisfy the conditions of their utilization. Lately, the NPs utilization in the NALDI technique gained a lot of interest among researches. Still, the issue of Ag NPs utilization in solar energy harvesting, bioimaging, SERS, and different medical preparation is not exhausted and needs new considerations.

Declaration of Competing Interest

The authors declare that they have no known competing financial interests or personal relationships that could have appeared to influence the work reported in this paper.

Acknowledgements

This work was financially supported in the frame of the project "Advanced Biocomposites for Tomorrow's Economy BIOG-NET", FNP POIR.04.04.00-00-1792/18-00, project is carried out within the TEAM-NET programme of the Foundation for Polish Science co-financed by the European Union under the European Regional Development Fund. Oleksandra Pryshchepa, Paweł Pomastowski and Bogusław Buszewski are members of Toruń Center of Excellence "Towards Personalized Medicine" operating under Excellence Initiative-Research University.

References

[1] Rogers B, Adams J, Pennathur S. Nanotechnology: understanding small systems. . 3rd ed.Boca Raton: CRC Press; 2014.
[2] European Commission. Definition – nanomaterials – environment – European commission. European Commission; 2015. https://ec.europa.eu/environment/chemicals/nanotech/faq/definition_en.htm (accessed March 8, 2020).
[3] Xing L, Xiahou Y, Zhang P, Du W, Xia H. Size control synthesis of monodisperse, quasi-spherical silver nanoparticles to realize surface-enhanced Raman scattering uniformity and reproducibility. ACS Appl Mater Interfaces 2019;11:17637–46. https://doi.org/10.1021/acsami.9b02052.
[4] Massey AG, Thompson NR, Johndon BFG. The chemistry of copper, silver and gold. Elsevier, Oxford; 1973. https://doi.org/10.1016/C2013-0-02676-X.
[5] Yang S, Liu P, Zhang Y, Guo Q-N, Chen Y. Effects of silver nanoparticles size and shape on light scattering. Optik (Stuttg) 2016;127:5722–8. https://doi.org/10.1016/j.ijleo.2016.03.071.
[6] Chun S, Grudinin D, Lee D, Kim S-H, Yi G-R, Hwang I. Roll-to-roll printing of silver oxide pastes and low temperature conversion to silver patterns. Chem Mater 2009;21:343–50. https://doi.org/10.1021/cm802475m.
[7] Švecová M, Ulbrich P, Dendisová M, Matějka P. SERS study of riboflavin on green-synthesized silver nanoparticles prepared by reduction using different flavonoids: what is the role of flavonoid used? Spectrochim Acta Part A Mol Biomol Spectrosc 2018;195:236–45. https://doi.org/10.1016/j.saa.2018.01.083.
[8] Ng K-M, Chau S-L, Tang H-W, Wei X-G, Lau K-C, Ye F, et al. Ion-desorption efficiency and internal-energy transfer in surface-assisted laser desorption/ionization: more implication(s) for the thermal-driven and phase-transition-driven desorption process. J Phys Chem C 2015;119:23708–20. https://doi.org/10.1021/acs.jpcc.5b05957.
[9] Yang M, Hashimoto K, Fujino T. Silver nanoparticles loaded on ammonium exchanged zeolite as matrix for MALDI-TOF-MS analysis of short-chain n-alkanes. Chem Phys Lett 2018;706:525–32. https://doi.org/10.1016/j.cplett.2018.07.002.
[10] Yang P, Xu Y, Chen L, Wang X, Mao B, Xie Z, et al. Encapsulated silver nanoparticles can be directly converted to silver nanoshell in the gas phase. Nano Lett 2015;15:8397–401. https://doi.org/10.1021/acs.nanolett.5b04328.
[11] Kang W-J, Cheng C-Q, Li Z, Feng Y, Shen G-R, Du X-W. Ultrafine Ag nanoparticles as active catalyst for electrocatalytic hydrogen production. ChemCatChem 2019;11:5976–81. https://doi.org/10.1002/cctc.201901364.
[12] Cao T, Li Z, Xiong Y, Yang Y, Xu S, Bisson T, et al. Silica-silver nanocomposites as regenerable sorbents for Hg0 removal from flue gases. Environ Sci Technol 2017;51:11909–17. https://doi.org/10.1021/acs.est.7b01701.
[13] Manivannan K, Cheng C-C, Anbazhagan R, Tsai H-C, Chen J-K. Fabrication of silver seeds and nanoparticle on core-shell Ag@SiO2 nanohybrids for combined

photothermal therapy and bioimaging. J Colloid Interface Sci 2019;537:604–14. https://doi.org/10.1016/j.jcis.2018.11.051.
[14] Hsu JC, Cruz ED, Lau KC, Bouché M, Kim J, Maidment ADA, et al. Renally excretable and size-tunable silver sulfide nanoparticles for dual-energy mammography or computed tomography. Chem Mater 2019;31:7845–54. https://doi.org/10.1021/acs.chemmater.9b01750.
[15] Li C, Yang W, Yuan R, Xu W. Antibody-responsive signal-off fluorescence of DNA-harbored silver nanoclusters for direct, rapid and sensitive immunoassay. Sens Actuators B 2019;301:127148. https://doi.org/10.1016/j.snb.2019.127148.
[16] Pomastowski P, Sprynskyy M, Žuvela P, Rafińska K, Milanowski M, Liu JJ, et al. Silver-lactoferrin nanocomplexes as a potent antimicrobial agent. J Am Chem Soc 2016;138:7899–909. https://doi.org/10.1021/jacs.6b02699.
[17] López-Carballo G, Higueras L, Gavara R, Hernández-Muñoz P. Silver ions release from antibacterial chitosan films containing in situ generated silver nanoparticles. J Agric Food Chem 2013;61:260–7. https://doi.org/10.1021/jf304006y.
[18] Yang C-H, Wang L-S, Chen S-Y, Huang M-C, Li Y-H, Lin Y-C, et al. Microfluidic assisted synthesis of silver nanoparticle–chitosan composite microparticles for antibacterial applications. Int J Pharm 2016;510:493–500. https://doi.org/10.1016/j.ijpharm.2016.01.010.
[19] Gurunathan S, Lee K, Kalishwaralal K, Sheikpranbabu S, Vaidyanathan R, Eom SH. Antiangiogenic properties of silver nanoparticles. Biomaterials 2009;30:6341–50. https://doi.org/10.1016/j.biomaterials.2009.08.008.
[20] Jadhav K, Deore S, Dhamecha D, Rajeshwari HR, Jagwani S, Jalalpure S, et al. Phytosynthesis of silver nanoparticles: characterization, biocompatibility studies, and anticancer activity. ACS Biomater Sci Eng 2018;4:892–9. https://doi.org/10.1021/acsbiomaterials.7b00707.
[21] Rycenga M, Cobley CM, Zeng J, Li W, Moran CH, Zhang Q, et al. Controlling the synthesis and assembly of silver nanostructures for plasmonic applications. Chem Rev 2011;111:3669–712. https://doi.org/10.1021/cr100275d.
[22] Sultana S, Rafiuddin MZ, Khan M. Shahadat, development of ZnO and ZrO2 nanoparticles: their photocatalytic and bactericidal activity. J Environ Chem Eng 2015;3:886–91. https://doi.org/10.1016/j.jece.2015.02.024.
[23] Medici S, Peana M, Nurchi VM, Zoroddu MA. Medical uses of silver: history, myths, and scientific evidence. J Med Chem 2019;62:5923–43. https://doi.org/10.1021/acs.jmedchem.8b01439.
[24] Ahn E-Y, Jin H, Park Y. Assessing the antioxidant, cytotoxic, apoptotic and wound healing properties of silver nanoparticles green-synthesized by plant extracts. Mater Sci Eng C 2019;101:204–16. https://doi.org/10.1016/j.msec.2019.03.095.
[25] Dubey P, Matai I, Kumar SU, Sachdev A, Bhushan B, Gopinath P. Perturbation of cellular mechanistic system by silver nanoparticle toxicity: cytotoxic, genotoxic and epigenetic potentials. Adv Colloid Interface Sci 2015;221:4–21. https://doi.org/10.1016/j.cis.2015.02.007.
[26] Walkey CD, Olsen JB, Song F, Liu R, Guo H, Olsen DWH, et al. Protein corona fingerprinting predicts the cellular interaction of gold and silver nanoparticles. ACS Nano 2014;8:2439–55. https://doi.org/10.1021/nn406018q.
[27] Juling S, Niedzwiecka A, Böhmert L, Lichtenstein D, Selve S, Braeuning A, et al. Protein corona analysis of silver nanoparticles links to their cellular effects. J Proteome Res 2017;16:4020–34. https://doi.org/10.1021/acs.jproteome.7b00412.
[28] Ma R, Levard C, Marinakos SM, Cheng Y, Liu J, Michel FM, et al. Size-controlled dissolution of organic-coated silver nanoparticles. Environ Sci Technol 2012;46:752–9. https://doi.org/10.1021/es201686j.
[29] Lewandowska-Andralojc A, Marciniak B. Five major sins in fluorescence spectroscopy of light-harvesting hybrid materials. ACS Energy Lett 2019;4:1898–901. https://doi.org/10.1021/acsenergylett.9b01146.
[30] Bhattacharjee S. DLS and zeta potential – what they are and what they are not? J Control Release 2016;235:337–51. https://doi.org/10.1016/j.jconrel.2016.06.017.
[31] Silva T, Pokhrel LR, Dubey B, Tolaymat TM, Maier KJ, Liu X. Particle size, surface charge and concentration dependent ecotoxicity of three organo-coated silver nanoparticles: comparison between general linear model-predicted and observed toxicity. Sci Total Environ 2014;468–469:968–76. https://doi.org/10.1016/j.scitotenv.2013.09.006.
[32] Beer C, Foldbjerg R, Hayashi Y, Sutherland DS, Autrup H. Toxicity of silver nanoparticles—nanoparticle or silver ion? Toxicol Lett 2012;208:286–92. https://doi.org/10.1016/j.toxlet.2011.11.002.
[33] Sun X, Shi J, Zou X, Wang C, Yang Y, Zhang H. Silver nanoparticles interact with the cell membrane and increase endothelial permeability by promoting VE-cadherin internalization. J Hazard Mater 2016;317:570–8. https://doi.org/10.1016/j.jhazmat.2016.06.023.
[34] Lesniak A, Salvati A, Santos-Martinez MJ, Radomski MW, Dawson KA, Åberg C. Nanoparticle adhesion to the cell membrane and its effect on nanoparticle uptake efficiency. J Am Chem Soc 2013;135:1438–44. https://doi.org/10.1021/ja309812z.
[35] Oćwieja M, Adamczyk Z, Morga M, Kubiak K. Silver particle monolayers — formation, stability, applications. Adv Colloid Interface Sci 2015;222:530–63. https://doi.org/10.1016/j.cis.2014.07.001.
[36] Biswas A, Bayer IS, Biris AS, Wang T, Dervishi E, Faupel F. Advances in top–down and bottom–up surface nanofabrication: techniques, applications & future prospects. Adv Colloid Interface Sci 2012;170:2–27. https://doi.org/10.1016/j.cis.2011.11.001.
[37] Kennedy DC, Orts-Gil G, Lai C-H, Müller L, Haase A, Luch A, et al. Carbohydrate functionalization of silver nanoparticles modulates cytotoxicity and cellular uptake. J Nanobiotechnol 2014;12:59. https://doi.org/10.1186/s12951-014-0059-z.
[38] Schauermann S, Nilius N, Shaikhutdinov S, Freund H-J. Nanoparticles for heterogeneous catalysis: new mechanistic insights. Acc Chem Res 2013;46:1673–81. https://doi.org/10.1021/ar300225s.
[39] Kibis LS, Stadnichenko AI, Pajetnov EM, Koscheev SV, Zaykovskii VI, Boronin AI. The investigation of oxidized silver nanoparticles prepared by thermal evaporation and radio-frequency sputtering of metallic silver under oxygen. Appl Surf Sci 2010;257:404–13. https://doi.org/10.1016/j.apsusc.2010.07.002.
[40] Miranzadeh M, Kassaee MZ. Solvent effects on arc discharge fabrication of durable silver nanopowder and its application as a recyclable catalyst for elimination of toxic p-nitrophenol. Chem Eng J 2014;257:105–11. https://doi.org/10.1016/j.cej.2014.06.088.
[41] Kylián O, Kuzminova A, Štefaníková R, Hanuš J, Solař P, Kúš P, et al. Silver/plasma polymer strawberry-like nanoparticles produced by gas-phase synthesis. Mater Lett 2019;253:238–41. https://doi.org/10.1016/j.matlet.2019.06.069.
[42] Zhang X-F, Liu Z-G, Shen W, Gurunathan S. Silver nanoparticles: synthesis, characterization, properties, applications, and therapeutic approaches. Int J Mol Sci 2016;17:1534. https://doi.org/10.3390/ijms17091534.
[43] Tien D-C, Tseng K-H, Liao C-Y, Huang J-C, Tsung T-T. Discovery of ionic silver in silver nanoparticle suspension fabricated by arc discharge method. J Alloys Compd 2008;463:408–11. https://doi.org/10.1016/j.jallcom.2007.09.048.
[44] Khan I, Bahuguna A, Krishnan M, Shukla S, Lee H, Min SH, et al. The effect of biogenic manufactured silver nanoparticles on human endothelial cells and zebrafish model. Sci Total Environ 2019;679:365–77. https://doi.org/10.1016/j.scitotenv.2019.05.045.
[45] Eisa WH, Zayed MF, Anis B, Abbas LM, Ali SSM, Mostafa AM. Clean production of powdery silver nanoparticles using *Zingiber officinale*: the structural and catalytic properties. J Clean Prod 2019;241:118398. https://doi.org/10.1016/j.jclepro.2019.118398.
[46] Desai R, Mankad V, Gupta SK, Jha PK. Size distribution of silver nanoparticles: UV-visible spectroscopic assessment. Nanosci Nanotechnol Lett 2012;4:30–4. https://doi.org/10.1166/nnl.2012.1278.
[47] Blommaerts N, Vanrompay H, Nuti S, Lenaerts S, Bals S, Verbruggen SW. Unraveling structural information of Turkevich synthesized plasmonic gold–silver bimetallic nanoparticles. Small 2019;15:1902791. https://doi.org/10.1002/smll.201902791.
[48] Polte J, Tuaev X, Wuithschick M, Fischer A, Thuenemann AF, Rademann K, et al. Formation mechanism of colloidal silver nanoparticles: analogies and differences to the growth of gold nanoparticles. ACS Nano 2012;6:5791–802. https://doi.org/10.1021/nn301724z.
[49] Bélteky P, Rónavári A, Igaz N, Szerencsés B, Tóth IY, Pfeiffer I, et al. Silver nanoparticles: aggregation behavior in biorelevant conditions and its impact on biological activity. Int J Nanomedicine 2019;14:667–87. https://doi.org/10.2147/IJN.S185965.
[50] Hegde H, Santhosh C, Sinha RK. Seed mediated synthesis of highly stable CTAB capped triangular silver nanoplates for LSPR sensing. Mater Res Express 2019;6:105075. https://doi.org/10.1088/2053-1591/ab3d8c.
[51] Liu T, Yin B, He T, Guo N, Dong L, Yin Y. Complementary effects of nanosilver and superhydrophobic coatings on the prevention of marine bacterial adhesion. ACS Appl Mater Interfaces 2012;4:4683–90. https://doi.org/10.1021/am301049v.
[52] Chen Z, Balankura T, Fichthorn KA, Rioux RM. Revisiting the polyol synthesis of Silver nanostructures: role of chloride in nanocube formation. ACS Nano 2019;13:1849–60. https://doi.org/10.1021/acsnano.8b08019.
[53] da Silva RR, Yang M, Choi S-I, Chi M, Luo M, Zhang C, et al. Facile synthesis of sub-20 nm silver nanowires through a bromide-mediated polyol method. ACS Nano 2016;10:7892–900. https://doi.org/10.1021/acsnano.6b03806.
[54] Huang T, Xu X-HN. Synthesis and characterization of tunable rainbow colored colloidal silver nanoparticles using single-nanoparticle plasmonic microscopy and spectroscopy. J Mater Chem 2010;20:9867–76. https://doi.org/10.1039/c0jm01990a.
[55] Agnihotri S, Mukherji S, Mukherji S. Size-controlled silver nanoparticles synthesized over the range 5–100 nm using the same protocol and their antibacterial efficacy. RSC Adv 2014;4:3974–83. https://doi.org/10.1039/C3RA44507K.
[56] Ben Moshe A, Markovich G. Synthesis of single crystal hollow silver nanoparticles in a fast reaction-diffusion process. Chem Mater 2011;23:1239–45. https://doi.org/10.1021/cm102991z.
[57] Yoo J, So H, Yang M, Lee K. Applied surface science effect of chloride ion on synthesis of silver nanoparticle using retrieved silver chloride as a precursor from the electronic scrap. Appl Surf Sci 2019;475:781–4. https://doi.org/10.1016/j.apsusc.2019.01.032.
[58] Tian Y, Liu H, Chen Y, Zhou C, Jiang Y, Gu C, et al. Seedless one-spot synthesis of 3D and 2D Ag nanoflowers for multiple phase SERS-based molecule detection. Sens Actuators B 2019;301:127142. https://doi.org/10.1016/j.snb.2019.127142.
[59] Le Trong H, Kiryukhina K, Gougeon M, Baco-Carles V, Courtade F, Dareys S, et al. Paramagnetic behaviour of silver nanoparticles generated by decomposition of silver oxalate. Solid State Sci 2017;69:44–9. https://doi.org/10.1016/j.solidstatesciences.2017.05.009.
[60] Bokhonov BB, Sharafutdinov MR, Whitcomb DR, Burleva LP. In situ self-assembly of silver nanoparticles. J Phys Chem C 2014;118:11980–9. https://doi.org/10.1021/jp501508a.
[61] Cai Y, Luo X, Maclean M, Qin Y, Duxbury M, Ding F. A single-step fabrication approach for development of antimicrobial surfaces. J Mater Process Technol 2019;271:249–60. https://doi.org/10.1016/j.jmatprotec.2019.04.012.
[62] Ashkarran AA. A novel method for synthesis of colloidal silver nanoparticles by arc discharge in liquid. Curr Appl Phys 2010;10:1442–7. https://doi.org/10.1016/j.cap.2010.05.010.
[63] Yasin HM, Ahmed W, Ali A, Bhatti AS, Rehman NU. Micro-plasma assisted synthesis of multifunctional D-fructose coated silver nanoparticles. Mater Res Express 2019;6:1050a2. https://doi.org/10.1088/2053-1591/ab3fed.
[64] Si MZ, Kang YP, Liu RM. Surface-enhanced Raman scattering (SERS) spectra of three kinds of azo-dye molecules on silver nanoparticles prepared by electrolysis. Appl Surf Sci 2012;258:5533–7. https://doi.org/10.1016/j.apsusc.2011.12.118.

[65] Stamplecoskie KG, Scaiano JC. Light emitting diode irradiation can control the morphology and optical properties of silver nanoparticles. J Am Chem Soc 2010;132:1825–7. https://doi.org/10.1021/ja910010b.
[66] Veisi H, Dadres N, Mohammadi P, Hemmati S. Green synthesis of silver nanoparticles based on oil-water interface method with essential oil of orange peel and its application as nanocatalyst for A3 coupling. Mater Sci Eng C 2019;105:110031. https://doi.org/10.1016/j.msec.2019.110031.
[67] Hernández-Morales L, Espinoza-Gómez H, Flores-López LZ, Sotelo-Barrera EL, Núñez-Rivera A, Cadena-Nava RD, et al. Study of the green synthesis of silver nanoparticles using a natural extract of dark or white *Salvia hispanica* L. seeds and their antibacterial application. Appl Surf Sci 2019;489:952–61. https://doi.org/10.1016/j.apsusc.2019.06.031.
[68] Sangar S, Sharma S, Vats VK, Mehta SK, Singh K. Biosynthesis of silver nanocrystals, their kinetic profile from nucleation to growth and optical sensing of mercuric ions. J Clean Prod 2019;228:294–302. https://doi.org/10.1016/j.jclepro.2019.04.238.
[69] Dakshayani SS, Marulasiddeshwara MB, Sharath SK, Golla R, Raghavendra Kumar P, Devaraja S, et al. Antimicrobial, anticoagulant and antiplatelet activities of green synthesized silver nanoparticles using Selaginella (Sanjeevini) plant extract. Int J Biol Macromol 2019;131:787–97. https://doi.org/10.1016/j.ijbiomac.2019.01.222.
[70] Anthony KJP, Murugan M, Jeyaraj M, Rathinam NK, Sangiliyandi G. Synthesis of silver nanoparticles using pine mushroom extract: a potential antimicrobial agent against *E. coli* and B. subtilis. J Ind Eng Chem 2014;20:2325–31. https://doi.org/10.1016/j.jiec.2013.10.008.
[71] Karimi S, Samimi T. Green and simple synthesis route of Ag@AgCl nanomaterial using green marine crude extract and its application for sensitive and selective determination of mercury. Spectrochim Acta Part A Mol Biomol Spectrosc 2019;222:117216. https://doi.org/10.1016/j.saa.2019.117216.
[72] Barbosa VT, Souza JKC, Alvino V, Meneghetti MR, Florez-Rodriguez PP, Moreira RE, et al. Biogenic synthesis of silver nanoparticles using Brazilian propolis. Biotechnol Prog 2019;35:1–9. https://doi.org/10.1002/btpr.2888.
[73] Shankar S, Rhim JW. Amino acid mediated synthesis of silver nanoparticles and preparation of antimicrobial agar/silver nanoparticles composite films. Carbohydr Polym 2015;130:353–63. https://doi.org/10.1016/j.carbpol.2015.05.018.
[74] Thomas RK, Sukumaran S, Sudarsanakumar C. An insight into the comparative binding affinities of chlorogenic acid functionalized gold and silver nanoparticles with ctDNA along with its cytotoxicity analysis. J Mol Liq 2019;287:110911. https://doi.org/10.1016/j.molliq.2019.110911.
[75] Kosa SA, Zaheer Z. Betanin assisted synthesis of betanin@silver nanoparticles and their enhanced adsorption and biological activities. Food Chem 2019;298:125014. https://doi.org/10.1016/j.foodchem.2019.125014.
[76] Song Z, Wu Y, Wang H, Han H. Synergistic antibacterial effects of curcumin modified silver nanoparticles through ROS-mediated pathways. Mater Sci Eng C 2019;99:255–63. https://doi.org/10.1016/j.msec.2018.12.053.
[77] Jiang Y, Huang J, Wu X, Ren Y, Li Z, Ren J. Controlled release of silver ions from AgNPs using a hydrogel based on konjac glucomannan and chitosan for infected wounds. Int J Biol Macromol 2020;149:148–57. https://doi.org/10.1016/j.ijbiomac.2020.01.221.
[78] Shahid-ul-Islam BS, Butola D, Verma. Facile synthesis of chitosan-silver nanoparticles onto linen for antibacterial activity and free-radical scavenging textiles. Int J Biol Macromol 2019;133:1134–41. https://doi.org/10.1016/j.ijbiomac.2019.04.186.
[79] Boutinguiza M, Comesaña R, Lusquiños F, Riveiro A, del Val J, Pou J. Production of silver nanoparticles by laser ablation in open air. Appl Surf Sci 2015;336:108–11. https://doi.org/10.1016/j.apsusc.2014.09.193.
[80] Villanueva ME, Lanterna AE, Vico RV. Hydrophobic silver nanoparticles interacting with phospholipids and stratum corneum mimic membranes in Langmuir monolayers. J Colloid Interface Sci 2019;543:247–55. https://doi.org/10.1016/j.jcis.2019.02.069.
[81] Hao N, Nie Y, Xu Z, Zhang JXJ. Ultrafast microfluidic synthesis of hierarchical triangular silver core-silica shell nanoplatelet toward enhanced cellular internalization. J Colloid Interface Sci 2019;542:370–8. https://doi.org/10.1016/j.jcis.2019.02.021.
[82] Jiménez E, Abderrafi K, Abargues R, Valdés JL, Martínez-Pastor JP. Laser-ablation-induced synthesis of SiO 2 -capped Noble metal nanoparticles in a single step. Langmuir 2010;26:7458–63. https://doi.org/10.1021/la904179x.
[83] Pryshchepa O, Sagandykova GN, Pomastowski P, Railean-Plugaru V, Król A, Rogowska A, et al. A new approach for spontaneous silver ions immobilization onto casein. Int J Mol Sci 2019;20:3864. https://doi.org/10.3390/ijms20163864.
[84] Railean-Plugaru V, Pomastowski P, Meller K, Złoch M, Rafinska K, Buszewski B. Lactococcus lactis as a safe and inexpensive source of bioactive silver composites. Appl Microbiol Biotechnol 2017;101:7141–53. https://doi.org/10.1007/s00253-017-8443-x.
[85] Hamouda RA, Hussein MH, Abo-elmagd RA, Bawazir SS. Synthesis and biological characterization of silver nanoparticles derived from the cyanobacterium *Oscillatoria limnetica*. Sci Rep 2019;9:1–17. https://doi.org/10.1038/s41598-019-49444-y.
[86] Swapnil G, Avinash I, Aniket G, Mahendra R, Annarita F, Novella I, et al. Antiviral activity of mycosynthesized silver nanoparticles against herpes simplex virus and human parainfluenza virus type 3. Int J Nanomedicine 2013;8:4303–14. https://doi.org/10.2147/IJN.S50070.
[87] Kodoth AK, Ghate VM, Lewis SA, Prakash B, Badalamoole V. Pectin-based silver nanocomposite film for transdermal delivery of Donepezil. Int J Biol Macromol 2019;134:269–79. https://doi.org/10.1016/j.ijbiomac.2019.04.191.
[88] Hun J, Jeong D, Kanmani P. Study on physical and mechanical properties of the biopolymer/silver based active nanocomposite films with antimicrobial activity. Carbohydr Polym 2019;224:115159. https://doi.org/10.1016/j.carbpol.2019.115159.
[89] Reymond-Laruinaz S, Saviot L, Potin V, del Carmen Marco de Lucas M. Protein–nanoparticle interaction in bioconjugated silver nanoparticles: a transmission electron microscopy and surface enhanced Raman spectroscopy study. Appl Surf Sci 2016;389:17–24. https://doi.org/10.1016/j.apsusc.2016.07.082.
[90] Qin D, Yang G, Wang Y, Zhou Y, Zhang L. Green synthesis of biocompatible trypsin-conjugated Ag nanocomposite with antibacterial activity. Appl Surf Sci 2019;469:528–36. https://doi.org/10.1016/j.apsusc.2018.11.057.
[91] Kim ST, Lee YJ, Hwang YS, Lee S. Study on aggregation behavior of Cytochrome C-conjugated silver nanoparticles using asymmetrical flow field-flow fractionation. Talanta 2015;132:939–44. https://doi.org/10.1016/j.talanta.2014.05.060.
[92] Lubitz I, Kotlyar A. Self-assembled G4-DNA-silver nanoparticle structures. Bioconjug Chem 2011;22:482–7. https://doi.org/10.1021/bc1004872.
[93] Railean-Plugaru V, Pomastowski P, Wypij M, Szultka-Mlynska M, Rafinska K, Golinska P, et al. Study of silver nanoparticles synthesized by acidophilic strain of actinobacteria isolated from the of *Picea sitchensis* forest soil. J Appl Microbiol 2016;120:1250–63. https://doi.org/10.1111/jam.13093.
[94] Almalki MA, Khalifa AYZ. Silver nanoparticles synthesis from Bacillus sp KFU36 and its anticancer effect in breast cancer MCF-7 cells via induction of apoptotic mechanism. J Photochem Photobiol B Biol 2020;204:111786. https://doi.org/10.1016/j.jphotobiol.2020.111786.
[95] Bromley KM, Patil AJ, Perriman AW, Stubbs G, Mann S. Preparation of high quality nanowires by tobacco mosaic virus templating of gold nanoparticles. J Mater Chem 2008;18:4796–801. https://doi.org/10.1039/b809585j.
[96] Singh R, Shedbalkar UU, Wadhwani SA, Chopade BA. Bacteriagenic silver nanoparticles: synthesis, mechanism, and applications. Appl Microbiol Biotechnol 2015;99:4579–93. https://doi.org/10.1007/s00253-015-6622-1.
[97] Mehta SM, Sequeira MP, Muthurajana H, D'Souza JS. Rapid synthesis of gold and silver nanoparticles using tryptone as a reducing and capping agent. Appl Nanosci 2018;8:759–69. https://doi.org/10.1007/s13204-018-0684-1.
[98] Durán N, Nakazato G, Seabra AB. Antimicrobial activity of biogenic silver nanoparticles, and silver chloride nanoparticles: an overview and comments. Appl Microbiol Biotechnol 2016;100:6555–70. https://doi.org/10.1007/s00253-016-7657-7.
[99] Thanh NTK, Maclean N, Mahiddine S. Mechanisms of nucleation and growth of nanoparticles in solution. Chem Rev 2014;114:7610–30. https://doi.org/10.1021/cr400544s.
[100] Dong M, Wang W, Wei W, Hu X, Qin M, Zhang Q, et al. Understanding the ensemble of growth behaviors of sub-10-nm silver nanorods using in situ liquid cell transmission electron microscopy. J Phys Chem C 2019;123:21257–64. https://doi.org/10.1021/acs.jpcc.9b05267.
[101] Suresh AK, Pelletier DA, Wang W, Morrell-Falvey JL, Gu B, Doktycz MJ. Cytotoxicity induced by engineered silver nanocrystallites is dependent on surface coatings and cell types. Langmuir 2012;28:2727–35. https://doi.org/10.1021/la2042058.
[102] Kang H, Buchman JT, Rodriguez RS, Ring HL, He J, Bantz KC, et al. Stabilization of silver and gold nanoparticles: preservation and improvement of plasmonic functionalities. Chem Rev 2019;119:664–99. https://doi.org/10.1021/acs.chemrev.8b00341.
[103] Zhang Q, Lee I, Joo JB, Zaera F, Yin Y. Core-shell nanostructured catalysts. Acc Chem Res 2013;46:1816–24. https://doi.org/10.1021/ar300230s.
[104] Jankiewicz BJ, Jamiola D, Choma J, Jaroniec M. Silica-metal core-shell nanostructures. Adv Colloid Interface Sci 2012;170:28–47. https://doi.org/10.1016/j.cis.2011.11.002.
[105] Nakamura T, Hirata N, Nagaoka S, Nakajima A. Two-photon photoemission spectroscopy for silver nanoparticles on a hydrogen-terminated Si(111) surface: metal nanoparticle-enhanced photoemission. Chem Phys Lett 2010;489:69–74. https://doi.org/10.1016/j.cplett.2010.02.010.
[106] Chook SW, Yau SX, Chia CH, Chin SX, Zakaria S. Carboxylated-nanoncellulose as a template for the synthesis of silver nanoprism. Appl Surf Sci 2017;422:32–8. https://doi.org/10.1016/j.apsusc.2017.05.242.
[107] Moglia I, Santiago M, Soler M, Olivera-Nappa A. Silver nanoparticle synthesis in human ferritin by photochemical reduction. J Inorg Biochem 2020;206:111016. https://doi.org/10.1016/j.jinorgbio.2020.111016.
[108] Giessen TW, Silver PA. Converting a natural protein compartment into a nanofactory for the size-constrained synthesis of antimicrobial silver nanoparticles. ACS Synth Biol 2016;5:1497–504. https://doi.org/10.1021/acssynbio.6b00117.
[109] Toster J, Swaminathan Iyer K, Burtovyy R, Burgess SSO, Luzinov IA, Raston CL. Regiospecific assembly of gold nanoparticles around the pores of diatoms: toward three-dimensional nanoarrays. J Am Chem Soc 2009;131:8356–7. https://doi.org/10.1021/ja901806y.
[110] De La Escosura A, Nolte RJM, Cornelissen JJLM. Viruses and protein cages as nanocontainers and nanoreactors. J Mater Chem 2009;19:2274–8. https://doi.org/10.1039/b815274h.
[111] Bulavchenko AI, Arymbaeva AT, Demidova MG, Popovetskiy PS, Plyusnin PE, Bulavchenko OA. Synthesis and concentration of organosols of silver nanoparticles stabilized by AOT: emulsion versus microemulsion. Langmuir 2018;34:2815–22. https://doi.org/10.1021/acs.langmuir.7b04071.
[112] Wu J, Tan LH, Hwang K, Xing H, Wu P, Li W, et al. DNA sequence-dependent morphological evolution of silver nanoparticles and their optical and hybridization properties. J Am Chem Soc 2014;136:15195–202. https://doi.org/10.1021/ja506150s.
[113] Chakraborty I, Feliu N, Roy S, Dawson K, Parak WJ. Protein-mediated shape control of silver nanoparticles. Bioconjug Chem 2018;29:1261–5. https://doi.org/10.1021/acs.bioconjchem.8b00034.
[114] Tsai CM, Hsu MS, Chen JC, Huang CL. Mechanistic study of shape evolution of silver nanoprisms in the presence of KSCN. J Phys Chem C 2012;116:461–7. https://doi.org/10.1021/jp209840n.

[115] Tang B, Xu S, An J, Zhao B, Xu W. Photoinduced shape conversion and reconstruction of silver nanoprisms. J Phys Chem C 2009;113:7025–30. https://doi.org/10.1021/jp810711a.
[116] Wonner K, Evers MV, Tschulik K. The electrochemical dissolution of single silver nanoparticles enlightened by hyperspectral dark-field microscopy. Electrochim Acta 2019;301:458–64. https://doi.org/10.1016/j.electacta.2019.01.129.
[117] Mock JJ, Smith DR, Schultz S. Local refractive index dependence of plasmon resonance spectra from individual nanoparticles. Nano Lett 2003;3:485–91. https://doi.org/10.1021/nl0340475.
[118] Sekine R, Moore KL, Matzke M, Vallotton P, Jiang H, Hughes GM, et al. Complementary imaging of silver nanoparticle interactions with green algae: dark-field microscopy, electron microscopy, and nanoscale secondary ion mass spectrometry. ACS Nano 2017;11:10894–902. https://doi.org/10.1021/acsnano.7b04556.
[119] Assis M, Robeldo T, Foggi CC, Kubo AM, Mínguez-Vega G, Condoncillo E, et al. Ag nanoparticles/α-Ag2WO4 composite formed by electron beam and femtosecond irradiation as potent antifungal and antitumor agents. Sci Rep 2019;9:9927. https://doi.org/10.1038/s41598-019-46159-y.
[120] Castro-González CG, Sánchez-Segura L, Gómez-Merino FC, Bello-Bello JJ. Exposure of stevia (*Stevia rebaudiana* B.) to silver nanoparticles in vitro: transport and accumulation. Sci Rep 2019;9:10372. https://doi.org/10.1038/s41598-019-46828-y.
[121] Choma J, Jamioła D, Ludwinowicz J, Jaroniec M. Deposition of silver nanoparticles on silica spheres and rods. Colloids Surf A Physicochem Eng Asp 2012;411:74–9. https://doi.org/10.1016/j.colsurfa.2012.07.004.
[122] Liu KG, Abbasi AR, Azadbakht A, Hu ML, Morsali A. Deposition of silver nanoparticles on polyester fiber under ultrasound irradiations. Ultrason Sonochem 2017;34:13–8. https://doi.org/10.1016/j.ultsonch.2016.04.006.
[123] Das B, Dash SK, Mandal D, Ghosh T, Chattopadhyay S, Tripathy S, et al. Green synthesized silver nanoparticles destroy multidrug resistant bacteria via reactive oxygen species mediated membrane damage. Arab J Chem 2017;10:862–76. https://doi.org/10.1016/j.arabjc.2015.08.008.
[124] Kim SW, Nam SH, An YJ. Interaction of silver nanoparticles with biological surfaces of *Caenorhabditis elegans*. Ecotoxicol Environ Saf 2012;77:64–70. https://doi.org/10.1016/j.ecoenv.2011.10.023.
[125] Guehrs E, Schneider M, Günther CM, Hessing P, Heitz K, Wittke D, et al. Quantification of silver nanoparticle uptake and distribution within individual human macrophages by FIB/SEM slice and view. J Nanobiotechnol 2017;15:1–11. https://doi.org/10.1186/s12951-017-0255-8.
[126] Adhikari L, Larm NE, Baker GA. Argentous deep eutectic solvent approach for scaling up the production of colloidal silver nanocrystals. ACS Sustain Chem Eng 2019;7:11036–43. https://doi.org/10.1021/acssuschemeng.9b01777.
[127] Robinson DA, White HS. Electrochemical synthesis of individual Core@Shell and hollow Ag/Ag2S nanoparticles. Nano Lett 2019;19:5612–9. https://doi.org/10.1021/acs.nanolett.9b02144.
[128] Tigger-Zaborov H, Maayan G. Aggregation of Ag(0) nanoparticles to unexpected stable chain-like assemblies mediated by 2,2′-bipyridine decorated peptoids. J Colloid Interface Sci 2019;533:598–603. https://doi.org/10.1016/j.jcis.2018.08.094.
[129] Ahmad F, Ashraf N, Bin Zhou R, Chen JJ, Liu YL, Zeng X, et al. Optimization for silver remediation from aqueous solution by novel bacterial isolates using response surface methodology: recovery and characterization of biogenic AgNPs. J Hazard Mater 2019;380:120906. https://doi.org/10.1016/j.jhazmat.2019.120906.
[130] Römer I, Wang ZW, Merrifield RC, Palmer RE, Lead J. High resolution STEM-EELS study of silver nanoparticles exposed to light and humic substances. Environ Sci Technol 2016;50:2183–90. https://doi.org/10.1021/acs.est.5b04088.
[131] Li J, Kang L, Wang B, Chen K, Tian X, Ge Z, et al. Controlled release and long-term antibacterial activity of dialdehyde nanofibrillated cellulose/silver nanoparticle composites. ACS Sustain Chem Eng 2019;7:1146–58. https://doi.org/10.1021/acssuschemeng.8b04799.
[132] Beleites M, Matyssek C, Blaschek HH, Seifert G. Near-field optical microscopy of femtosecond-laser-reshaped silver nanoparticles in dielectric matrix. Nanoscale Res Lett 2012;7:2–5. https://doi.org/10.1186/1556-276X-7-315.
[133] Sethi A, Rafiee M, Chandra S, Ahmed H, McCormack S. Unified methodology for fabrication and quantification of gold nanorods, gold core silver shell nanocuboids, and their polymer nanocomposites. Langmuir 2019;35:13011–9. https://doi.org/10.1021/acs.langmuir.9b01481.
[134] Burratti L, Ciotta E, Bolli E, Kaciulis S, Casalboni M, De Matteis F, et al. Fluorescence enhancement induced by the interaction of silver nanoclusters with lead ions in water. Colloids Surf A Physicochem Eng Asp 2019;579:123634. https://doi.org/10.1016/j.colsurfa.2019.123634.
[135] Sivakumar P, Priyatharshni S, Kumar K. Fluorescent silver nanoparticles for sensitive and selective detection of dopamine. Mater Chem Phys 2020;240:122167. https://doi.org/10.1016/j.matchemphys.2019.122167.
[136] Rogowska A, Rafińska K, Pomastowski P, Walczak J, Railean-Plugaru V, Buszewska-Forajta M, et al. Silver nanoparticles functionalized with ampicillin. Electrophoresis 2017;38:2757–64. https://doi.org/10.1002/elps.201700093.
[137] Teeparuksapun K, Prasongchan N, Thawonsuwan A. Alpha-lipoic acid functionalized Silver nanoparticles for colorimetric detection of copper ion. Anal Sci 2019;35:371–7. https://doi.org/10.2116/analsci.18P442.
[138] Liu CW, Lin Y-R, Fang C-S, Latouche C, Kahlal S, Saillard J-Y. [Ag 7 (H){E 2 P(OR) 2 } 6] (E = Se, S): precursors for the fabrication of silver nanoparticles. Inorg Chem 2013;52:2070–7. https://doi.org/10.1021/ic302482p.
[139] Piao MJ, Kang KA, Lee IK, Kim HS, Kim S, Choi JY, et al. Silver nanoparticles induce oxidative cell damage in human liver cells through inhibition of reduced glutathione and induction of mitochondria-involved apoptosis. Toxicol Lett 2011;201:92–100. https://doi.org/10.1016/j.toxlet.2010.12.010.
[140] Shah V, Bharatiya B, Mishra MK, Ray D, Shah DO. Molecular insights into sodium dodecyl sulphate mediated control of size for silver nanoparticles. J Mol Liq 2019;273:222–30. https://doi.org/10.1016/j.molliq.2018.10.042.
[141] Maiti N, Thomas S, Debnath A, Kapoor S. Raman and XPS study on the interaction of taurine with silver nanoparticles. RSC Adv 2016;6:56406–11. https://doi.org/10.1039/c6ra09569k.
[142] Sharp JC, Yao YX, Campbell CT. Silver nanoparticles on Fe 3 O 4 (111): energetics by Ag adsorption calorimetry and structure by surface spectroscopies. J Phys Chem C 2013;117:24932–6. https://doi.org/10.1021/jp408956x.
[143] Abbass AE, Swart HC, Coetsee E, Kroon RE. Enhanced terbium emission due to plasmonic silver nanoparticles in bismuth silicate. J Am Ceram Soc 2016;99:876–80. https://doi.org/10.1111/jace.14011.
[144] Campos A, Troc N, Cottancin E, Pellarin M, Weissker HC, Lermé J, et al. Plasmonic quantum size effects in silver nanoparticles are dominated by interfaces and local environments. Nat Phys 2019;15:275–80. https://doi.org/10.1038/s41567-018-0345-z.
[145] Sadovnikov SI, Vovkotrub EG. Thermal stability of nanoparticle size and phase composition of nanostructured Ag2S silver sulfide. J Alloys Compd 2018;766:140–8. https://doi.org/10.1016/j.jallcom.2018.06.351.
[146] Hsiao IL, Bierkandt FS, Reichardt P, Luch A, Huang YJ, Jakubowski N, et al. Quantification and visualization of cellular uptake of TiO2 and Ag nanoparticles: comparison of different ICP-MS techniques. J Nanobiotechnol 2016;14:1–13. https://doi.org/10.1186/s12951-016-0203-z.
[147] Azodi M, Sultan Y, Ghoshal S. Dissolution behavior of silver nanoparticles and formation of secondary silver nanoparticles in municipal wastewater by single-particle ICP-MS. Environ Sci Technol 2016;50:13318–27. https://doi.org/10.1021/acs.est.6b03957.
[148] Lee WC, Lee BT, Lee S, Hwang YS, Jo E, Eom IC, et al. Optimisation, evaluation and application of asymmetrical flow field-flow fractionation with single particle inductively coupled plasma mass spectrometry (SP-ICP-MS) to characterise silver nanoparticles in environmental media. Microchem J 2016;129:219–30. https://doi.org/10.1016/j.microc.2016.06.030.
[149] Mozhayeva D, Engelhard C. Separation of Silver nanoparticles with different coatings by capillary electrophoresis coupled to ICP-MS in single particle mode. Anal Chem 2017;89:9767–74. https://doi.org/10.1021/acs.analchem.7b01626.
[150] Boughriba S, Souissi N, Jridi M, Li S, Nasri M. Thermal, mechanical and microstructural characterization and antioxidant potential of *Rhinobatos cemiculus* gelatin films supplemented by titanium dioxide doped silver nanoparticles. Food Hydrocoll 2020;103:105695. https://doi.org/10.1016/j.foodhyd.2020.105695.
[151] Liu M, Chao J, Deng S, Wang K, Li K, Fan C. Dark-field microscopy in imaging of plasmon resonant nanoparticles. Colloids Surf B Biointerfaces 2014;124:111–7. https://doi.org/10.1016/j.colsurfb.2014.06.001.
[152] Huang B, Bates M, Zhuang X. Super-resolution fluorescence microscopy. Annu Rev Biochem 2009;78:993–1016. https://doi.org/10.1146/annurev.biochem.77.061906.092014.
[153] Kästner C, Böhmert L, Braeuning A, Lampen A, Thünemann AF. Fate of fluorescence labels – their adsorption and desorption kinetics to silver nanoparticles. Langmuir 2018;34:7153–60. https://doi.org/10.1021/acs.langmuir.8b01305.
[154] O'Connor DJ, Sexton BA, Smart RSC. Surface analysis methods in materials science. Berlin, Heidelberg: Springer Berlin Heidelberg; 2003. https://doi.org/10.1007/978-3-662-05227-3.
[155] Yu X, Arey B, Chatterjee S, Chun J. Improving in situ liquid SEM imaging of particles. Surf Interface Anal 2019;51:1325–31. https://doi.org/10.1002/sia.6700.
[156] Kim KH, Akase Z, Suzuki T, Shindo D. Charging effects on SEM/SIM contrast of metal/insulator system in various metallic coating conditions. Mater Trans 2010;51:1080–3. https://doi.org/10.2320/matertrans.M2010034.
[157] Stabentheiner E, Zankel A, Pölt P. Environmental scanning electron microscopy (ESEM)—a versatile tool in studying plants. Protoplasma 2010;246:89–99. https://doi.org/10.1007/s00709-010-0155-3.
[158] Antisari LV, Laudicina VA, Gatti A, Carbone S, Badalucco L, Vianello G. Soil microbial biomass carbon and fatty acid composition of earthworm Lumbricus rubellus after exposure to engineered nanoparticles. Biol Fertil Soils 2015;51:261–9. https://doi.org/10.1007/s00374-014-0972-1.
[159] Williams DB, Carter CB. Transmission electron microscopy: a textbook for materials science. New York: Springer; 2009.
[160] De Yoreo JJ, Sommerdjik NAJM. Investigating materials formation with liquid-phase and cryogenic TEM. Nat Rev Mater 2016;1:16035. https://doi.org/10.1038/natrevmats.2016.35.
[161] Collins L, Liu Y, Ovchinnikova OS, Proksch R. Quantitative electromechanical atomic force microscopy. ACS Nano 2019;13:8055–66. https://doi.org/10.1021/acsnano.9b02883.
[162] Vobornik D, Vobornik S. Scanning near-field optical microscopy. Bosn J Basic Med Sci 2008;8:63–71. https://doi.org/10.17305/bjbms.2008.3000.
[163] Liu BJ, Lin KQ, Hu S, Wang X, Lei ZC, Lin HX, et al. Extraction of absorption and scattering contribution of metallic nanoparticles toward rational synthesis and application. Anal Chem 2015;87:1058–65. https://doi.org/10.1021/ac503612b.
[164] Dziubakiewicz E, Buszewski B. Principles of electromigration techniques. In: Buszewski B, Dziubakieicz E, Szumski M, editors. Electromigr. tech. Heidelberg: Springer-Verlag; 2013. p. 5–26. https://doi.org/10.1007/978-3-642-35043-6_2.
[165] Mudalige TK, Qu H, Van Haute D, Ansar SM, Linder SW. Capillary electrophoresis and asymmetric flow field-flow fractionation for size-based separation of engineered metallic nanoparticles: a critical comparative review. TrAC Trends Anal Chem 2018;106:202–12. https://doi.org/10.1016/j.trac.2018.07.008.
[166] Garcia MA. Surface plasmons in metallic nanoparticles: fundamentals and applications. J Phys D Appl Phys 2011;44:283001. https://doi.org/10.1088/0022-3727/44/28/283001.

[167] Hooshmand N, El-Sayed MA. Collective multipole oscillations direct the plasmonic coupling at the nanojunction interfaces. Proc Natl Acad Sci 2019;116:19299–304. https://doi.org/10.1073/pnas.1909416116.
[168] Wijaya YN, Kim J, Choi WM, Park SH, Kim MH. A systematic study of triangular silver nanoplates: one-pot green synthesis, chemical stability, and sensing application. Nanoscale 2017;9:11705–12. https://doi.org/10.1039/c7nr03077k.
[169] Luo M, Huang H, Choi S-I, Zhang C, da Silva RR, Peng H-C, et al. Facile synthesis of Ag nanorods with no plasmon resonance peak in the visible region by using Pd decahedra of 16 nm in size as seeds. ACS Nano 2015;9:10523–32. https://doi.org/10.1021/acsnano.5b05053.
[170] Pansare AV, Shedge AA, Chhatre SY, Das D, Murkute P, Pansare SV, et al. AgQDs employing black box synthetic strategy: photocatalytic and biological behavior. JOL 2019;212:133–40. https://doi.org/10.1016/j.jlumin.2019.04.014.
[171] Monago-Maraña O, Durán-Merás I, Galeano-Díaz T, Muñoz De La Peña A. Fluorescence properties of flavonoid compounds. Quantification in paprika samples using spectrofluorimetry coupled to second order chemometric tools. Food Chem 2016;196:1058–65. https://doi.org/10.1016/j.foodchem.2015.10.041.
[172] Socrates GG. Infrared and Raman characteristic group frequencies: tables and charts. . 3rd ed.Chichester, West Sussex: John Wiley & Sons, Ltd; 2004.
[173] Syed B, Nagendra Prasad MN, Satish S. Synthesis and characterization of silver nanobactericides produced by Aneurinibacillus migulanus 141, a novel endophyte inhabiting *Mimosa pudica* L. Arab J Chem 2019;12:3743–52. https://doi.org/10.1016/j.arabjc.2016.01.005.
[174] Bowie BT, Chase DB, Lewis IR, Griffiths PR. Anomalies and artifacts in Raman spectroscopy. In: Griffiths PR, editor. Handb. vib. spectrosc. Chichester, UK: John Wiley & Sons, Ltd; 2006. https://doi.org/10.1002/0470027320.s3103.
[175] Hanrahan MP, Fought EL, Windus TL, Wheeler LM, Anderson NC, Neale NR, et al. Characterization of silicon nanocrystal surfaces by multidimensional solid-state NMR spectroscopy. Chem Mater 2017;29:10339–51. https://doi.org/10.1021/acs.chemmater.7b03306.
[176] Retout M, Brunetti E, Valkenier H, Bruylants G. Limits of thiol chemistry revealed by quantitative analysis of mixed layers of thiolated-PEG ligands grafted onto gold nanoparticles. J Colloid Interface Sci 2019;557:807–15. https://doi.org/10.1016/j.jcis.2019.09.047.
[177] Marbella LE, Millstone JE. NMR techniques for noble metal nanoparticles. Chem Mater 2015;27:2721–39. https://doi.org/10.1021/cm504809c.
[178] Pawłowski R, Kiełbasiński K, Sobik P, Pawłowski B, Wita H, Konefał R, et al. Obtaining of silver nanopowders by the thermal decomposition of fatty silver salts with various chain length. Mater Res Express 2019;6:065046. https://doi.org/10.1088/2053-1591/ab086b.
[179] Marbella LE, Andolina CM, Smith AM, Hartmann MJ, Dewar AC, Johnston KA, et al. Gold-cobalt nanoparticle alloys exhibiting tunable compositions, near-infrared emission, and high T 2 relaxivity. Adv Funct Mater 2014;24:6532–9. https://doi.org/10.1002/adfm.201400988.
[180] Jones LC, Buras Z, Gordon MJ. Partial hydrogenation of C 2H 2 on Ag-doped pt nanoparticles. J Phys Chem C 2012;116:12982–8. https://doi.org/10.1021/jp304632v.
[181] Lee JH, Okuno Y, Cavagnero S. Sensitivity enhancement in solution NMR: emerging ideas and new frontiers. J Magn Reson 2014;241:18–31. https://doi.org/10.1016/j.jmr.2014.01.005.
[182] Zhi Hu J. Magic angle spinning NMR metabolomics. Metabolomics 2016;6. https://doi.org/10.4172/2153-0769.1000e147.
[183] Ma G, Allen HC. Handbook of spectroscopy. Wiley-VCH Verlag GmbH: Weinheim; 2003. https://doi.org/10.1002/3527602305.
[184] Radu T, Benea D, Ciceo-Lucacel R, Barbu-Tudoran L, Simon S. X-ray photoelectron spectroscopic characterization of Ag nanoparticles embedded bioglasses. J Phys Chem C 2012;116:17975–9. https://doi.org/10.1021/jp306035n.
[185] Han Y, Xu Q, Wang W, Zhu J. Atomic-scale insight into the metal–support interaction: a case for Ag nanoparticles on ordered ZrO 2 (111) thin films. J Phys Chem C 2015;119:4235–41. https://doi.org/10.1021/jp5129035.
[186] Kjærvik M, Hermanns A, Dietrich P, Thissen A, Bahr S, Ritter B, et al. Detection of suspended nanoparticles with near-ambient pressure X-ray photoelectron spectroscopy. J Phys Condens Matter 2017;29:474002. https://doi.org/10.1088/1361-648X/aa8b9d.
[187] Dahle S, Meuthen J, Viöl W, Maus-Friedrichs W. Adsorption of silver on glucose studied with MIES, UPS, XPS and AFM. Appl Surf Sci 2013;284:514–22. https://doi.org/10.1016/j.apsusc.2013.07.126.
[188] Scudiero L, Wei H, Eilers H. Photoemission spectroscopy and atomic force microscopy investigation of vapor-phase codeposited silver/poly(3-hexylthiophene) composites. ACS Appl Mater Interfaces 2009;1:2721–8. https://doi.org/10.1021/am900582w.
[189] Pal R, Sikder AK, Saito K, Funston AM, Bellare JR. Electron energy loss spectroscopy for polymers: a review. Polym Chem 2017;8:6927–37. https://doi.org/10.1039/C7PY01459G.
[190] Bunaciu AA, Udriştioiu E Gabriela, Aboul-Enein HY. X-Ray diffraction: instrumentation and applications. Crit Rev Anal Chem 2015;45:289–99. https://doi.org/10.1080/10408347.2014.949616.
[191] Shen G, Chen D. Transparent silver-nanoparticles/nanorods-decorated zinc oxide nanowires. J Phys Chem C 2010;114:21088–93. https://doi.org/10.1021/jp107213q.
[192] Holder CF, Schaak RE. Tutorial on powder X-ray diffraction for characterizing nanoscale materials. ACS Nano 2019;13:7359–65. https://doi.org/10.1021/acsnano.9b05157.
[193] Guo W, Hu S, Zhang J, Zhang H. Elimination of oxide interferences and determination of ultra-trace silver in soils by ICP-MS with ion–molecule reactions. Sci Total Environ 2011;409:2981–6. https://doi.org/10.1016/j.scitotenv.2011.04.011.
[194] Tang J, Xiong L, Wang S, Wang J, Liu L, Li J, et al. Distribution, translocation and accumulation of silver nanoparticles in rats. J Nanosci Nanotechnol 2009;9:4924–32. https://doi.org/10.1166/jnn.2009.1269.
[195] Kéri A, Kálomista I, Ungor D, Bélteki Á, Csapó E, Dékány I, et al. Determination of the structure and composition of Au-Ag bimetallic spherical nanoparticles using single particle ICP-MS measurements performed with normal and high temporal resolution. Talanta 2018;179:193–9. https://doi.org/10.1016/j.talanta.2017.10.056.
[196] Naasz S, Weigel S, Borovinskaya O, Serva A, Cascio C, Undas AK, et al. Multi-element analysis of single nanoparticles by ICP-MS using quadrupole and time-of-flight technologies. J Anal At Spectrom 2018;33:835–45. https://doi.org/10.1039/C7JA00399D.
[197] Wagener S, Dommershausen N, Jungnickel H, Laux P, Mitrano D, Nowack B, et al. Textile functionalization and its effects on the release of silver nanoparticles into artificial sweat. Environ Sci Technol 2016;50:5927–34. https://doi.org/10.1021/acs.est.5b06137.
[198] Priebe A, Barnes J-P, Edwards TEJ, Pethö L, Balogh I, Michler J. 3D imaging of nanoparticles in an inorganic matrix using TOF-SIMS validated with STEM and EDX. Anal Chem 2019;91:11834–9. https://doi.org/10.1021/acs.analchem.9b02545.
[199] Dhanya S, Saumya V, Rao TP. Synthesis of silver nanoclusters, characterization and application to trace level sensing of nitrate in aqueous media. Electrochim Acta 2013;102:299–305. https://doi.org/10.1016/j.electacta.2013.04.017.
[200] Oliveira E, Santos HM, Garcia-Pardo J, Diniz M, Lorenzo J, Rodríguez-González B, et al. Synthesis of functionalized fluorescent silver nanoparticles and their toxicological effect in aquatic environments (Goldfish) and HEPG2 cells. Front Chem 2013;1:1–11. https://doi.org/10.3389/fchem.2013.00029.
[201] Rafińska K, Pomastowski P, Buszewski B. Study of *Bacillus subtilis* response to different forms of silver. Sci Total Environ 2019;661:120–9. https://doi.org/10.1016/j.scitotenv.2018.12.139.
[202] Loeschner K, Navratilova J, Grombe R, Linsinger TPJ, Købler C, Mølhave K, et al. In-house validation of a method for determination of silver nanoparticles in chicken meat based on asymmetric flow field-flow fractionation and inductively coupled plasma mass spectrometric detection. Food Chem 2015;181:78–84. https://doi.org/10.1016/j.foodchem.2015.02.033.
[203] Mudalige TK, Qu H, Sánchez-Pomales G, Sisco PN, Linder SW. Simple functionalization strategies for enhancing nanoparticle separation and recovery with asymmetric flow field flow fractionation. Anal Chem 2015;87:1764–72. https://doi.org/10.1021/ac503683n.
[204] Štěpánová S, Kašička V. Recent applications of capillary electromigration methods to separation and analysis of proteins. Anal Chim Acta 2016;933:23–42. https://doi.org/10.1016/j.aca.2016.06.006.
[205] Qu H, Mudalige TK, Linder SW. Capillary electrophoresis coupled with inductively coupled mass spectrometry as an alternative to cloud point extraction based methods for rapid quantification of silver ions and surface coated silver nanoparticles. J Chromatogr A 2016;1429:348–53. https://doi.org/10.1016/j.chroma.2015.12.033.
[206] Michalke B, Vinković-Vrček I. Speciation of nano and ionic form of silver with capillary electrophoresis-inductively coupled plasma mass spectrometry. J Chromatogr A 2018;1572:162–71. https://doi.org/10.1016/j.chroma.2018.08.031.
[207] Hanauer M, Pierrat S, Zins I, Lotz A, Sönnichsen C. Separation of nanoparticles by gel electrophoresis according to size and shape. Nano Lett 2007;7:2881–5. https://doi.org/10.1021/nl071615y.
[208] Meenakshisundaram S, Krishnamoorthy V, Jagadeesan Y, Vilwanathan R, Balaiah A. *Annona muricata* assisted biogenic synthesis of silver nanoparticles regulates cell cycle arrest in NSCLC cell lines. Bioorg Chem 2020;95:103451. https://doi.org/10.1016/j.bioorg.2019.103451.
[209] Thiagamani SMK, Rajini N, Siengchin S, Varada Rajulu A, Hariram N, Ayrilmis N. Influence of silver nanoparticles on the mechanical, thermal and antimicrobial properties of cellulose-based hybrid nanocomposites. Compos Part B Eng 2019;165:516–25. https://doi.org/10.1016/j.compositesb.2019.02.006.
[210] Zheng Q, Zhang Y, Montazerian M, Gulbiten O, Mauro JC, Zanotto ED, et al. Understanding glass through differential scanning calorimetry. Chem Rev 2019;119:7848–939. https://doi.org/10.1021/acs.chemrev.8b00510.
[211] Haq S, Rehman W, Waseem M, Meynen V, Awan SU, Saeed S, et al. Fabrication of pure and moxifloxacin functionalized silver oxide nanoparticles for photocatalytic and antimicrobial activity. J Photochem Photobiol B Biol 2018;186:116–24. https://doi.org/10.1016/j.jphotobiol.2018.07.011.
[212] Dong C, Wang Z, Zhang Y, Ma X, Iqbal MZ, Miao L, et al. High-performance colorimetric detection of thiosulfate by using silver nanoparticles for smartphone-based analysis. ACS Sensors 2017;2:1152–9. https://doi.org/10.1021/acssensors.7b00257.
[213] Mogal SI, Gandhi VG, Mishra M, Tripathi S, Shripathi T, Joshi PA, et al. Single-step synthesis of silver-doped titanium dioxide: influence of silver on structural, textural, and photocatalytic properties. Ind Eng Chem Res 2014;53:5749–58. https://doi.org/10.1021/ie404230q.
[214] Chapter 4. The future is flat—two-dimensional nanomaterials. Nanotechnology. Cambridge, England: Royal Society of Chemistry; 2016. p. 85–114. https://doi.org/10.1039/9781782628873-00085.
[215] Harris LK, Theriot JA. Surface area to volume ratio: a natural variable for bacterial morphogenesis. Trends Microbiol 2018;26:815–32. https://doi.org/10.1016/j.tim.2018.04.008.
[216] Graf C, Nordmeyer D, Sengstock C, Ahlberg S, Diendorf J, Raabe J, et al. Shape-dependent dissolution and cellular uptake of silver nanoparticles. Langmuir 2018;34:1506–19. https://doi.org/10.1021/acs.langmuir.7b03126.
[217] Aherne D, Ledwith DM, Gara M, Kelly JM. Optical properties and growth aspects of silver nanoprisms produced by a highly reproducible and rapid synthesis at room temperature. Adv Funct Mater 2008;18:2005–16. https://doi.org/10.1002/adfm.200800233.

[218] Vankayala R, Kuo C-L, Sagadevan A, Chen P-H, Chiang C-S, Hwang KC. Morphology dependent photosensitization and formation of singlet oxygen (1Δg) by gold and silver nanoparticles and its application in cancer treatment. J Mater Chem B 2013;1:4379. https://doi.org/10.1039/c3tb20806k.
[219] Nejati S, Mohseni Vadeghani E, Khorshidi S, Karkhaneh A. Role of particle shape on efficient and organ-based drug delivery. Eur Polym J 2020;122:109353. https://doi.org/10.1016/j.eurpolymj.2019.109353.
[220] Dasgupta S, Auth T, Gompper G. Shape and orientation matter for the cellular uptake of nonspherical particles. Nano Lett 2014;14:687–93. https://doi.org/10.1021/nl403949h.
[221] Kulkarni AP, Munechika K, Noone KM, Smith JM, Ginger DS. Phase transfer of large anisotropic plasmon resonant silver nanoparticles from aqueous to organic solution. Langmuir 2009;25:7932–9. https://doi.org/10.1021/la900600z.
[222] Hartland GV, Besteiro LV, Johns P, Govorov AO. What's so hot about electrons in metal nanoparticles? ACS Energy Lett 2017;2:1641–53. https://doi.org/10.1021/acsenergylett.7b00333.
[223] Jiang P, Dong Y, Yang L, Zhao Y, Xie W. Hot electron-induced carbon–halogen bond cleavage monitored by in situ surface-enhanced Raman spectroscopy. J Phys Chem C 2019;123:16741–6. https://doi.org/10.1021/acs.jpcc.9b03238.
[224] Han F, Guan Z, Tan TS, Xu Q-H. Size-dependent two-photon excitation photoluminescence enhancement in coupled noble-metal nanoparticles. ACS Appl Mater Interfaces 2012;4:4746–51. https://doi.org/10.1021/am301121k.
[225] Wang W-L, Yang C-S. Silver nanoparticles embedded titania nanotube with tunable blue light band gap. Mater Chem Phys 2016;175:146–50. https://doi.org/10.1016/j.matchemphys.2016.03.005.
[226] Guo L, Yin H, Xu M, Zheng Z, Fang X, Chong R, et al. In situ generated plasmonic silver nanoparticle-sensitized amorphous titanium dioxide for ultrasensitive photoelectrochemical sensing of formaldehyde. ACS Sensors 2019;4:2724–9. https://doi.org/10.1021/acssensors.9b01204.
[227] Tsendzughul NT, Ogwu AA. Physicochemical aspects of the mechanisms of rapid antimicrobial contact-killing by sputtered silver oxide thin films under visible light. ACS Omega 2019;4:16847–59. https://doi.org/10.1021/acsomega.9b01856.
[228] Mahmoud KH, Abbo M. Synthesis, characterization and optical properties of gelatin doped with silver nanoparticles. Spectrochim Acta Part A Mol Biomol Spectrosc 2013;116:610–5. https://doi.org/10.1016/j.saa.2013.07.106.
[229] Luo W, Hu W, Xiao S. Size effect on the thermodynamic properties of silver nanoparticles. J Phys Chem C 2008;112:2359–69. https://doi.org/10.1021/jp0770155.
[230] Chiu C, Hong P, Lin J. Clay-mediated synthesis of silver nanoparticles exhibiting low-temperature melting. Langmuir 2011;27:11690–6. https://doi.org/10.1021/la202661n.
[231] Alarifi HA, Atiş M, Özdoğan C, Hu A, Yavuz M, Zhou Y. Determination of complete melting and surface premelting points of silver nanoparticles by molecular dynamics simulation. J Phys Chem C 2013;117:12289–98. https://doi.org/10.1021/jp311541c.
[232] Sagandykova GN, Pomastowski PP, Kaliszan R, Buszewski B. Modern analytical methods for consideration of natural biological activity. TrAC Trends Anal Chem 2018;109:198–213. https://doi.org/10.1016/j.trac.2018.10.012.
[233] Anwar A, Mungroo MR, Anwar A, Sullivan WJ, Khan NA, Siddiqui R. Repositioning of Guanabenz in conjugation with gold and silver nanoparticles against pathogenic amoebae *Acanthamoeba castellanii* and *Naegleria fowleri*. ACS Infect Dis 2019;5:2039–46. https://doi.org/10.1021/acsinfecdis.9b00263.
[234] Lu L, Sun RW-Y, Chen R, Hui C-K, Ho C-M, Luk JM, et al. Silver nanoparticles inhibit hepatitis B virus replication. Antivir Ther 2008;13:253–62.
[235] Teodoro JS, Simões AM, Duarte FV, Rolo AP, Murdoch RC, Hussain SM, et al. Assessment of the toxicity of silver nanoparticles in vitro: a mitochondrial perspective. Toxicol In Vitro 2011;25:664–70. https://doi.org/10.1016/j.tiv.2011.01.004.
[236] AshaRani P, Hande MP, Valiyaveettil S. Anti-proliferative activity of silver nanoparticles. BMC Cell Biol 2009;10:65. https://doi.org/10.1186/1471-2121-10-65.
[237] Sachdev A, Matai I, Gopinath P. Dual-functional carbon dots–silver@zinc oxide nanocomposite: in vitro evaluation of cellular uptake and induction of apoptosis. J Mater Chem B 2015;3:1217–29. https://doi.org/10.1039/C4TB02043J.
[238] Zhang R, Piao MJ, Kim KC, Kim AD, Choi J-Y, Choi J, et al. Endoplasmic reticulum stress signaling is involved in silver nanoparticles-induced apoptosis. Int J Biochem Cell Biol 2012;44:224–32. https://doi.org/10.1016/j.biocel.2011.10.019.
[239] Liu J, Wang Z, Liu FD, Kane AB, Hurt RH. Chemical transformations of nanosilver in biological environments. ACS Nano 2012;6:9887–99. https://doi.org/10.1021/nn303449n.
[240] Srivastava M, Singh S, Self WT. Exposure to silver nanoparticles inhibits selenoprotein synthesis and the activity of thioredoxin reductase. Environ Health Perspect 2012;120:56–61. https://doi.org/10.1289/ehp.1103928.
[241] Gordon O, Vig Slenters T, Brunetto PS, Villaruz AE, Sturdevant DE, Otto M, et al. Silver coordination polymers for prevention of implant infection: thiol interaction, impact on respiratory chain enzymes, and hydroxyl radical induction. Antimicrob Agents Chemother 2010;54:4208–18. https://doi.org/10.1128/AAC.01830-09.
[242] Xu FF, Imlay JA. Silver(I), mercury(II), cadmium(II), and zinc(II) target exposed enzymic iron-sulfur clusters when they toxify *Escherichia coli*. Appl Environ Microbiol 2012;78:3614–21. https://doi.org/10.1128/AEM.07368-11.
[243] Erdogan O, Abbak M, Demirbolat GM, Birtekocak F, Aksel M, Pasa S, et al. Green synthesis of silver nanoparticles via *Cynara scolymus* leaf extracts: the characterization, anticancer potential with photodynamic therapy in MCF7 cells. PLoS One 2019;14:e0216496. https://doi.org/10.1371/journal.pone.0216496.
[244] Kaveh R, Li Y-S, Ranjbar S, Tehrani R, Brueck CL, Van Aken B. Changes in *Arabidopsis thaliana* gene expression in response to silver nanoparticles and silver ions. Environ Sci Technol 2013;47:10637–44. https://doi.org/10.1021/es402209w.
[245] Mei N, Zhang Y, Chen Y, Guo X, Ding W, Ali SF, et al. Silver nanoparticle-induced mutations and oxidative stress in mouse lymphoma cells. Environ Mol Mutagen 2012;53:409–19. https://doi.org/10.1002/em.21698.
[246] Banti CN, Giannoulis AD, Kourkoumelis N, Owczarzak AM, Poyraz M, Kubicki M, et al. Mixed ligand–silver(i) complexes with anti-inflammatory agents which can bind to lipoxygenase and calf-thymus DNA, modulating their function and inducing apoptosis. Metallomics 2012;4:545. https://doi.org/10.1039/c2mt20039b.
[247] Park H-J, Kim JY, Kim J, Lee J-H, Hahn J-S, Gu MB, et al. Silver-ion-mediated reactive oxygen species generation affecting bactericidal activity. Water Res 2009;43:1027–32. https://doi.org/10.1016/j.watres.2008.12.002.
[248] Dibrov P, Dzioba J, Gosink KK, Häse CC. Chemiosmotic mechanism of antimicrobial activity of Ag+ in vibrio cholerae. Antimicrob Agents Chemother 2002;46:2668–70. https://doi.org/10.1128/AAC.46.8.2668-2670.2002.
[249] Kittler S, Greulich C, Diendorf J, Köller M, Epple M. Toxicity of silver nanoparticles increases during storage because of slow dissolution under release of silver ions. Chem Mater 2010;22:4548–54. https://doi.org/10.1021/cm100023p.
[250] Ivask A, Kurvet I, Kasemets K, Blinova I, Aruoja V, Suppi S, et al. Size-dependent toxicity of silver nanoparticles to bacteria, yeast, algae, crustaceans and mammalian cells in vitro. PLoS One 2014;9:e102108. https://doi.org/10.1371/journal.pone.0102108.
[251] Tang B, Xu S, Hou X, Li J, Sun L, Xu W, et al. Shape evolution of silver nanoplates through heating and photoinduction. ACS Appl Mater Interfaces 2013;5:646–53. https://doi.org/10.1021/am302072u.
[252] Lucky SS, Soo KC, Zhang Y. Nanoparticles in photodynamic therapy. Chem Rev 2015;115:1990–2042. https://doi.org/10.1021/cr5004198.
[253] Saavedra JRM, Asenjo-Garcia A, García de Abajo FJ. Hot-electron dynamics and thermalization in small metallic nanoparticles. ACS Photon 2016;3:1637–46. https://doi.org/10.1021/acsphotonics.6b00217.
[254] Du B, Tung C-H. Enzyme-assisted photodynamic therapy based on nanomaterials. ACS Biomater Sci Eng 2020;6:2506–17. https://doi.org/10.1021/acsbiomaterials.9b00968.
[255] Fuertes G, Sánchez-Muñoz OL, Pedrueza E, Abderrafi K, Salgado J, Jiménez E. Switchable bactericidal effects from novel silica-coated silver nanoparticles mediated by light irradiation. Langmuir 2011;27:2826–33. https://doi.org/10.1021/la1045282.